Oxidative Transformation of Curcumin: Products and Reaction Mechanisms

By

Odaine Gordon

Dissertation

Submitted to the Faculty of the

Graduate School of Vanderbilt University

in partial fulfillment of the requirements

for the degree of

DOCTOR OF PHILOSOPHY

in

Pharmacology

May, 2014

Nashville, Tennessee

Approved by:

Sean Davies

Claus Schneider

Brian Bachmann

Daniel Liebler

J. Scott Daniels

ACKNOWLEDGEMENTS

I would like to express sincere gratitude to Dr. Claus Schneider for his exceptional mentorship throughout my graduate school tenure. I was granted tremendous freedom in performing my research, with commensurate levels of guidance and support throughout, which has allowed me to develop into an independent scientist and professional.

The members of my committee, Drs. Sean Davies, Brian Bachmann, Scott Daniels, and Daniel Liebler, provided further guidance and critical review of my experiments. I would like to thank them for serving in that capacity, for the additional consultations between committee meetings, and for the generous contribution of their time.

I thank my collaborators Dr. Adam Ketron and his advisor Dr. Neil Osheroff with whom I worked on the topoisomerase project and had my first peer reviewed publication.

My colleagues in the Schneider lab, Katie Sprinkel and Drs. Leigh Ann Graham, and Paula Luis, along with past members Drs. Markus Griesser, Noemi Tejera, and Takashi Suzuki, all contributed to the completion of this project. I am grateful for their scientific contributions, and equally for their friendships that made every day in the lab a joyous one.

Drs. Donald Stec and Wade Calcutt of the NMR and LC-MS core facilities were invaluable resources in the use of their facility instruments.

My pre-doctoral training was supported by F31 AT007287, Ruth L. Kirschstein National Research Service Award (NRSA) for individual pre-doctoral fellowship training from the National Center for Complementary and Alternative Medicine at the National Institutes of Health (NCCAM/NIH) and training grant T32 GM07628 from the NIH. Other support came from the following grants awarded to Dr. Claus Schneider: R01 AT006896 from the NCCAM/NIH; R03 CA159382 from the (NCI/NIH); and Pilot awards from the Vanderbilt Center in Molecular Toxicology, DDRC, GI-SPORE, and VICB.

DEDICATION

I dedicate this dissertation to my grandparents Luther and Imogene Martin who are my biggest inspiration.

To my parents Joseph and Sandra Gordon for their love, tremendous sacrifices, constant support and encouragement that helped me to persevere throughout the many years of studies.

My siblings Natalee, Latania, Devenia, Keron, Toriean, and Kevon Gordon for being my source of motivation.

My extended family of aunts, uncles and cousins have helped to instill in me the values of discipline and hard work and always encouraged me to aim high.

And to the many friends with whom I shared this amazing journey!

TABLE OF CONTENTS

III. OXIDATIVE TRANSFORMATION OF CURCUMIN-GLUCURONIDE

LIST OF FIGURES

LIST OF TABLES

List of Abbreviations

AChE	Acetylcholinesterase
APC	Adenomatous polyposis coli gene
BCP	Bicyclopentadione
COX-2	Cyclooxygenase-2
DMBA	7,12-Dimethylbenz[α]anthracene
ESI	Electrospray ionization
GSH	Glutathione
IKK	IκB kinase
HRP	Horseradish peroxidase
HR/MS	High resolution mass spectrometry
Log P	Log10 of oil-water partition coefficient
m/*z*	Mass-to-charge ratio
NF−κB	Nuclear factor kappa B
SPLET	Sequential proton loss electron transfer
TPA	12-O-tetradecanoyl-phorbol-13-acetate
UGT	UDP-glucuronosyltransferase
UV-Vis	Ultraviolet-visible light

Chapter 1

Introduction

1. Curcumin

1.1. Introduction to curcumin

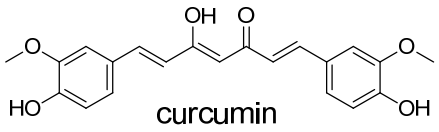

FIGURE 1.1 Structure of curcumin.

The chemical structure of curcumin is shown in Figure 1.1. Curcumin is a major secondary metabolite of the perennial Asian plant turmeric (*Curcuma longa* L). Curcumin was identified as the active principle of turmeric in 1815, and its structure determined after crystallization in 1870 (Ravindran, Prasad, and Aggarwal 2009). Turmeric is only one representative of more than 80 *curcuma* species of the ginger family, *Zingiberaceae* (Leong-Skornicková et al. 2007; Sasikumar 2005). Turmeric is widely cultivated in many Asian countries particularly in India where it is grown mostly for dietary use, and is a major component of the spice curry. Additionally, turmeric is recognized for its medicinal properties, and has been used for centuries in the treatment of a variety of ailments including eczema, arthritis, ulcers, asthma, anemia and many others (Goel, Kunnumakkara, and Aggarwal 2008). Resulting from extensive studies over the last few decades, curcumin has emerged as a promising anti-cancer agent and has been shown to target multiple and diverse signaling pathways involved in disease causation and progression (Aggarwal & Harikumar 2009; Singh & Khar 2006). The

attractiveness of curcumin as a therapeutic agent is enhanced by its safety, affordability, and history of long-term use (Chandran and Goel 2012; Belcaro et al. 2010).

1.2 Curcuminoids

Curcuminoids refer to the mixture of curcumin and its two structurally related isomers, demethoxycurcumin and bisdemethoxycurcumin, shown in Figure 1.2. (Tonnesen and Karlsen 1985). Demethoxycurcumin and bisdemethoxycurcumin lack one or both of the methoxy groups attached to the phenolic rings in curcumin, respectively. Together, curcuminoids constitute about 4–6% of the mass of dried turmeric rhizome. Curcumin is by far the most abundant, accounting for more than 80% of the total curcuminoids (Jacob et al. 2007). Commercial preparations of curcumin contain a mixture of about 80% curcumin, 15% demethoxycurcumin and 5% bisdemethoxycurcumin (Goel, Kunnumakkara, and Aggarwal 2008).

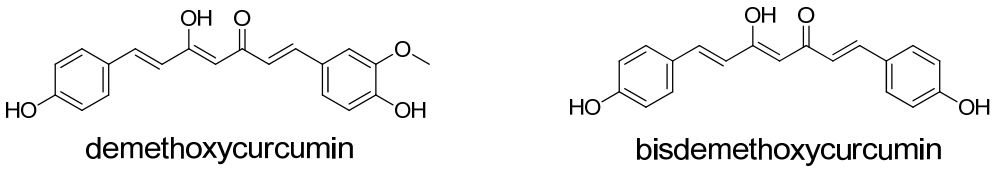

FIGURE 1.2 Structure of the minor curcuminoids.

1.3 Chemical and physical properties of curcumin

The IUPAC name of curcumin, also referred to as diferuloylmethane, is (1E,6E)-1,7-bis(4-hydroxy-3-methoxyphenyl)-1,6-heptadiene-3,5-dione. It has a

molecular formula of $C_{21}H_{20}O_6$, corresponding to a molecular weight of 368.37. Curcumin is a yellow-orange crystalline powder with maximum absorbance at 430 nm and melting point of 183 °C (Goel, Kunnumakkara, and Aggarwal 2008). Curcumin exhibits hydrophobic and (slight) hydrophilic properties owing to its aliphatic heptadienone linker and polar β-dicarbonyl and phenolic groups, respectively (Balasubramanian 2006; Grynkiewicz and Ślifirski 2012). Curcumin is sparingly soluble in water, but shows greater solubility in some organic solvents such as acetone, ethyl acetate, acetonitrile and ethanol. Its reported partition coefficient (Log P) ranges from 2.5 to 3.3 (Grynkiewicz and Ślifirski 2012). Curcumin is a bis-α,β-unsaturated β-diketone, and exists in equilibrium with its enol tautomer (Chignell et al. 1994). Studies involving ^{1}H, ^{13}C NMR, and infrared spectroscopy have shown that the enolate form predominates in alkaline solution (Sun et al. 2010; Jacob et al. 2007). Further, the enolate form is energetically favored since curcumin then exists as a completely conjugated and planar structure (Sun et al. 2002; Sun et al. 2010). In the enolate conformation in alkaline conditions, the phenolic hydroxyl is the major site of curcumin reactivity; curcumin donates a proton and an electron from either of its phenolic hydroxyls via the 'Sequential

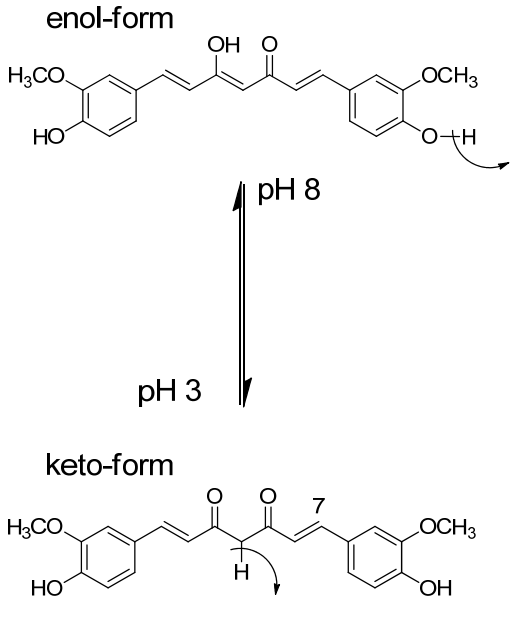

FIGURE 1.3 Enol (pH 8) versus bis-keto (pH 3) tautomers of curcumin, and their different site of H-donation.

Proton Loss Electron Transfer' (SPLET) mechanism, resulting in a phenoxyl radical. (Litwinienko and Ingold 2004). The donation of a phenolic H underlies curcumin's antioxidant activity and its instability at alkaline pH (Strimpakos and Sharma 2008; Griesser et al. 2011; Wang et al. 1997). In contrast, under acidic conditions, the bis-keto form of curcumin predominates and it becomes a potent H donor from the weak central C–H bond (Sun et al. 2002; Litwinienko and Ingold 2004; Pandya et al. 2012; Jacob et al. 2007) (Figure 1.3). Up to eight different conformational isomers of the enolic curcumin have been proposed from crystallization studies, with three crystalline forms exhibiting varying degrees of solubility identified depending on the type of solvents used for extraction and purification. All three crystalline forms exist as the β-keto–enol tautomer but differ in their hydrogen bonding, molecular packing, and the relative orientation of the keto–enol groups in neighboring molecules. Form 1, the type typically seen in commercial preparations of curcumin, has a slightly twisted conformation. Forms 2 and 3 show a linear, planar conformation and have a slight increase in solubility compared to form 1 (Grynkiewicz and Ślifirski 2012; Sanphui et al. 2011).

1.4 Therapeutic potential of curcumin

Like many other natural products with 'roots' in ethno-medicine, curcumin is now the subject of extensive research and is among the most studied plant derived medicinal chemicals (Grynkiewicz and Ślifirski 2012). Curcumin is widely recognized for its potent anti-inflammatory effects, and is associated with reduction in neutrophil and macrophage infiltration, inhibition of pro-inflammatory

chemokines, and suppression of NF-κB, COX-2, iNOS, IL-8 and other pro-inflammatory targets *in vitro* and in animal models (Wilken et al. 2011; Weisberg, Leibel, and Tortoriello 2008; Weber et al. 2006). Inflammation is central to the progression of many chronic diseases such as cancer, cardiovascular disease, diabetes, neurodegenerative disease, and arthritis, and curcumin is being investigated in the treatment and prevention of these diseases (Hong et al. 2010; Chandran and Goel 2012; Chanpoo et al. 2010; Weisberg, Leibel, and Tortoriello 2008; Ono et al. 2004; Quitschke, Steinhauff, and Rooney 2013). Suppression of prostaglandin (PGs) synthesis through the inhibition of COX-2, for example, is associated with decreasing inflammation and cancer cell proliferation. (Suzuki et al. 2009; Valacchi et al. 2004; Marcu et al. 2006; Weisberg, Leibel, and Tortoriello 2008; Chen et al. 2007).

Epidemiological studies have linked the high consumption of curcumin/turmeric in India (up to 1.5 g per person daily) to the lower overall incidence of colorectal, pancreatic, lung, breast, and prostate cancers when compared to Western countries where little curcumin is consumed (Aggarwal and Harikumar 2009). Furthermore, second generation migrants from India show higher cancer prevalence than their first generation counterpart, further solidifying an environmental (or dietary) basis for the discrepancy in cancer prevalence (Wilken et al. 2011; Sinha et al. 2003).

Pre-clinical studies of curcumin in rodent models show efficacy against colonic, stomach, liver, breast, pancreatic, brain and lung cancers (Johnson & Mukhtar 2007; Singh & Khar 2006; Singh et al. 2013; Ranjan et al. 2013; Perry et

al. 2010; Su et al. 2010). Curcumin exhibits chemopreventive effects against cancer caused from germline mutation in the *APC* gene in C57BL/6J-Min/+ mice that show spontaneous intestinal adenomas, or cancer caused from the carcinogens DMBA, benzo[a]pyrene, and azoxymethane that induce lymphomas, stomach and colon carcinogenesis, respectively (Mahmoud et al. 2000; Huang, Newmark, and Frenkel 1997; Huang et al. 1998). The chemopreventive effects of curcumin in mouse models support its role in the low incidence of cancers in regions where turmeric forms a major part of the diet. Curcumin is also able to reduce tumors once they are formed in animals. Studies conducted in tumor xenograft mice shows that curcumin can reduce or cure brain tumors, pancreatic tumors, lymphomas, and others (Perry et al. 2010; Aoki et al. 2007; Ranjan et al. 2013; Li et al. 2009).

In mouse models of diabetes, curcumin treatment results in improvements in obesity, blood glucose levels, as well as glucose and insulin tolerance. Curcumin was shown to significantly decrease body weight and fat content even with increasing caloric intake, and protects pancreatic islets against disease related damage. The improvements in glycemic status were coupled with decreased NF-κB signaling, reduced macrophage infiltration into adipose

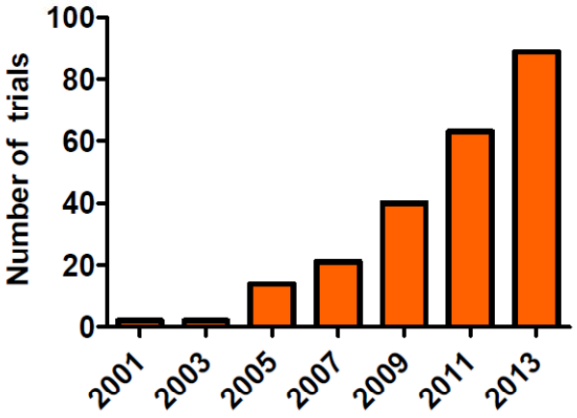

FIGURE 1.4 Number of curcumin clinical trials registered at www.clinicaltrials.gov. every other year since 2001.

tissue, and higher circulating adiponectin levels (Weisberg, Leibel, and Tortoriello 2008; Chanpoo et al. 2010). Curcumin also shows efficacy in models of depression, Alzheimer's disease, and cardiovascular disease (Olszanecki et al. 2005; Zhao et al. 2013; Quitschke, Steinhauff, and Rooney 2013).

Extensive preclinical data showing efficacy for curcumin led to studies in human diseases. There is a growing number of clinical studies involving curcumin, reaching 92 as of March 2014, up from 2 studies in 2001 (Figure 1.4). A study by Hishikawa et al. investigated turmeric in three Alzheimer's disease (AD) patients with severe cognitive, behavioral and psychological decline. The patients were given 100 mg/day curcumin for 12 weeks. The authors reported significant improvement in behavioral symptoms with no adverse effects seen even after 1 y of taking the drug (Hishikawa et al. 2012). The mechanism of action for curcumin in AD has not been elucidated. Current strategies for treating the disease use inhibitors of glutamate and acetylcholinesterase (AChE). Curcumin has been shown to protect against glutamate excitotoxicity (Wang et al., 2008) and inhibit AChE in *in vitro* assays. Furthermore, curcumin shows memory-enhancing effects in rodent models (Ahmed & Gilani, 2009), exhibits anti-amyloid activity (Ono et al., 2004) and can lessen inflammation in the brain (Akiyama, 2000) as possible mechanisms of its effects on AD.

Studies in arthritis patients report improvements in disease activity and improved overall quality of life in patients taking 200 mg (open label) or 500 mg meriva curcumin per day (Belcaro et al. 2010; Chandran and Goel 2012). Additionally, curcumin shows efficacy in patients with ulcerative colitis, diabetes,

colorectal cancer, and other diseases (Hishikawa et al. 2012; Hanai et al. 2006; Chuengsamarn et al. 2014; He et al. 2011).

1.5 Curcumin as an antioxidant

The effects of curcumin were first attributed to its antioxidant properties (Jurrmann, Brigelius-Flohé, and Böl 2005). Curcumin has a uniquely conjugated phenolic structure making it a particularly good radical trapping antioxidant (Al-Amiery et al. 2013). Curcumin can reduce oxidative damage in cells by preventing lipid peroxidation, increasing reduced glutathione by inducing its biosynthesis, and scavenging small free radical species like HO• and ROO• (Barzegar and Moosavi-Movahedi 2011; Jat et al. 2013). There was some contention in the literature over the relative importance of the phenolic hydroxyl versus the central methylenic hydrogen in mediating the antioxidant effect of curcumin. Jovanovic and his collaborators concluded that curcumin donates its H-atom from the central methylenic group in aqueous acidic buffer and in acetonitrile solutions (Jovanovic et al. 2001). It was later proposed that under physiological conditions, curcumin is a typical phenolic antioxidant and donates an H-atom from one of its phenolic hydroxyls (Barclay et al. 2000; Priyadarsini et al. 2003; Barzegar and Moosavi-Movahedi 2011). The meta-methoxy groups were suggested to further increase its antioxidant activity (Sun et al. 2002).

During anti-oxidant reactions, the donation of an H-atom and electron to an oxidized species creates a second radical (albeit a more stable one) in the antioxidant molecule (a phenoxyl radical in the case of curcumin). This

secondary radical must then be terminated by another radical species. An important clue to understanding the anti-oxidant mechanism of a compound is the structural elucidation of the terminated antioxidant product (Masuda et al. 1999). Masuda et al conducted model studies of curcumin oxidation using 2,2'-azobis(isobutyronitrile) to produce the curcumin radical in acetonitrile. The authors reported isolating chain cleavage products vanillin and ferulic acid, as well as dimers of curcumin. A mechanism was proposed in which curcumin is first converted to the phenolic radical that moves to a carbon centered position along the heptadienone chain resulting in the formation of a quinone methide. The dimers, they further proposed, were formed from coupling of two different carbon-centered radical species, and vanillin and ferulic acid formed from radical chain cleavage. Studies in our lab show that in aqueous solution, the terminal product(s) involves the stable incorporation of oxygen into the molecule to form a bicyclopentadione, with no products from inter-molecular curcumin reactions observed (Griesser et al. 2011; Gordon & Schneider 2012). The reaction of curcumin to generate the bicyclopentadione is the main focus of the work presented in this dissertation.

1.6 Intermolecular interactions of curcumin.

In addition to its anti-inflammatory and anti-oxidant effects, curcumin exhibits antiviral, antibacterial, antifungal, antineoplastic, and antiangiogenic bioactivities (Barclay et al. 2000; Nafisi et al. 2009; Perry et al. 2010; F. Chen and Shi 2002). Curcumin modulates more than 100 cellular targets in i*n vitro*

studies using cell-based systems (Anand et al. 2008). Curcumin has been shown to affect transcription factors (AP-1, PPAR-γ), cytokines (IL-1, IL-2, IL-5, IL-12), enzymes (MMP-1, GST, 5-LOX), growth factors (EGF, VEGF, TGFβ1), kinases (PKA, PKB, JNK, MAPK) and survival pathways (p53, Bcl-2) in many cell types (Johnson and Mukhtar 2007; Jurrmann, Brigelius-Flohe, and Bol 2005; Valacchi et al. 2004; Awasthi et al. 2000; S. Singh and Khar 2006; Ravindran, Prasad, and Aggarwal 2009).

Affecting this many targets is a remarkable feat for any single molecule. The chemical mechanisms whereby curcumin is able to achieve this is one conundrum associated with its biological effects. The chemical properties of the curcumin molecule provide many inferences into the nature of its interactions with protein targets and may explain its interaction with some of its targets. The following features of curcumin are implicated in mediating its intermolecular interactions: lipophilicity; Michael reaction acceptor capacity; H-bond donating capacity of the *β*-diketo and phenolic hydroxyl moieties; and its rotamerization capacity (Figure 1.5).

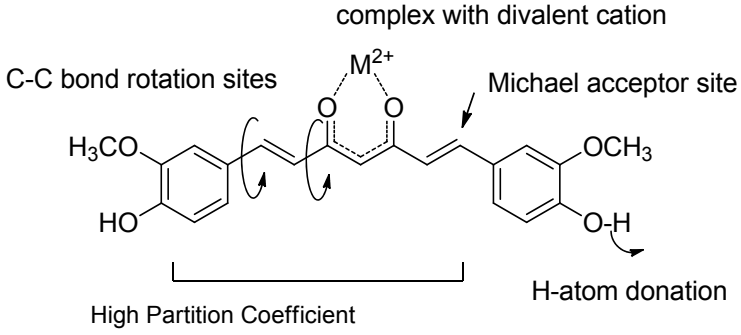

FIGURE 1.5 Chemical properties of curcumin

The high lipophilicity of curcumin has been attributed to the aliphatic heptadienone linker connecting the more polar methoxyphenol rings. Lipophilicity allows for non-covalent interactions with hydrophobic residues in proteins (Liu et al. 2008). Molecular docking studies show interactions between curcumin and alanine and tyrosine residues in human immunoglobulin G (Liu et al. 2008). Docking studies of curcumin in COX-1 active site show that the aliphatic chain region of curcumin is surrounded by hydrophobic amino acids, including leucine, alanine, and valine (Heger et al. 2014a; Selvam et al. 2005). Curcumin also binds in the minor and major groove of DNA at AT-rich regions (Bera et al. 2008; Nafisi et al. 2009). The strong hydrophobic binding of curcumin to its target proteins stabilizes further covalent interactions between the two molecules (Leung and Kee 2009).

The Michael acceptor capacity of curcumin allows for covalent interactions with nucleophilic residues in proteins (thiolates and amines) at its *α*,*β*-unsaturated carbonyl positions (Figure 1.5). A common Michael reaction involving curcumin is with glutathione (GSH). The GSH tripeptide is composed of γ-glutamate-cysteine-glycine and is known for its nucleophilic reaction with *α*,*β*-unsaturated carbonyl compounds (Ketterer 1988; Awasthi et al. 2000). Incubation of curcumin with GSH led to a concentration and time-dependent decrease in the curcumin chromophore at 430 nm, due to the disruption in the conjugated system resulting from covalent adduction (Awasthi et al. 2000). Curcumin-GSH adducts have been confirmed by HPLC, LC-MS and NMR

studies (ON Gordon, unpublished). One study suggesting covalent adduction of curcumin with p300 in cells uses the lack of reactivity of the protein with tetrahydrocurcumin (which lacks the *α*,*β*-unsaturated carbonyl) as evidence of Micheal reaction with curcumin (Marcu et al. 2006). Covalent interaction of curcumin with many of its target proteins has not been demonstrated.

Lastly, curcumin undergoes rotamerization about multiple a C–C bonds. This conformational flexibility maximizes the number of interactions between curcumin and its targets, as evident from the docking studies in which curcumin tends to adopt different configurations for each molecular target (Heger et al. 2014a). Curcumin retains its planar structure when interacting with B-form DNA minor grooves, and becomes nonplanar when bound to amyloid protein and PKC (Heger et al. 2014a; Koonammackal, Nellipparambil, and Sudarsanakumar 2011).

These interactions highlight the versatility of curcumin in its ability to associate with other molecules, but only its antioxidant and Michael acceptor functions are expected to contribute significantly to its ability to modulate signaling in these proteins. The Michael acceptor capacity and antioxidant effects of curcumin however do not account for the many and varied targets identified. The chemical mechanisms whereby curcumin is able to affect its proteins targets therefore remain to be determined.

1.7 Curcumin bioavailability

A second conundrum associated with the biological effects of curcumin is that efficacy is often demonstrated in tissues that show low to undetectable levels of the unconjugated compound. Curcumin is poorly absorbed across the gastrointestinal (GI) tract and is extensively metabolized in the liver and intestines, accounting for the submicromolar levels of the unconjugated compound observed in blood after oral dosage (Holder, Plummer, and Ryan 1978; Wahlström and Blennow 1978; Hoehle et al. 2006) Yang et al. administered 10 mg/kg of curcumin intravenously to rats and reported maximum serum levels 0.36 μg/mL after 45 min. A very high oral dose of 500 mg/kg curcumin gave only 0.06 μg/mL, and 1 g/kg dose produced a maximum serum curcumin level of only 0.5 μg/mL after 45 min. The comparatively low plasma levels of curcumin seen after the oral doses support significant first pass metabolism of curcumin (Yang et al. 2007). Similar plasma levels of curcumin are reported in other animal studies (Holder, Plummer, and Ryan 1978; Pan, Huang, and Lin 1999).

Curcumin was undetectable in the serum in studies in human subjects given a single oral dose of 0.5 or 10 g curcumin. Only one of three subjects who received a 10 g dose had detectable serum levels of 0.03 to 0.06 μg/mL after 1, 2, and 4 hours. An increase to a 12 g dose resulted in detectable levels in only one of three subjects with comparable serum levels over the same time period (Lao et al. 2006). These results are consistent with data from other studies in which glucuronide conjugates of curcumin and its reduced metabolites are the

predominant form of the compound detected in plasma (Vareed et al. 2008; Pawar et al. 2012; Awasthi et al. 2000).

Multiple approaches are being employed to improve the uptake of curcumin from the gut, including complexes with nanoparticles, liposomes, micelles and phospholipids. The studies described above used curcumin-C3 complex marketed/developed by Sabinsa. Curcumin-C3 is a mixture of the three curcuminoids (curcumin, demethoxycurcumin and bisdemethoxycurcumin) in a patented ratio and is reported to enhance the bioavailability of curcumin. Another often-used formulation is meriva curcumin patented by Indena SpA, Milan, Italy. The meriva curcumin formulation contains soy lecithin and microcrystalline cellulose with an overall curcumin content of 20%. A comparison of 340 mg/Kg unformulated curcumin and meriva curcumin corresponding to an equal amount of the compound was conducted in rats. In the first group, 99% of curcumin was present in plasma as glucuronide conjugates, with the remaining 1% being curcumin sulphate and free curcumin. The meriva curcumin group showed 23 fold increase in glucuronides, but only a 5 fold increase in curcumin (Marczylo et al. 2007). Curcumin levels in the plasma therefore remains low, and only marginal improvements in efficacy have been reported with these formulations.

Even though the low bioavailability is considered the main limitation to the clinical efficacy of curcumin, pre-clinical studies in rodents do report efficacy with plasma exposures that one would consider sub-therapeutic. Examples include systemic effects of dietary curcumin (0.01%–0.25% w/w) in treating inflammatory eye disorders (Wang et al. 2011) and glioma in the brain (Perry et al. 2010; Aoki

et al. 2007). These effects either suggest extraordinary potency for systemic curcumin, or suggest a role for its more abundant metabolites.

1.8 Curcumin metabolism

Studies assessing the metabolism of curcumin in rat liver slices, microsomes, and cytosol yields octahydrocurcumin, hexahydrocurcumin tetrahydrocurcumin and dihydrocurcumin (Hoehle et al. 2006). Thus, the phase I metabolism of curcumin involves the successive reduction of the unsaturated heptadieneone chain (Figure 1.5). Alcohol dehydrogenase is required for the formation of tetrahydrocurcumin and hexahydrocurcumin, the abundant reduced metabolites, while unidentified microsomal enzyme(s) catalyze the reduction of hexahydrocurcumin to octahydrocurcumin (Hoehle et al. 2006).

The reported conjugation metabolites of curcumin are glucuronide and/or sulfate conjugates; the major conjugation metabolites were formed in varied but significant amounts (Vareed et al. 2008; Ireson et al. 2001). None of the postulated cytochrome P450 metabolites (demethylation or hydroxylation) of curcumin were detected, suggesting these enzymes are not involved to an appreciable extent in curcumin metabolism of curcumin in the liver (Hoehle et al. 2006).

Analyses of curcumin metabolism *in vivo* are consistent with the *in vitro* data, indicating reduction of the unsaturated heptadienone chain of curcumin and subsequent conjugation to glucuronic acid or sulfates (usually inferred after hydrolysis with β-glucuronidase and arylsulfatase) forms the major metabolites.

The first detailed study on the *in vivo* metabolism of curcumin was conducted in rats by Holder et al. using [^{3}H]-curcumin (Holder, Plummer, and Ryan 1978). After an oral dose of 0.6 mg [^{3}H]curcumin, about 90% of the radioactivity was detected in the feces, suggesting biliary excretion of curcumin and its metabolites. Similar data were obtained when [^{3}H]curcumin was administered intravenously. Most of the excretion occurred within the first 24 h of administration, with very little compound detected in the tissues beyond 3 days. Glucuronide conjugates represented more than 95% of the metabolites recovered from the bile. Most of the glucuronide was conjugated to tetra- and hexahydrocurcumin. Sulfates accounted for about 2% of the metabolites (Holder, Plummer, and Ryan 1978).

After oral administration of 8 g curcumin in human subjects, curcumin-glucuronide and curcumin-sulfate were detected in plasma at 1.5 to 1.7 μM and 0.21 to 0.35 μM, respectively. Hexahydrocurcumin and hexahydrocurcumin glucuronide were also present in minor amounts (Lao et al. 2006).

Several studies have also explored the tissue distribution of curcumin. Among these are studies conducted by Ravindranath & Chandrasekhara, showing that after oral administration of 400 mg of curcumin to rats, only traces of the parent compound could be found in tissues such as the liver and kidney. After 30 min, about 90% of curcumin was found in the stomach and small intestine, but only 1% was present at 24 h, with less than 3% of the curcumin found in the tissues. In a similar evaluation of the tissue distribution using [^{3}H]curcumin diluted with cold curcumin, radioactivity was detectable in blood,

liver, and kidneys after oral administration of 400, 80, or 10 mg of the compound. With a high dose of 400 mg [^{3}H]curcumin, large amounts of the radioactivity were present in tissues 12 days after dosing. [^{3}H]Curcumin remained in the body for 72 h to 12 days with doses of 10 mg and 400 mg (Ravindranath and Chandrasekhara 1981).

1.9 Chemical instability of curcumin *in vitro*

The instability of curcumin at alkaline conditions (pH 7 to pH 10) was reported in 1985 by Tonnesen & Karlsen. The reported products of the degradation were ferulic acid, vanillin, feruloylmethane, and condensation products of feruloylmethane. The products were identified by GC-MS comparison with authentic standards.

A more detailed account of this degradation was later provided by Wang et al. The authors showed that curcumin undergoes degradation at alkaline pH in aqueous buffer, cell culture medium, and human blood. In 0.1 M phosphate buffer at pH 7.2, curcumin degrades rapidly with 90% of the chromophore at 423 nm disappearing over 10 minutes. Curcumin was more stable in media containing 10% serum or in human plasma in which it has a half-life of about 8 h (Strimpakos and Sharma 2008; Wang et al. 1997). Curcumin degradation is also slower in the presence of thiol-based antioxidants such as glutathione, and divalent ions such as Zn^{2+}, Cu^{2+}, Mg^{2+}, and Se^{2+} (Zebib, Mouloungui, and Noirot 2010). No appreciable degradation of curcumin occurs below pH 7.

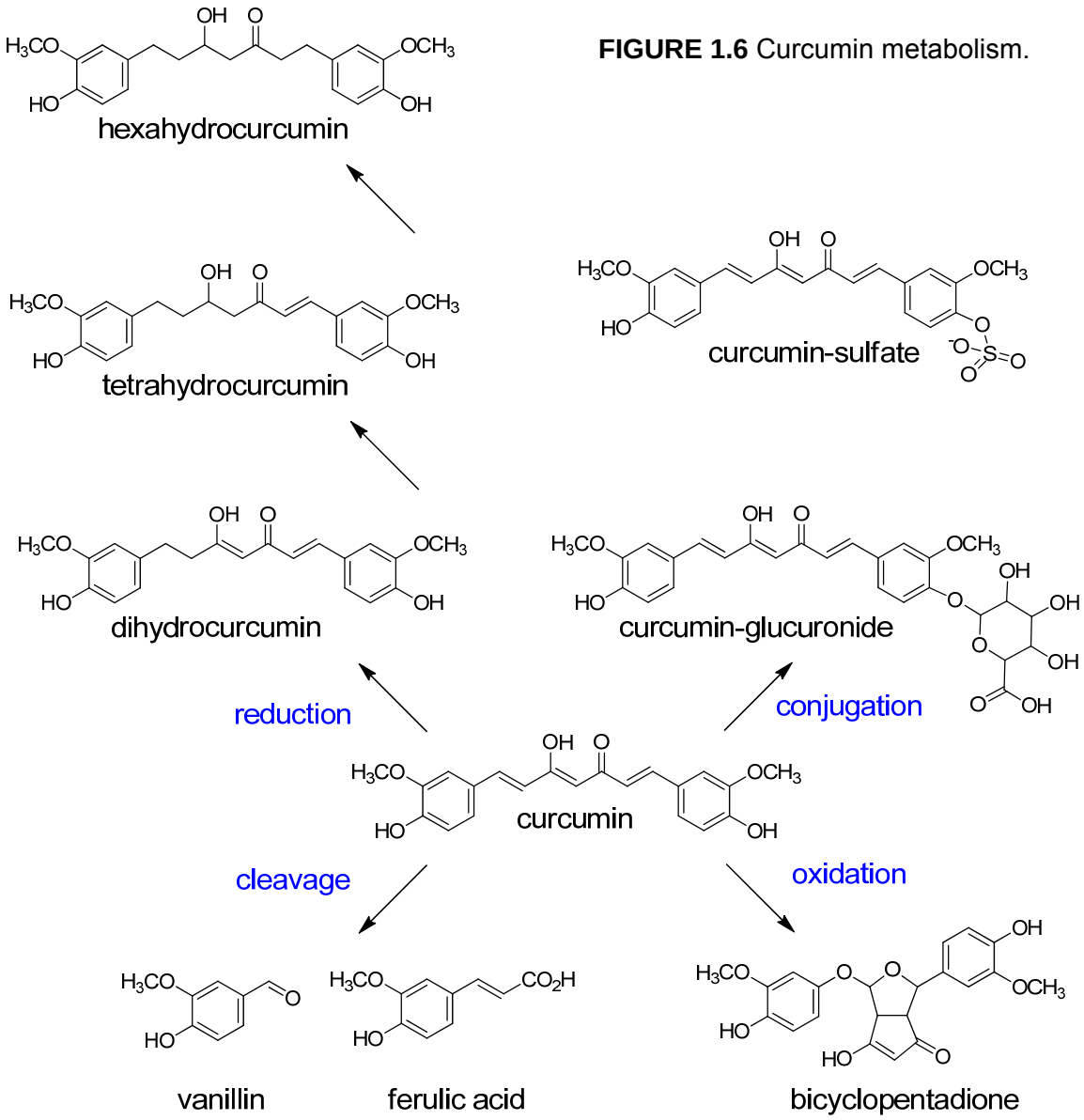

FIGURE 1.6 Curcumin metabolism.

.Wang et al. identified vanillin, ferulic acid and feruloyl methane (**Figure 1.6**) as minor products of this degradation with the major product tentatively identified as trans-6-(4'-hydroxy-3'-methoxyphenyl)-2,4-dioxo-5-hexenal. The identification of vanillin, ferulic acid and feruloyl methane was based on retention time comparisons with authentic standards. Due to limited sample availability, the major product was only tentatively identified based on LC–ESI–MS. Its structure

was inferred based on a molecular weight (MW) of 248, even though the MS spectrum showed several more prominent ions at higher *m*/*z* values (Wang et al. 1997).

Recent studies in our laboratory showed that transformation of curcumin in alkaline buffer is an autoxidation, and identified the major reaction products as a dioxygenated bicyclopentadione and its two less abundant configurational isomers. The chain cleavage products vanillin, ferulic acid and feruloyl methane, were not detected in these analyses. (Griesser et al. 2011; Gordon and Schneider 2012). We proposed a mechanism for autoxidation of curcumin initiated by hydrogen abstraction from one of the phenolic hydroxyls to form a phenoxyl radical that rearranges to a reactive quinone methide and carbon centered radical. The radical mediates intramolecular cyclization of C2 to C6 to give the cyclopentadione ring, and the incorporation of molecular oxygen (O_2) into the to form the final bicyclopentadione product. This reaction mechanism is discussed in detail in chapter 2.

Curcumin also exhibits poor stability towards irradiation with ultraviolet and visible light. Curcumin absorbs strongly in the visible wavelength range (λmax 430 nm) making it susceptible to photo-degradation. In ethanol-extracted curcumin in the crystalline state, exposure to sunlight over 5 days yielded chain cleavage products vanillin (34%), ferulic aldehyde (0.5%), ferulic acid (0.5%) and vanillic acid (0.5%) and other unidentified products. The similar analysis using methanol-extracted curcumin yielded the same products, but in different abundances: vanillin (2%), ferulic aldehyde (0.2%), ferulic acid (0.1%) and

vanillic acid (1.5%), suggesting that the crystalline form of curcumin used affects the rate of degradation (Khurana and Ho 1988). Under UV (254 nm) irradiation in aqueous buffer, 50% of the curcumin chromophore detected at 405 nm disappear over 8 h, compared to 36% over 24 h when stored in a dark place. The rate of UV induced degradation was also higher with increasing pH, with 70% degradation seen in 2 h at pH 8 (Lee et al. 2013).

The low bioavailability of curcumin, coupled by its chemical instability, has led to the notion that metabolites are mediators of some of its effects. To date, there is little evidence to support a role for the aforementioned chain cleavage, reduced or conjugated metabolites. Our recent discovery that curcumin undergoes oxidative transformation to generate the bicyclopentadione through reactive intermediates has refueled the hypothesis of metabolites as ultimate mediators of these effects. We hypothesize that the oxidative metabolism of curcumin contributes to its biological effects.

1.10 Reactive protein thiols as biological sensors.

The oxidative degradation of curcumin is proposed to progress through electrophilic quinone methide and epoxide intermediates to form the final bicyclopentadione product (Griesser et al. 2011). Many of the protein targets of curcumin are regulated by covalent adduction to electrophiles at reactive cysteine residues. Cysteine thiols are a major site of reactivity in proteins and show high reactivity towards electrophiles. Many drugs and environmental chemicals are metabolized to generate reactive electrophiles that modify proteins

and DNA (Dennehy et al. 2006). Cysteine thiols are considered soft electrophiles exhibiting the characteristic low electronegativity and high polarizability. Electrophiles preferentially react with nucleophiles of comparable 'hardness'. Thus, α,β-unsaturated carbonyls, quinones and epoxides, all soft electrophiles, show selectivity towards Michael reaction with cysteine thiols (Lopachin and Decaprio 2005). This reaction selectivity confers specificity to electrophiles in their targeting of cellular proteins for modification.

Protein targets of curcumin regulated by reactive cysteines include the transcription factor NF-κB (Pandey et al. 2007). NF-κB is an important target of curcumin and plays a prominent role in inflammation and cancer (Valacchi et al. 2004; S. Singh and Khar 2006). In the resting state, NF-κB lingers in the cystosol in complex with its inhibitor IκB . Activation of NF-κB ultimately depends on phosphorylation of its upstream regulator IκB kinase (IKK). When activated by phosphorylation, IKK in turn phosphorylates IκB to relieve its inhibition of NF-κB, which is then freed to enter to nucleus (Denk et al. 2001). Electrophilic adduction to cysteine 179 in IKK has been shown to prevent its activation leading to the inhibition of NF-κB (Pandey et al. 2007). Curcumin can interact with IKK to inhibit its phosphorylation and prevent the translocation of NF-κB to the nucleus (Cohen, Veena, Srivatsan, & Wang, 2009). While covalent adduction of curcumin to IKK has not been demonstrated, a similar natural phenolic compound, butein, was shown to directly modify IKK cysteine residue 179 to inhibit NF-kB (Pandey et al. 2007). The electrophilic lipid oxidation product acrolein also adducts to IKK at (unidentified) reactive cysteine residues to inhibit NF-κB (Valacchi et al.,

2004). Curcumin, and its more reactive quinone methide and epoxide metabolites in particular, could be acting via a similar mechanism.

Another example of a curcumin target regulated by reactive thiols is the Keap1 protein, which mediates the activation of the transcription factor Nrf2. Electrophlic modification of cysteine thiols in Keap1 leads to Nrf2 translocation to the nucleus and transcription of antioxidant defense genes. Other examples of proteins with reactive thiols are various PPAR phosphatases, peroxiredoxins, and thioredoxin (Dennehy et al. 2006).

Cysteine thiols are subjected to oxidation by ROS. Oxidized thiols form sulfenic (Cys-SOH), sulfinic (Cys-SO_2H), and sulfonic acids (Cys-SO_3H) depending on the degree of oxidation (Cooper et al. 2002; Reddie and Carroll 2008). The first oxidation product of Cys-SH is the sulfenic acid. Sulfenic acids are unstable, reversible, and easily oxidized to sulfinic and sulfonic acids. Sulfenic acids exhibit both nucleophile and electrophile properties, and exhibit different reactivity compared to thiols (Vaidya, Ingold, and Pratt 2009). Sulfenic acids exist only transiently and undergo further oxidation to the sulfinic acid, or react with another nucleophilic thiol to form a disulfide bond. The formation of the disulfide bond serves as a means of regenerating the native protein through the actions of glutaredoxin enzymes (Figure 1.7). Acting as an electrophile, sulfenic acids react selectively with a model β-diketone, 5,5-dimethyl-1,3-cyclohexanedione (dimedone) (Poole et al. 2005.). It is therefore likely that molecules that share this β-diketone, such the bicyclopentadione product of

curcumin oxidation, would also adduct to protein sulfenic acids to modulate protein signaling.

Sulfonic acid is the most highly oxidized and is irreversible. This non-enzymatic modification of proteins mediates apoptosis, cell migration, inflammation, and other cellular processes. The nature of the oxidation is controlled by the oxidative state of the cell, or the actions of reducing enzymes including families of peroxiredoxin (PRX) that either reduce or promote oxidation (Jeong et al. 2011; Wetzelberger et al. 2010).

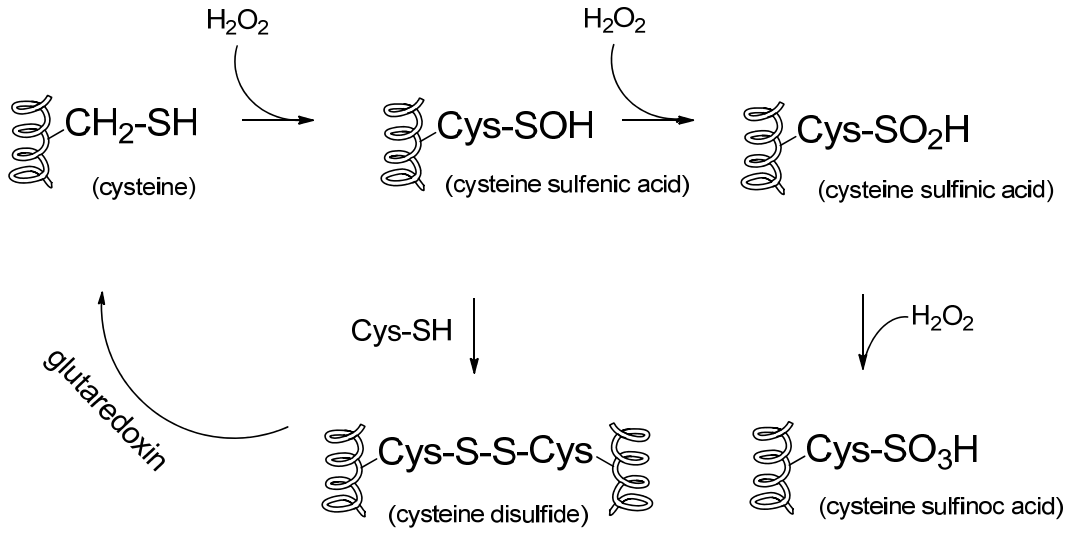

FIGURE 1.7 Redox cycling of sulfenic acids.

1.11 Glucuronidation reactions

Conjugation with glucuronic acid is the major route of phase-II metabolism of curcumin. Glucuronidation involves the direct condensation of a drug with the activated form of glucuronic acid, UDP–glucuronic acid (UDPGA). Conjugation

with the polar glucuronic acid moiety is an important and common means of eliminating drugs from the body (Ritter 2000). As a general rule, drugs are lipophilic, distribute readily into the tissues, and are not easily excreted from the body. The resulting drug-glucuronide conjugate is much more hydrophilic and is more readily excreted in the urine and bile. Furthermore, glucuronidation is generally a deactivation reaction generating less biologically and chemically active metabolites. A wide variety of chemicals are subjected to glucuronidation, with the common feature being the presence of an appropriate functional group (-NH, -OH, -SH or -COOH). Glucuronidation occurs in the liver, small intestine, and colon (Ritter 2000; Johnson and Mukhtar 2007).

The re-formation of the unconjugated form of the drug from the *O*-glucuronide conjugates is achieved through the action of β-glucuronidase enzymes located in lysosomes of most cell types and in gut microbes (Sperker et al. 2000; B Sperker, Backman, and Kroemer 1997). Glucuronide conjugates are often secreted through the bile into the intestine where they are hydrolyzed to reform the aglycone compound and then reabsorbed. This process, called enterohepatic circulation, serves to increase exposure to the parent drug. Re-absorption of the unhydrolyzed drug is otherwise very inefficient. Tissue specific hydrolysis of glucuronide conjugates has been described in cancers. In these tissues, there is increased β-glucuronidase activity, resulting in secretion of the enzyme into the extracellular space where hydrolysis of the glucuronide conjugates occurs. The highly hydroplilic glucuronides do not penetrate the cell and may not be otherwise subjected to the actions of the enzyme (Weyel et al.

2000). Furthermore, the action of β-glucuronidases in tumors can selectively activate glucuronide 'prodrugs' into the active aglycone specifically at the tumor site, thereby reducing systemic exposure to the compound.

1.2. Specific Aims

My research project is based on the discovery in our lab that curcumin undergoes a previously unrecognized oxidative transformation to generate a novel bicyclopentadione derivative of curcumin as the major product. Initial studies into the mechanism of transformation suggest a reaction via reactive quinone methide and epoxide intermediates to form the final bicyclopentadione products. However, studies on the reaction mechanism were incomplete, and other products of the transformation remained to be identified.

Our finding that curcumin undergoes oxidative metabolism *in vitro* to generate bioactive compounds could be a major step forward understanding how curcumin exerts its chemopreventive and therapeutic effects. Furthermore, oxidative metabolites of curcumin could represent new lead compounds with improved efficacy to overcome the many therapeutic limitations of curcumin.

The specific aims of the project were as follows:

Specific Aims:

a) To identify the products of curcumin oxidative transformation.

b) To determine the mechanism of formation of curcumin oxidative products.

c) To assess the oxidative transformation of curcumin-glucuronide

Chapter 2

MECHANISTIC STUDIES INTO THE OXIDATIVE TRANSFORMATION OF CURCUMIN

2.1 Introduction

Curcumin is a naturally occurring chemopreventive agent isolated from the rhizome of the *Curcuma longa* plant. Curcumin possesses anti-inflammatory, anti-oxidant, and anti-cancer properties *in vitro* and in animal models by modulating up to 100 cellular targets, but its chemical mechanisms of action are still unclear (Goel, Kunnumakkara, and Aggarwal 2008). Curcumin exhibits very low bioavailability resulting from poor absorption and extensive metabolism that renders it undetectable in most tissues after oral dosage (Vareed et al. 2008; Metzler et al. 2013; Pan, Huang, and Lin 1999). Curcumin undergoes metabolic glucuronidation and sulfation, as well as reduction of its dienone double bonds (Ireson et al. 2001). *In vitro*, curcumin undergoes spontaneous degradation at physiological pH (Wang et al. 1997). Attempts at identifying the products of the pH dependent transformation of curcumin have proved elusive, with only minor products vanillin, ferulic acid, and feruloyl methane identified. The major product was recently identified as a dioxygenated bicyclopentadione by our group (Griesser et al. 2011).

The low bioavailability of curcumin has been credited for the lack of therapeutic efficacy in past clinical trials. Thus, overcoming the low bioavailability

of curcumin has been explored as a route towards improving its clinical efficacy (Pawar et al. 2012). Recent research in the field has led to significant improvements in the bioavailability of curcumin, mainly through developing complex formulations involving encapsulation by phospholipid or nanoparticles. However, only marginal effects on clinical efficacy have been reported so far with these novel formulations (Belcaro et al. 2010; Marczylo et al. 2007).

As an alternative to the 'bioavailability' approach, we have pursued research aimed at understanding the chemical basis for the pleiotropic effects of curcumin. Questions about the chemical bases for the effects of curcumin are pertinent given its virtual absence from organs, such as the brain, where efficacy have been demonstrated (Aoki et al. 2007). Moreover, curcumin mediates its effects by targeting up to 100 different cellular targets, a remarkable achievement for any one molecule. With these discrepancies it became hard to attribute all the biological effects to the parent curcumin and metabolites are implicated as ultimate mediators of some of these effect (Shen and Ji 2009; Shen and Ji 2012). There is little evidence to support major roles for the known metabolites (conjugation, reduction, or chain cleavage products) in the biological activities of curcumin.

Our discovery that curcumin undergoes oxidative transformation to generate novel products has refueled the hypothesis of metabolites as ultimate mediators of curcumin's effects. Consistent with the earlier studies on curcumin reaction in buffer, we found that curcumin degrades rapidly at pH 7.5 (Wang et al. 1997; Griesser et al. 2011). Contrary to earlier reports, however, we found

that the major reaction is an autoxidation to generate a dioxygenated bicyclopentadione as the final product (Figure 2.1), with the chain cleavage to form vanillin a minor reaction.

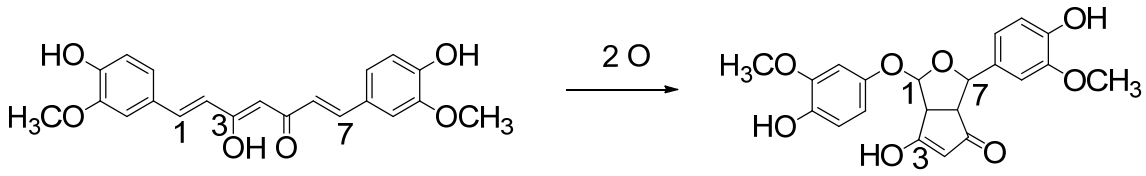

Figure 2.1 Autoxidation of curcumin generates a dioxygenated bicyclopentadione as the major product.

Spectrophotometric analysis of curcumin autoxidation showed the disappearance of its 430 nm chromophore, suggesting disruption of the conjugated system along the heptadienone linker. A new chromophore at 263 nm is formed concomitantly with the disappearance of curcumin (Wang et al. 1997; Griesser et al. 2011). None of the isolated products of curcumin autoxidation showed a 263 nm chromophore, suggesting the existence of other yet unidentified products. HPLC-UV and LC-ESI-MS showed one major peak for the bicyclopentadione and two minor peaks identified as its configurational isomers. The molecular weight (MW) of 400 supports the incorporation of two oxygen atoms (MW 32) during degradation of curcumin (MW 368). The bicyclopentadione structure was ultimately confirmed after 1D and 2D NMR analyses. The bicyclopentadione is the same compound tentatively identified by Wang et al as trans-6-(4'-hydroxy-3'-methoxyphenyl)-2,4-dioxo-5-hexenal, since

both compounds shared identical MS^2 spectra (Wang et al. 1997; Griesser et al. 2011).

Prompted by the structural elucidation of the bicyclopentadione product, analyses into the incorporation of oxygen into the molecule were performed in an oxygen electrode. The data showed the consumption of molecular oxygen at a rate equivalent to the degradation of curcumin, suggesting the incorporation of molecular oxygen (O_2) into the molecule during the reaction. It was further determined that COX-2 catalyzes the same transformation of curcumin at its peroxidase active site (Griesser et al. 2011). Studies conducted by other groups on the interaction of COX-1 peroxidase with other natural phenols, e.g. resveratrol, indicate that phenolic hydroxyls serve as an electron source during catalysis by peroxidases and are thereby oxidized to a phenoxyl radical (Szewczuk et al. 2005). Thus, catalysis by peroxidases, as well as the alkaline-pH dependence of the autoxidative transformation, led to a proposed mechanism of curcumin transformation initiated by H-abstraction from one of its phenolic hydroxyls to form a phenoxyl radical. Curcumin is completely conjugated therefore the phenoxyl radical is delocalized and migrates into the heptadieneone chain at C2, forming a quinone methide in the process. The cyclopentadione ring of the bicyclopentadione is formed from the radical at C2 undergoing 5-exo cyclization onto C6. The newly formed radical at C6 mediates the incorporation of molecular oxygen O_2 into the molecule that progresses to form the bicyclocpentadione. LC-MS analysis of the bicyclopentadione formed in $H_2{}^{18}O$

suggest that only one of the oxygen incorporated from O_2 is retained in the molecule, and the other replaced with oxygen from H_2O (Griesser et al. 2011).

The main aims of my project are to determine the complete profile of products formed during curcumin autoxidative transformation, and to elucidate their mechanism of formation. I used radiolabeled [$^{14}C_2$]curcumin in autoxidation studies to isolate and structurally identify four intermediates and six novel products formed from curcumin oxidative transformation. Our studies allowed us to refine and expand what was known from the previously proposed reaction mechanism.

2.2 Materials and Methods

2.2.1 Materials

Curcumin was synthesized as previously described (Pabon 1964). A 5 mM stock solution of curcumin in ethanol was prepared on the day of the experiments. Oxygen-18 labeled water (97 atom-% ^{18}O) was obtained from Isotec. Oxygen-$^{18}O_2$ (99 atom-% ^{18}O) and deuterium oxide (D, 97%) were from Sigma. [^{14}C]Methyl iodide (2 mCi/mmol) was from American Radiolabeled Chemicals, Inc., St. Louis, MO. [d_3]Methyl iodide (99.5%) acetylvanillin, 3,4-dihydroxybenzaldehyde, 3,4,dimethyl-benzaldehyde and all other reagents were from Sigma. Chelex-100 resin was from Bio-Rad, Hercules, CA.

2.2.2 Synthesis of isotopic analogs of vanillin and curcumin

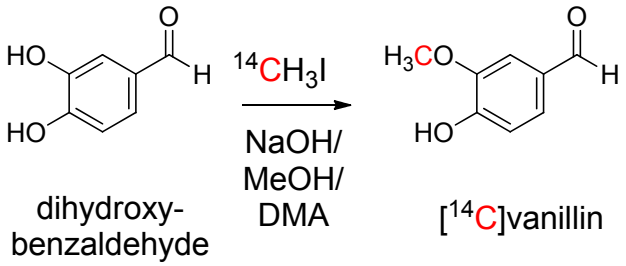

FIGURE 2.2 Synthesis of [^{14}C]vanillin

[^{14}C]Vanillin

3,4-Dihydroxybenzaldehyde (15 mg, 0.1 mmol) was dissolved in 4 M methanolic NaOH (50 µl) and diluted with dimethylacetamide (200 µl). [^{14}C]Methyl iodide (7 mg, 0.05 mmol, 2 mCi/mmol) in toluene (100 µl) was added dropwise to the solution. The reaction was stirred for 2 h, acidified with 1 M HCl, and extracted three times with 500 µl dichloromethane (Figure 2.2). The solvent was evaporated, and the product was isolated using RP-HPLC (Method A) to yield 3.5 mg [^{14}C]vanillin (52 µCi, 52% radiochemical yield; purity 98% by HPLC). The identity of [^{14}C]vanillin was confirmed by comparison of its RP-HPLC retention time and UV spectra with an authentic standard. LC-MS analysis was not performed in order to avoid contamination of the instrument with radioactive material.

[$^{14}C_2$]Curcumin

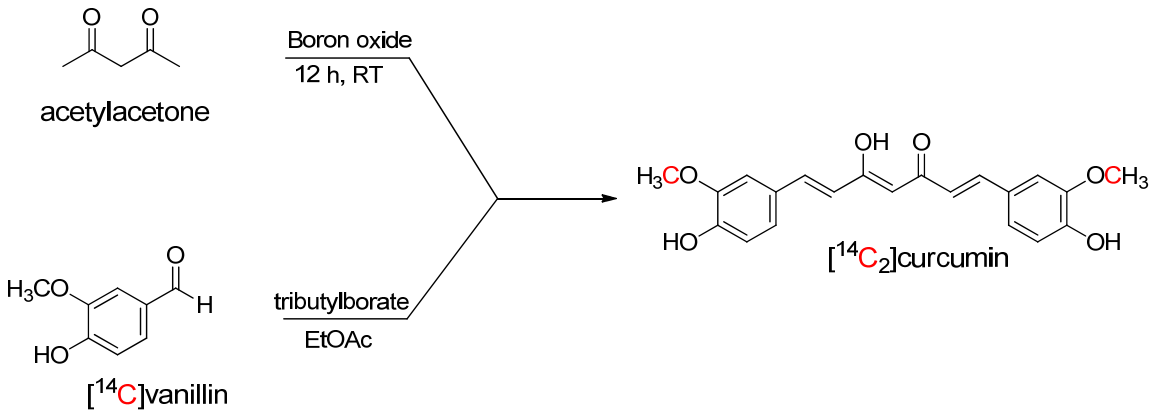

FIGURE 2.3 Synthesis of [$^{14}C_2$]curcumin.

Boron oxide (20 mg, 0.3 mmol) and acetylacetone (40 µl, 0.4 mmol) were stirred for 16 h to form a white paste. An aliquot (20 µl) of the paste dissolved in ethyl acetate (360 µl) was added to 3.5 mg [^{14}C]vanillin (0.03 mmol, 52 µCi) dissolved in tributyl-borate (21 µl). The mixture was stirred for 5 min after which a 10% dilution of butylamine in ethyl acetate (2 µl) was added every 10 min for 40 min. The reaction was stirred for 16 h overnight. The next day, 0.4 M HCl (100 µl; heated to 60 ºC) was added to the reaction and stirred for 1 h (Figure 2.3). [$^{14}C_2$]Curcumin was extracted into ethyl acetate (4 × 200 µl) and purified using RP-HPLC (Method A) to yield 1.2 mg purified [$^{14}C_2$]curcumin (13 µCi; 4 mCi/mmol; 25% radiochemical yield; purity 97% by HPLC).^{1}H NMR (CD_3OD, 600 MHz): δ = 3.91 (s, 6H), 5.97 (s, 1H), 6.64 (d, 2H, J = 15.0 Hz), 6.82 (d, 2H, J = 7.9 Hz), 7.1 (d, 2H, J = 7.5 Hz), 7.22 (s, 2H), 7.57 (d, 2H, J = 15.0 Hz) ppm.

[d_3]Vanillin

[d_3]Vanillin was prepared as described for [^{14}C]vanillin starting from 3,4-dihydroxybenzaldehyde (50 mg, 0.35 mmol) and [d_3]methyl iodide (50 mg, 0.35 mmol) in toluene (100 µl). The product was isolated using RP-HPLC (Method B) to yield [d_3]vanillin (26 mg; 47% yield; purity 91% by HPLC). LC-MS: 154.1 ([M − H]$^-$). ^{1}H NMR (CD_3OD, 600 MHz): δ = 5.28 (s, 1H), 6.77 (d, 1H, *J* = 8.1 Hz) , 6.86 (dd, 1H, *J* = 8.1; 1.8 Hz) , 6.98 (d, 1H, *J* = 1.8 Hz), 9.75 (s, 1H) ppm.

3'-OCD_3,4"-O-methylcurcumin

3'-OCD_3,4"-O-methylcurcumin (Figure 2.4) was from a 1:1 reaction [d_3]vanillin and 3,4-dimethoxybenzaldehyde. Boron oxide (20 mg, 0.3 mmol) and acetylacetone (40 µl, 0.4 mmol) were stirred for 16 h to form a white paste. This is added to 1:1 mixture of [d_3]vanillin and 3,4-dimethoxybenzaldehyde (20mg, 0.9 mmol each) dissolved in tributyl-borate (200 µl) and ethyl-acetate (300 µl). The mixture was stirred for 5 min after which 1 µl of butylamine was added every 10 min for 40 min. The reaction was stirred for 16 h overnight. The next day, 0.4 M HCl (500 µl; heated to 60 ºC) was added to the reaction and stirred for 1 h. 3'-OCD_3,4"-O-methylcurcumin was extracted into ethyl acetate (4 × 200 µl) and purified using RP-HPLC (Method A) LC-MS: 416 ([M − H]$^-$).

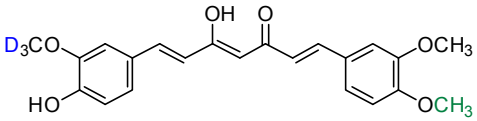

3'-OCD_3,4"-O-methylcurcumin

FIGURE 2.4 Structure of 3'-OCD_3,4"-O-methylcurcumin

[$^{13}C_5$]Curcumin

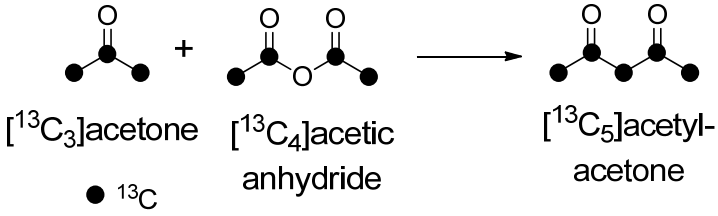

FIGURE 2.5 Synthesis of [$^{13}C_5$]acetylacetone

[$^{13}C_3$]Acetone (120 µl, 2 mmol) and [$^{13}C_4$]acetic anhydride (500 µl, 5 mmol) were placed in a 1-ml reaction vial and cooled in an ice-salt bath. Boron trifluoride diethyl etherate (400 µl, 3 mmol) was added slowly over the course of 3 min. The reaction was stirred for 4 h and then poured into 3 ml of 10 M sodium acetate heated to 80 ºC. The reaction was extracted twice using 500 µl dichloromethane to yield 12 mg (0.1 mmol; 5% yield) [$^{13}C_5$]acetylacetone (Figure 2.5). [$^{13}C_5$]Curcumin was prepared as described for [$^{14}C_2$]curcumin starting from boron oxide (47 mg, 0.7 mmol) and [$^{13}C_5$]acetylacetone (12 mg) dissolved in dichloromethane (100 µl). Vanillin (250 mg), tributylborate (800 µl) in 800 µl ethyl acetate, and butylamine (5 µl) were added. The products were loaded onto a 2-g Supelco DSC-18 cartridge in 30% acetonitrile and eluted using 100% acetonitrile. [$^{13}C_5$]curcumin was purified using RP-HPLC (Method A; 51% yield; purity 92% by HPLC). LC-MS: 372.2 ($[M-H]^-$).^{1}H NMR (CD_3OD, 600 MHz): δ = 3.91 (s, 6H), 5.97 (s, 1H), 6.64 (d, 2H, J = 15.7 Hz), 6.82 (d, 2H, J = 8.1 Hz), 7.1 (dd, 2H, J = 8.3; 1.8 Hz), 7.21 (d, 2H, J = 1.7 Hz), 7.58 (d, 2H, J = 15.7 Hz) ppm.

2.2.3 Analytical procedures for synthesized compounds

RP-HPLC

Products were analyzed and purified by RP-HPLC using an Agilent 1200 series diode array system equipped with a Waters Symmetry C18 5-μm column (4.6 × 250 mm). The column was eluted with a linear gradient of MeCN/H_2O/HOAc 20/80/0.01 to 80/20/0.01 (by vol.) over 20 min and a flow rate of 1 ml/min (Method A). Semi-preparative RP-HPLC using a Waters Symmetry C18 column (300 × 19 mm) was eluted with a solvent of MeOH/H_2O/HOAc (40/60/0.01, by vol.; Method B) or MeCN/H_2O/HOAc (55/45/0.01, by vol; Method C) or MeOH/H_2O/HOAc (75/25/0.01, by vol.; Method D) at a flow rate of 10 ml/min.

LC-MS

LC-MS was performed using a Thermo LTQ ion trap instrument equipped with an electrospray ionization interface. The instrument was operated in the negative ion mode, and mass spectra were acquired at a rate of 2 s/scan. The settings for the heated capillary (300 °C), spray voltage (4.0 kV), spray current (0.22 μA), auxiliary (37 mTorr), and sheath gas (16 mTorr) were optimized using direct infusion of a solution of curcumin (20 ng/μl) in MeCN/H_2O 95/5, by volume, containing 10 mM NH_4OAc. Samples were introduced using a Waters Symmetry Shield C18 3.5-μm column (2.1 × 100 mm) eluted with a gradient of MeCN/H_2O (5/95, by volume, containing 10 mM NH_4OAc) to MeCN/H_2O (95/5, by volume,

containing 10 mM NH_4OAc) over 10 min followed by 3 min of isocratic elution and re-equilibration in the starting solvent (Method E).

NMR

NMR spectra were recorded using a Bruker AV-II 600 MHz spectrometer equipped with a TCI cryoprobe. Chemical shifts are reported in ppm relative to the non-deuterated solvent peak of methanol-d_4 ($\delta = 3.34$ ppm).

2.2.4 Oxidation of curcumin *in vitro*

Curcumin autoxidation

Curcumin was diluted to a concentration of 50 µm in 50 mM $NaPO_4$ buffer pH 7.5 for 20 minutes (or as indicated). For extraction, the sample was loaded onto a preconditioned 30 mg Waters HLB cartridge. After washing with water the cartridge was eluted with 2x 500 µl MeOH. The solvent was evaporated under a stream of nitrogen and the residue dissolved in acetonitrile for RP-HPLC analysis. For product identification, 20x 50 ml reactions were conducted in parallel. Extraction was performed as described above. For autoxidation of [$^{14}C_2$]curcumin, 250k cpm was added to 500 µl buffer (30 uM curcumin). 250 µl of the crude reaction were injected at 30 minutes and 2 hrs.

Reaction progress

Products **6a** and **6b** were isolated from 2 ml curcumin autoxidation reactions at 20 min. The products were dissolved in 10 mM NH_4OAc buffer pH 7.4 and an aliquot analyzed using LC-MS at 15 or 45 min intervals over 6 hrs.

Preparation of ^{18}O labeled metabolites

Autoxidative transformation of curcumin was conducted using 100 µl of buffer. 5 µl of a 1 M stock solution of NH_4OAc buffer pH 8 was diluted with 95 µl of $H_2{}^{18}O$ (97 atom-% ^{18}O). Curcumin, 2 µl from a 5 mM stock solution in ethanol, was added, and the reaction was allowed to proceed for 30 min. A reaction using unlabeled H_2O was conducted in parallel.

For NMR analysis, the autoxidative reaction was scaled up to 100 ml in 10 mM NH_4OAc buffer pH 8. After 20 min, the reaction is loaded onto a 2 mg HLB cartridge and eluted with MeOH. The MeOH solution is evaporated under a stream of nitrogen and re-dissolved in 500 µl $H_2{}^{18}O$ after 6 h, the reaction is acidified and before RP-HPLC purification of the bicyclopentadiones.

Preparation of deuterium-labeled metabolites

For LC-MS analysis, autoxidative transformation of curcumin was conducted using 100 µl of buffer. 5 µl of a 1 m stock solution of NH_4OAc buffer pH 8 was diluted with 95 µl of D_2O (D, 97%). Curcumin, 2 µl from a 5 mM stock solution in ethanol was added and the reaction was allowed to proceed for 30 min. A reaction using unlabeled H_2O was performed in parallel.

For NMR analysis, the autoxidative reaction was scaled up to 100 ml in ammonium acetate buffer pH 8. After 20 minutes (when the spiroepoxides **7** are the abundant products) the reaction is loaded onto a 2 mg HLB cartridge and eluted with MeOH. The MeOH solution was evaporated under a stream of nitrogen and re-dissolved in 500 μl D_2O at room temperature. After 6 h, the reaction is acidified before RP-HPLC purification of the bicyclopentadiones.

Synthesis of diguaiacol standard

Guaiacol (2 mg, 0.02 mmol) was dissolved to a final concentration of 16 mM in 1 ml of a 10 mM pyrophosphate buffer containing H_2O_2 (0.35 mM), GSH (1.6 mg, 5mM) and manganase acetate (0.04 mg, 1mM). The reaction was allowed to proceed at room temperature for 12 h before extraction on a preconditioned 50 mg Waters HLB cartridge eluted with MeOH. The sample was analyzed on RP-HPLC using a Waters Symmetry C18 5-μm column (4.6 × 250 mm) eluted with a gradient of 20% MeCN to 80% MeCN in 0.01% aqueous acetic acid over 20 min and the diguaiacol product, eluting at retention time 12 min, isolated for LC-MS analysis. LC-MS: 245 ($[M-H]^-$).

2.2.5 Analytical procedures

HPLC Analysis

The transformation reactions were analyzed using a Waters Symmetry C18 5-μm column (4.6 × 250 mm) eluted with a gradient of 20% MeCN to 80% MeCN in 0.01% aqueous acetic acid over 20 min followed by 10 min of isocratic elution. To isolate individual metabolites, 2% or 10% MeCN in $NH_4C_2H_3O_2$ pH 7.5 buffer mobile phase is used. All samples run at flow rate of 1 ml/min. Elution of the products was monitored using an Agilent 1200 diode array detector.

LC-MS Analysis

For LC-MS analyses a Finnigan TSQ Quantum triple quadrupole MS instrument equipped with an electrospray interface was used. The instrument was operated in the negative ion mode, and mass spectra were acquired at a rate of 2 s/scan. The heated capillary was set at 300 °C, and the spray voltage was set at 4.4 kV. For LC-MS analysis of oxygen incorporation from 18O-buffer (MSn analyses), a Thermo Finnigan LTQ ion trap instrument was used. The settings for the heated capillary (300 °C), spray voltage (4.0 kV), spray current (0.22 μA), auxiliary (37 mTorr) and sheath gas (16 mTorr) were optimized using direct infusion of a solution of curcumin (20 ng/μl) in MeCN /H_2O 95/5, by vol., containing 10 mm NH_4OAc. Samples were introduced into both instruments using a Waters Symmetry Shield C18 3.5-μm column (2.1 × 100 mm) eluted with acetonitrile/water (3/97, by vol., containing 10 mm NH_4OAc) isocratic over 20 min.

NMR

Samples were dissolved in 150 µl of methanol-d_4 in a 3 mm tube, and the NMR spectra were recorded using a Bruker DRX 600 MHz spectrometer equipped with a cryoprobe. Chemical shifts are reported in ppm relative to residual non-deuterated solven peakt (δ 3.30 for methanol-d_4). The pulse frequencies for the H,H-COSY, HSQC, and HMBC experiments were taken from the Bruker library. The spectra were acquired at 284 K.

2.3 Results

2.3.1 Spectrophotometric analysis of curcumin oxidation

Spectrophotometric analysis of curcumin autoxidation in phosphate buffer (10 mM, pH 7.4) shows the fast disappearance of the curcumin chromophore at λmax 430 nm within 10 min, giving rise to product(s) with prominent absorbance at 263 nm (Figure 2.6A). The 263 nm chromophore is formed concomitantly with the disappearance of curcumin and then decreased slowly over the next 45 min (Figure 2.6B). Further studies showed that the 263 nm chromophore will disappear slowly over 2 h with about 50% of that chromophore persisting over time, suggesting the presence of both stable and intermediate species (data not shown).

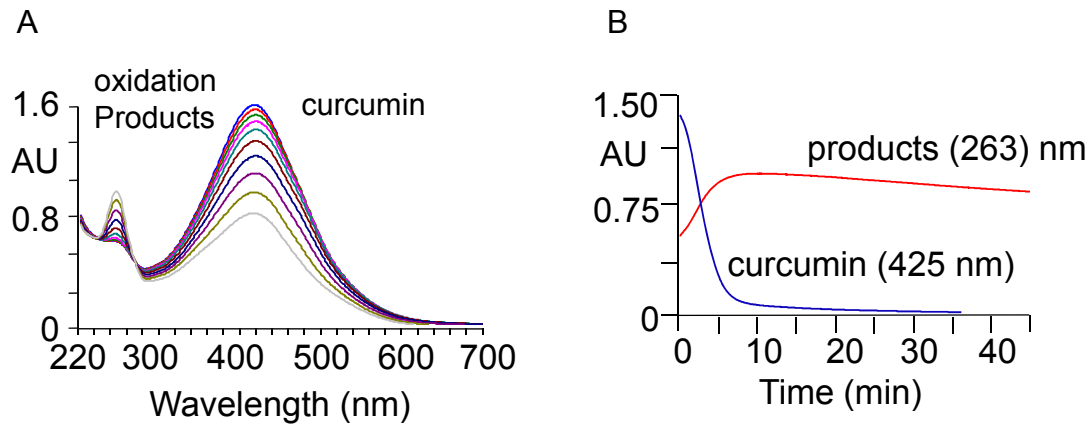

FIGURE 2.6: UV/VIS analysis of curcumin autoxidation. (**A**) The reaction is scanned from 700-220 at t=0 min and t=10 min. (**B):** Time drive analysis of curcumin autoxidation, monitoring 430 nm (curcumin) and 263 nm (oxidized curcumin) over 45 min.

2.3.2 RP-HPLC analysis of curcumin oxidation

The dioxygenated bicyclopentadiones were previously identified as products of curcumin autoxidation. (Griesser et al. 2011). Spectrophotometric and HPLC analyses of the reaction suggest the formation of additional reaction products bearing prominent 263 nm absorbance. Furthermore, the complex structure of the bicyclopentadione suggests the involvement of multiple reaction intermediates during its formation. In this study, I set out to determine a complete profile of products formed from curcumin autoxidation. To this end, I synthesized [$^{14}C_2$]curcumin in which the radiolabel is inserted into the inert methoxy groups, and used it as a tracer in RP-HPLC analysis.

An autoxidation reaction of [$^{14}C_2$]curcumin was analyzed on RP-HPLC with diode array and in-line radioactivity detection at 45 min, without extraction. The radio-chromatogram, presented in Figure 2.7, shows unreacted curcumin eluting at 26 min, and the main bicyclopentadione product **8a** and its isomers **8b,**

c eluting at 17 and 18 min respectively, substantiating our previous publication designating the bicyclopentadione as major product of this reaction (Griesser et al. 2011). The chromatogram further shows a series of more polar peaks **1-7** and **9** that were not previously identified. The most polar of the products (**1**-**4**) were collected as a group and further resolved into 5 distinct peaks (Figure 2.6B). Peak **7** represents diastereomeric isomers **(7a, b)** that were not resolved on this system.

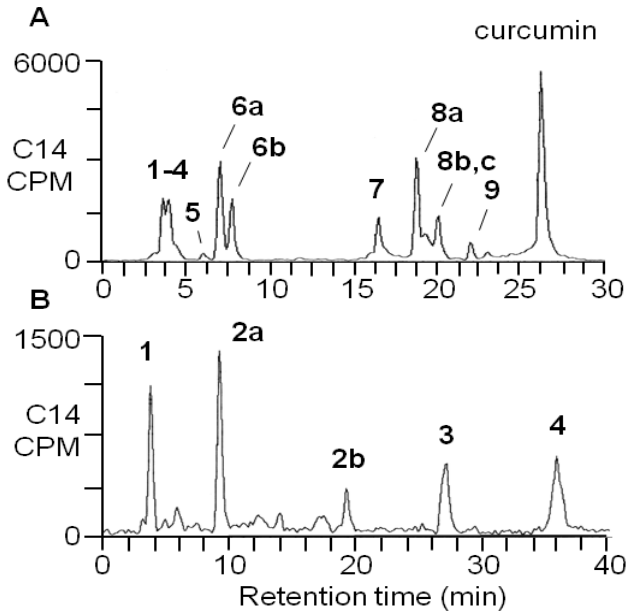

FIGURE 2.7 (**A**): Separation of [$^{14}C_2$]curcumin autoxidation products by RP-HPLC. The [$^{14}C_2$]curcumin stock solution (3 mM in ethanol) was diluted to a final concentration of 5 µM in 300 µl Pi buffer. After 50 min incubation at room temperature, a 100 µl aliquot was injected on HPLC and eluted with a 10% MeCN in NH_4OAc pH 7.5 isocratic for 10 min, followed by linear gradient to 80% MeCN over 20 min. The effluent was monitored by radio-detection. (**B**) The group of peaks **1**-**4** was re-injected on 2% MeCN for further separation.

There are several factors that made isolation of these metabolites unsuccessful until now. The unusual polarity of the metabolites made extraction from aqueous buffer difficult and hinders their detection by HPLC due to very

early elution times. Also, compounds **6** and **7** are acid labile and do not survive acidification during typical workup and HPLC analysis.

2.3.2 Identification of curcumin oxidation products

To obtain a sufficient quantity of the compounds for NMR analysis, large scale curcumin autoxidation reactions were performed and each novel product (**2**-**7** and **9)** isolated for further structural analysis using LC/ESI/MS, ESI/HR/MS (summarized in Table 2 of the Appendix) and a combination of ^{1}H, COSY, HSQC and HMBC and NOESY NMR analyses (summarized in Table B1-8 of the Appendix). Peak **1** contained multiple putative cleavage products (based on LC-MS analysis) that were not sufficiently abundant for complete structural characterization by NMR.

The structures of **2** - **9** are presented in Figure 2.8. All the novel products have the characteristic cyclopentadione ring formed of C2 to C6 found in the bicyclopentadione product **8** and incorporate oxygen atoms at C1 and C7. The exceptions are **5** that does not incorporate oxygen but instead has a carbon-carbon bond between C1 and C7, and **9** that is diguaiacol.

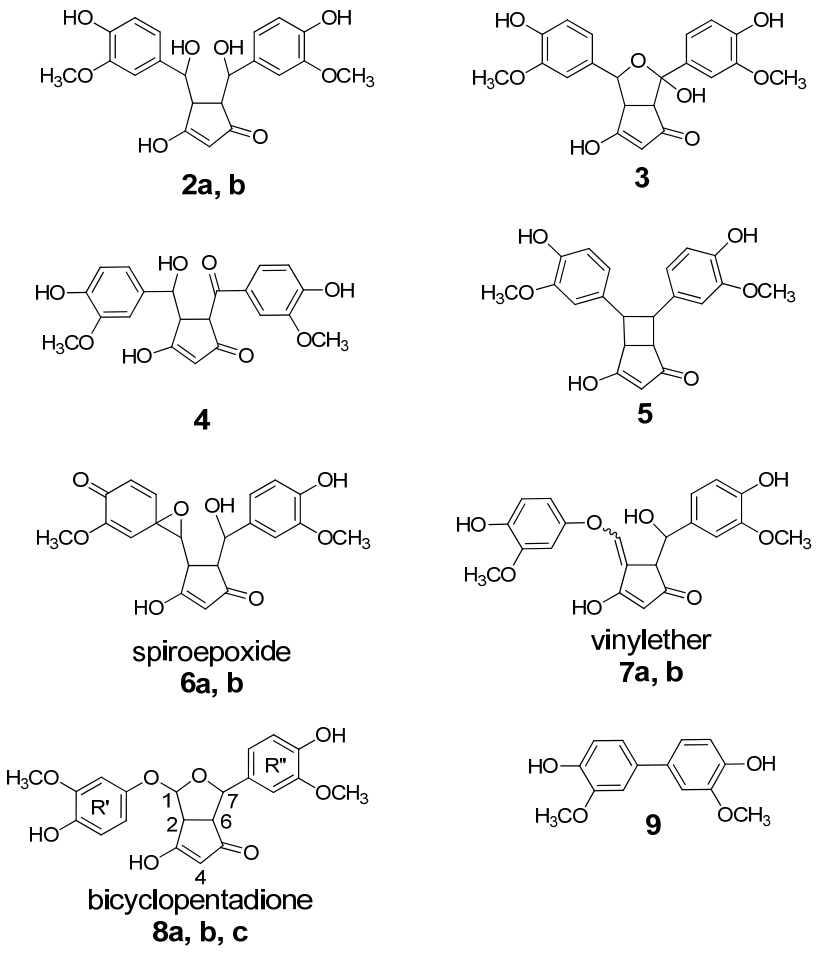

FIGURE 2.8 Products of curcumin autoxidative transformation.

Product **2a**, asymmetrical dihydroxy-cyclopentadione

Product **2a** is highly polar dihydroxy-cyclopentadione derivative, and is the asymmetrical analog of **2b**. It was eluted at 9 min (Figure 2.7).

ESI/HR/MS analysis in negative mode of **2a** showed *m/z* 401.1249. **2a** is nominally a 2H reduction product of **3**. MS^2 analysis (product ions of *m/z* 401) yielded these major fragment ions: *m/z* 401 ($[M-H]^-$); 249 (base ion); and 151.

^1H NMR spectra showed 11 proton and 2 MeO peaks. Six of the protons, at 7.0 - 6.5 ppm belonged to the phenolic moiety, suggesting the rings are in the

phenolic form. The proton–proton cross-peaks observed in the COSY analysis supported our assignment of H1, H2, H6 and H7 as being part of the same spin system, and H4 as an isolated proton.

The HSQC signals between 144 and 146 ppm substantiated four sp2 quaternary carbons attached to oxygen atoms. H1 and H7 are both sp3 hybridized and connected to oxygen, with shifts of 73 ppm and 77 ppm respectively. Since H4 is a singlet at 3.84 ppm, we concluded that in the *β*-diketo moiety exists in a keto- enol form. HMBC crosspeaks between each MeO peak and C3' or C3" allowed for their assignment to the different aromatic rings. ^{1}H and ^{13}C NMR chemical shifts and characteristic couplings are summarized in Table B1.

Product **2b**, symmetrical dihydroxy-cyclopentadione

Product **2b** is a highly polar dihydroxy-cyclopentadione derivative, and is the symmetrical analog of **2a**. It was eluted at 19 min (Figure 2.7)

ESI/HR/MS analysis in negative mode of the metabolite 5 showed *m/z* 401.1261. MS^2 analysis of product **2b** (product ions of *m/z* 401) yielded these major fragment ions: *m/z* 401 ($[M-H]^-$), 249; and 151.

^{1}H NMR spectra showed 5 proton and 1 MeO peaks, representing half the symmetrical molecule. Three of the protons, at 7.0 - 6.50 ppm, belonged to the phenolic moieties. H1/H7 and H2/H6 are sp3 hybridized with shifts of 4.55 ppm and 2.64 ppm respectively. A proton peak for H4 was not seen presumably due to rapid exchange with deuterium.

The HSQC signals at 144 pmm and 147 ppm substantiated four sp2 quaternary carbons attached to oxygen atoms. The 72 ppm peak for C1/C7 and 51 ppm peak for C2/C6 supports our conclusion that they are all sp3 hybridized, with C1/C7 connected to any oxygen. ^{1}H and ^{13}C NMR chemical shifts and characteristic couplings are summarized in Table B2.

Product **3,** hemiketal cyclopentadione

Product **3** is a highly polar hemiketal-cyclopentadione derivative, and exists in equilibrium with its hydroxy-keto **4**. It was eluted at 28 min (Figure 2.6).

ESI/HR/MS analysis of **3** showed *m*/*z* 399.1084 representing an increase of 32 amu compared with that of curcumin. MS^2 analysis (product ions of *m/z* 399) yielded these major fragment ions: *m/z* 399 ($[M-H]^-$); 247 (base ion); 355; 313; and 151.

^{1}H NMR spectra showed 10 proton and 2 two MeO peaks. Six protons, at 7.0 - 6.2 ppm, occurred in the aromatic region of the spectra, suggesting the rings are in the phenolic form. The proton–proton cross-peaks observed in the COSY analysis supported the assignment of H1, H2 and H6 as being part of the same spin system, and H4 as an isolated proton. No proton was seen at C7.

The HSQC signals between 143 and 150 ppm substantiated four sp2 quaternary carbon atoms attached to oxygen atoms. C1 is connected to an oxygen, as suggested by its chemical shift of 70.0 ppm. On the basis of the 104.2 ppm chemical shift for C4, and the singlet peak for H4 (5.04 ppm), we concluded that in the *β*-diketo moiety exists keto-enol configuration. HMBC crosspeaks

between each MeO peak and C3' or C3" allowed for their assignment the different aromatic rings. No coupling into C3, C5 or C7 was observed and their chemical shifts were not determined ^{1}H and ^{13}C NMR chemical shifts and characteristic couplings are summarized in Table B3.

Product **4**, hydroxy-keto -cyclopentadione

Product **4** is a highly polar keto-hydroxy cyclopentadione derivative, and exists in equilibrium with its hemiketal **3**. It was eluted at 36 min (Figure 2.6).

ESI/HR/MS analysis of **4** in negative ion mode showed *m/z* 399.1099 representing an increase of 32 amu compared with that of curcumin. MS^2 analysis (product ions of *m/z* 399) yielded these major fragment ions: *m/z* 399 ($[M-H]^-$); 247 (base ion); 355; 313; and 151.

^{1}H NMR spectra showed 9 proton and 2 MeO peaks. Six protons, at 7.40 - 6.50 ppm, belonged to the phenolic moieties. The proton–proton cross-peaks observed in the COSY analysis supported the assignment of H1, H2 and H6 as being part of the same spin system, and H4 as an isolated proton. No proton was seen at C7.

The HSQC signals between 144 and 151 ppm substantiated four sp2 quaternary carbons attached to oxygen atoms. C1 is bonded to an hydroxyl group, with chemical shift of 69.6 ppm. The C2 to C6 bond was determined from their (J_2) coupling in the HMBC. No proton peak was observed for H4, presumably due to rapid exchange for deuterium in the NMR solvent. No coupling into C3, C5, C4 or C7 was observed and their chemical shifts were not

determined. ^{1}H and ^{13}C NMR chemical shifts and characteristic couplings are summarized in Table B4.

Product **5**, cyclobutane-cyclopentadione

Product **5**, a highly polar cyclobutane cyclopentadione eluting at 6 min (Figure 2.7), does not incorporate oxygen.

ESI/HR/MS analysis of **5** in negative ion mode showed accurate molecular ion peak at *m/z* 367.1195, matching that of curcumin. MS^2 analysis showed the existence of precursor ion ($[M-H]^-$) at *m/z* = 367, and major fragment ions at 217 (base ion), 271, and 173.

^{1}H NMR spectra showed 6 proton and 1 MeO peaks, representing half the symmetrical molecule. Three of the protons, at 6.60 - 6.40 ppm, belonged to the phenolic moiety and suggested an aromatic confirmation of both rings. H1/H7 and H2/H6 are sp3 hybridized with chemical shifts of 3.76 ppm and 3.34 ppm respectively. H4 is a singlet at 4.7 ppm. The proton–proton cross-peaks observed in the COSY analysis supported the assignment of H1/H7 and H2/6 as neighboring protons (*J*=3.18), and H4 as an isolated proton.

The HSQC signals at 144 ppm and 147 ppm correspond to the four sp2 quaternary carbons attached to oxygen atoms in the aromatic rings. The 46 ppm and 47 ppm shifts for C1/C7 and C2/C6, respectively, support our conclusion that they are all sp3 hybridized and are not connected to oxygen. On the basis of the 104.2 ppm chemical shift for C4, and the singlet peak for H4 (4.76 ppm), we

concluded that in the *β*-diketo moiety exists keto-enol configuration. ^{1}H and ^{13}C NMR chemical shifts and characteristic couplings are summarized in Table B5.

Products **6a** and **6b,** spiro-epoxide-cyclopentadiones

Products **6a** and **6b** are diastereomeric spiroepoxy cyclopentadiones eluting at 10 min (Figure 2.7).

ESI/HR/MS analysis in negative ion mode of products **6a** and **6b** showed *m/z* 399.1088 and 399.1086, respectively, representing an increase of 32 amu compared with that of curcumin. MS^2 analysis showed the existence of precursor ion ($[M-H]^-$) at *m/z* = 399 and major fragments at 259 (base ion), 355, and 315.

^{1}H NMR spectra of **6a** showed 11 proton and 2 two MeO peaks. Only 5 protons occurred in the aromatic region of the spectra, with H2' shifted upfield to 5.25 ppm indicating that the R' ring is no longer aromatic. The proton–proton cross-peaks observed in the COSY analysis supported the assignment of H1, H2, H6 and H7 as being part of the same spin system, with H4 an isolated proton. H7, at 5.20 ppm, is connected to a hydroxyl, with H1 (3.28 ppm) connected to the epoxide.

The HSQC data supported the assignment of the tertiary protons, while the HMBC data were used to unequivocally determine the assignment of the quaternary signals: The 60 ppm chemical shift for C1' supports the loss of aromaticity in the R' ring. Both C1 and C7 are sp3 hybridized and connected to oxygen, with chemical shifts of 70 and 71 pmm, respectively. The C2 to C6 bond

was determined from HMBC cross-peaks between C1 and C6, as well as cross-peaks between C2 and C7. On the basis of the 103.5 ppm chemical shift for C4, and the singlet peak for H4 (4.9 ppm), we concluded that in the *β*-diketo moiety exists keto-enol configuration. C3 and C5 have chemical shifts of 205 and 206 ppm, respectively. HMBC crosspeaks between each MeO peak and C3' or C3" allowed for their assignment the different rings.

The NMR data for **6a** closely match that of **6b**, with only minor variations in the chemical shifts. One noteworthy difference is the coupling constant (*J*) between H6 and H7, which is 2.7 Hz for **6a** and 7.6 Hz for **6b**.

^{1}H and ^{13}C NMR chemical shifts and characteristic couplings are summarized in Table B6 (**6a**) and Table B7 (**6b**).

Product **7a**, vinylether-cyclopentadione

Product **7a** was identified as a dioxygenated, vinyl-ether metabolite. Chromatographic separation was achieved using a RP-HPLC with pH 7.5 10 mM NH_4OAc buffer. It was eluted at 16 min (Figure 2.7). Products **7a** co-elutes with its diastereomer **7b,** which was not sufficiently stable for NMR analysis. Both compounds were identical with respect to HPLC retention time, MS, MS-MS, and UV analyses.

ESI/HR/MS analysis of **7a** in negative ion mode showed accurate molecular ion peak at *m/z* 399.1084, representing an increase of 32 amu compared with that of curcumin. Tandem MS studies showed the existence of

precursor ion ($[M-H]^-$) at *m/z* = 399 and intense fragments at 247 (base ion), 355, 313 and 151.

^{1}H NMR spectra showed 10 proton and 2 MeO peaks. Six of the protons, at 6.9 - 6.3 ppm, belong to the phenolic moiety and suggested an aromatic conformation of both rings. The most downfield shifted proton was H1′ at 7.15 ppm, and is connected to the C1=C2 double bond and an oxygen that forms the ether bond between C1 and C1'. The proton–proton cross-peaks observed in the COSY analysis supported the assignment of H6 and H7 as neighboring protons (*J* = 4.04 Hz), and H4 and H1 as isolated protons.

The HSQC supported the assignment of the tertiary protons, while the HMBC data was used to unequivocally determine the assignment of the quaternary signals; five signals in the HSQC between 145 and 150 ppm substantiated four sp2 quaternary carbon attached to oxygen atoms. C2 is a also a quaternary sp2 carbon, with chemical shift of 106 ppm. C7 is connected to oxygen, with chemical shift of 73.1 ppm. The C2 to C6 cyclization was determined from HMBC cross-peaks between C1 and C6, as well as cross-peaks between C2 and C7. On the basis of the 187.6 ppm and 210.1 ppm chemical shifts for the quaternary signals of C3 and C5, respectively, we concluded that the β-diketo moiety exists in a C5 keto, C3 enol conformation. Furthermore, C4 is a singlet at 109.4 ppm. HMBC crosspeaks between each MeO peaks and C3' or C3" allowed for their assignment to the different aromatic rings. ^{1}H and ^{13}C-NMR chemical shifts and characteristic couplings are summarized in Table B8.

Product **9**, diguaiacol

Product **9** was identified as diguaiacol. It was eluted at 23 min (Figure 2.7). ESI/MS analysis in negative mode of **9** showed *m/z* 245. MS^2 analysis (product ions of *m/z* 245) yielded these major fragment ions: *m/z* 245 ($[M-H]^-$), 185, and 157.

^1H NMR spectra showed 3 aromatic protons occurring between 6.5 and 7.5 ppm, and 1 MeO peak at 1.8 ppm, representing half the symmetrical molecule. The HSQC data showed 3 peaks (for the 6 protons) in the 110 - 120 ppm region of the spectrum, supporting our conclusion that these protons are attached to sp^2 hybridized carbons. The HMBC data further corroborated the proton assignment as well of assignment of the quaternary signals.

2.3.3 Mechanistic studies into curcumin oxidation

Reaction progress: Identification of reaction intermediates

The identification of **6a** and **6b** as spiroepoxides prompted further study into their reaction since a similar structure was proposed as an intermediate to the bicyclopentadione. Furthermore we knew from handling the spiroepoxides that they were chemically unstable.

LC-MS analysis of isolated fractions of **6a** and **6b** in pH 7.5 buffer over 6 h is shown in Figure 2.9. **6a** disappeared within the first 3 h to form **7a** which then formed the bicyclopentadiones **8b** and **8c** (Figure 2.9B). The parallel reaction with **6b** showed similar reaction, however, **6b** reacted faster (than **6a**) and disappeared within 1 h to form **7b**. **7b** persisted over the 3 h, with only small

amounts of transformation to **8a** detected. Figures 2.9 C and D show the time course for formation of the bicyclopentadiones over a 6 h from by plotting the relative abundance of **6**, **7** and **8** from ion chromatograms generated during the same experiment. Products **2**-**5** showed no reaction after further incubation for up to 12 hrs (data not shown).

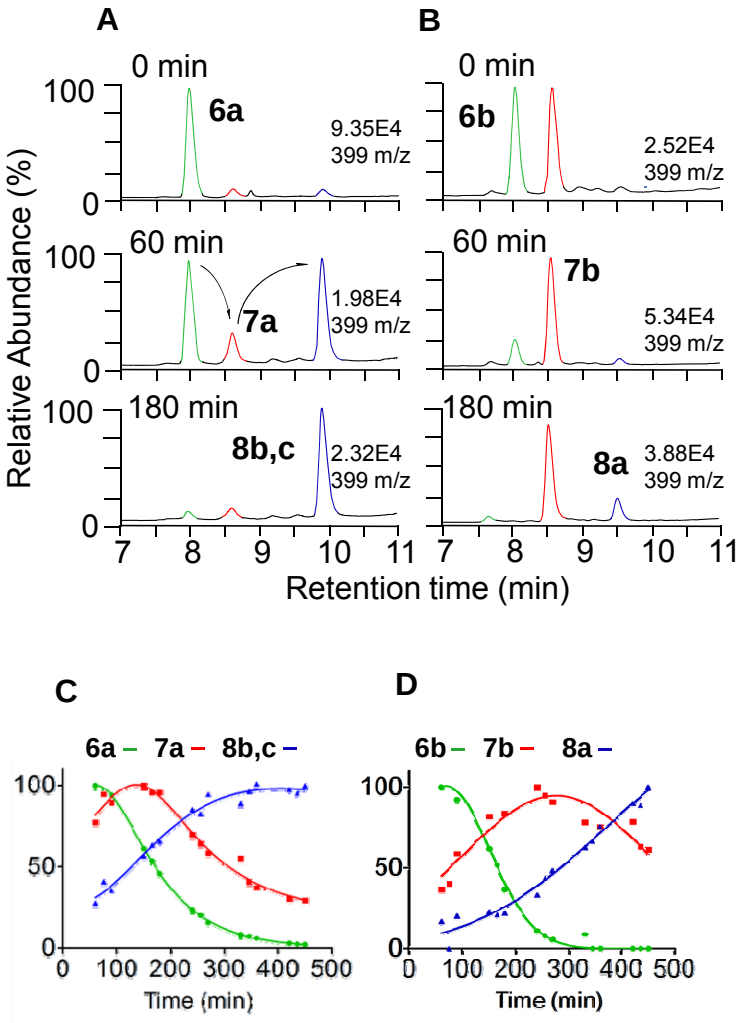

FIGURE 2.9 Conversion of the intermediates **6a** (A) and **6b** (B) to the **8** via intermediates **7a** and **7b**. Ion chromatograms were recorded every 15 min during a 6 hr incubation of **6a** and **6b** at room temperature. The products were monitored at m/z 399. (C and D) Time course of bicyclopentadione formation. The curves were obtained by fitting to the Gaussian distribution.

Analysis of oxygen incorporation into the bicyclopentadione

In a previous publication from our laboratory, Griesser et al. showed that only one of the two newly incoporated oxygen in the bicyclopentadione was from H_2O, with the other coming from O_2. (Griesser et al. 2011). It was proposed that the reaction with H_2O occured with an early quinone methide intermediate, but this was never shown directly. The isolation of oxygenated reaction intermediates allowed us to re-examine the step in the reaction scheme at which the reaction with H_2O occurs. I performed curcumin autoxidation in buffer made of 50% $H_2{}^{18}O$ and analyzed each product for the incorporation of the heavy atom using LC-ESI-MS. As shown in Figure 2.10, only the vinylether **7** and bicyclopentadione **8** contained ^{18}O from $H_2{}^{18}O$ as evident from the 50% enrichment of the 401 (+2 amu) ion. The spiroepoxide **6** and products **2**-**4** did not incorporate ^{18}O, suggesting that the reaction with H_2O occured during the transformation of **6** to **7**. Neither **7** nor **8** exchanged ^{18}O after incubations in $H_2{}^{18}O$ buffer.

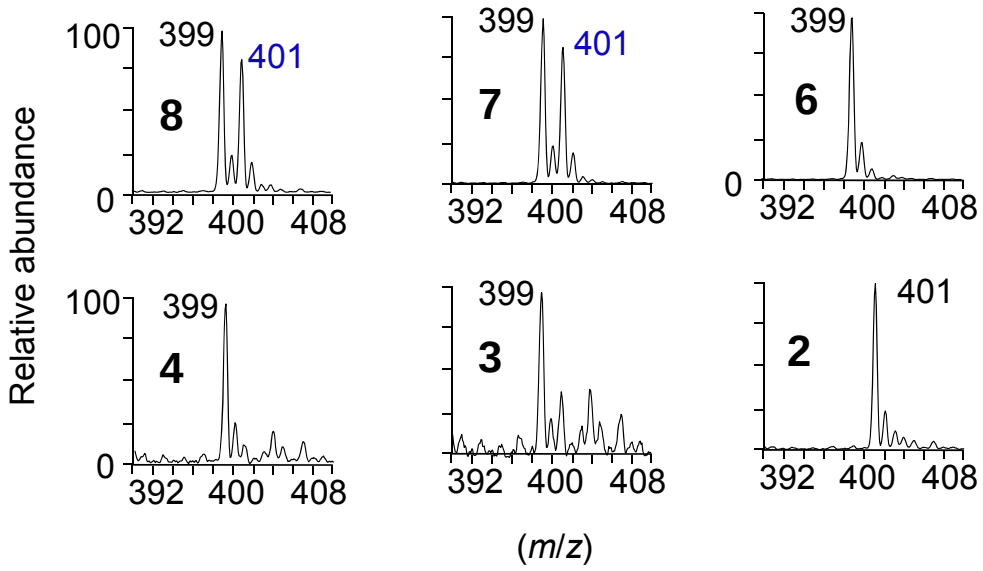

FIGURE 2.10. Partial LC-ESI mass spectra of curcumin autoxidation products formed in a 1:1 mixture of H_2O and $H_2{}^{18}O$.

Site of oxygen incorporation in the bicyclopentadione.

The proposed reaction mechanism in which H_2O reacts with an early quinone methide intermediate positions the oxygen from H_2O into the tetrahydrofuran ring between C1 and C7 of **8** (Griesser et al. 2011). While LC-MS studies supported that assignment of the oxygen, the data were not unequivocal. In re-examining these studies, I used more specific and sensitive LC-MS and NMR methods to determine which of the two newly incorporated oxygen atoms was from H_2O and which was from O_2.

In the first of two approaches I sought to generate unambiguous fragmentation of ^{18}O-**8** formed in $H_2{}^{18}O$ to determine the part of the molecule that has the ^{18}O label. CID of the unlabeled **8** (at *m*/*z* 399) and ^{18}O-labeled **8** (*m*/*z* 401) showed a base ion at m/z 247 or 249, respectively, suggesting that the 247 fragment contained the heavy atom. Both spectra also shared fragments at *m*/*z*

151 and *m*/*z* 353 (Figure 2.11A & B). Since the 247/249 fragment could be reasonably generated in a manner to include either oxygen, we modified our approach to use an unsymmetrical analog of **8** (3'-OCD_3,4"-Omethyl-8) to obtain unambiguous fragments (Figure 2.11 B). We generated 3'-OCD_3,4"-Omethyl-**8** from autoxidation of the corresponding curcumin analog that has deuterium for hydrogen in the methoxy of one ring, and paramethoxy group at the second phenolic ring. CID of the $[M-H]^-$ molecular ions at m/z 416 and 418 (for the ^{18}O-product) showed a fragment ion at m/z 250 or 252, respectively, as the base peak (Figure 2.11C & D). These data suggest that the base peak fragments, bearing the d_3- label, also have the labeled oxygen atom. Based on these results, the major fragment ions m/z 249 or m/z 252, contains the bicyclic ring moiety with one of the phenolic rings attached. Together, these data suggest that the ^{18}O derived from $H_2{}^{18}O$ formed the ether bond between carbons 1 and 1'.

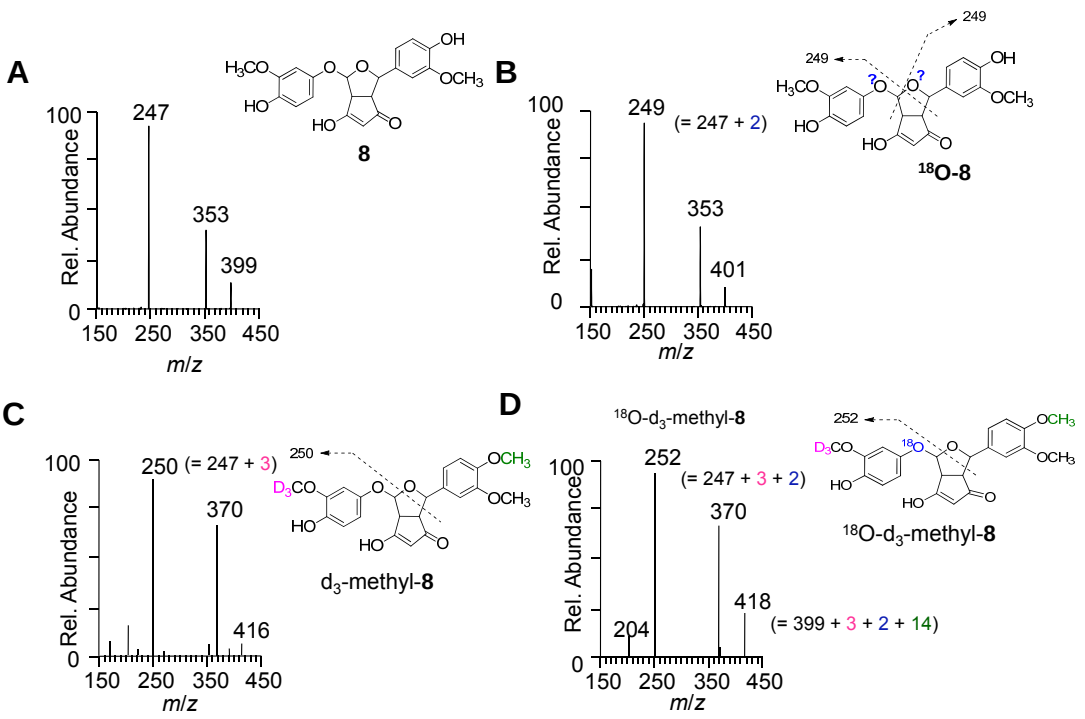

FIGURE 2.11. LC-MS-MS spectra of **8** and 3'-OCD_3,4"-Omethyl-**8**, respectively, formed in H_2O or $H_2{}^{18}O$.

NMR Characterization of Oxygen-18-Labeled BCP analogs.

To corroborate the LC-MS/MS data, I conducted ^{13}C NMR analysis of **8** generated in $H_2{}^{18}O$ or $^{18}O_2$ that were then mixed in a 1:1 ratio with unlabeled **8** to observe the small upfield shift in the carbon signal connected to the heavy isotope (Baillie et al. 2001). When **8** was generated in $^{18}O_2$:O_2, the C-1 signal (at 96.9 ppm) and C-7 signal (79.3 ppm) were shifted by 0.02 ppm indicating that both carbons were connected to the oxygen (in the tetrahydrofuran ring) derived from O_2. (Figure. 2.12A). When **8** was generated in $H_2{}^{18}O$:H_2O, the C1 signal was shifted by 0.02 ppm but no shift was observed for C-7 (Figure. 2.12B) suggesting that the oxygen connecting C1 to C1' in the phenolic ring was derived from H_2O. We did not observe the expected shift of the C1' signal. Nonetheless,

the data corroborate the previous the LC-MS/MS analysis and show that the oxygen from H_2O is positioned between C1 and the aromatic ring (C1').

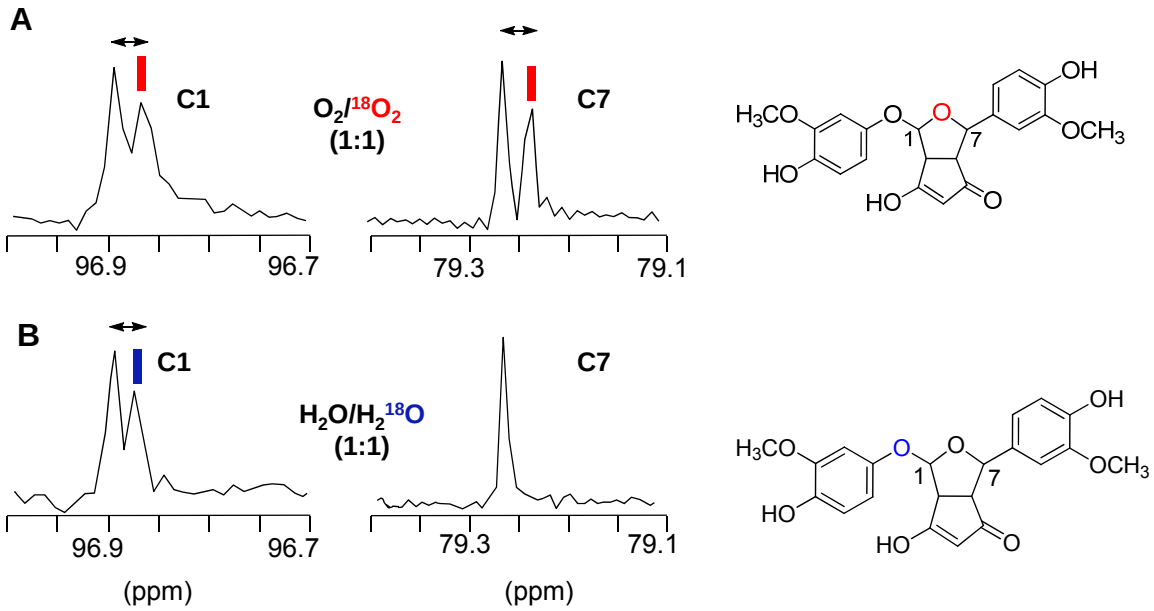

FIGURE 2.12. Partial ^{13}C NMR spectra of **8** formed in a 1:1 mixture of (A) O_2 and $^{18}O_2$ and (B) H_2O and $H_2{}^{18}O$ showing the signals for C-1 and C-7 are shown.

Analysis of the bicyclopentadione formed in D_2O

The molecular structure of **7a** shows a C1-C2 double bond that becomes saturated during the formation of **8**. To confirm the existence and location of this double bond in **7,** I conducted curcumin autoxidation in D_2O buffer and assessed for the incorporation of deuterium into **8** by NMR. Partial ^1H NMR spectra of **8** formed in D_2O buffer shows the incorporation of deuterium at C2, as indicated by the lack of a proton signal. The expected coupling of H2 into the neighboring H6 carbon was also lacking, further confirming the incorporation of deuterium at C2

(Figure 2.13A & B). The ^{1}H spectra for **8** and [D]-**8** were otherwise identical. This data supports the existence of the C1-C2 double bond in **7.**

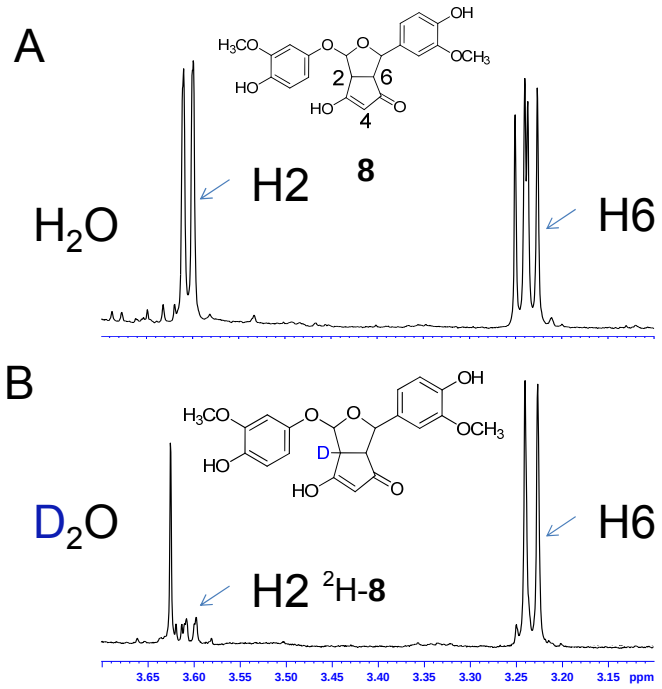

FIGURE 2.13 Partial ^{1}H NMR spectra of the bicyclopentadione formed in regular buffer (A) and D_2O buffer (B).

Autoxidation of methylcurcumin

Curcumin autoxidation is initiated by hydrogen abstraction from either of the two phenolic hydroxyls in the symmetrical molecule. After hydrogen abstraction, the ring bearing the phenoxyl radical and eventual quinone methide will determine the position of the incorporated oxygen atoms in the final product **8**. To determine whether the ether bond at C1 in **8** will connect the ring that has the additional methyl group, or the other ring where H-abstraction is permitted and therefore contained quinone methide and phenoxyl radical. I performed oxidation of methylcurcumin (using the oxidant $K_3[FeCN)_6]$) to generate the

corresponding methyl-**8**. Methylcurcumin does not undergo autoxidation. NMR analysis showed that the methyl group was found exclusively in the ring connected to C7 rather than the ring connected through the ether bond at C1 (Figure 2.14). This places the ether bond on the side of the molecule where the H-abstraction occurred to form the quinone methide. The implications of this finding is further discussed in the next section. Partial NMR spectra from the identification of methyl-8 are shown in Figure B1 of the Appendix.

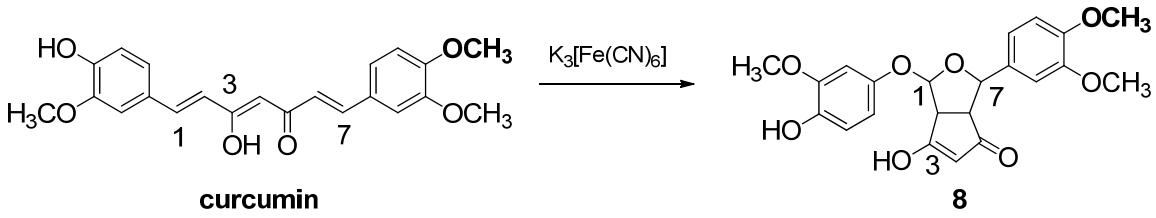

curcumin **8**

FIGURE 2.14 Oxidation of methylcurcumin.

2.3.4 Curcumin metabolism in human S9 liver fractions.

We have shown that curcumin is a substrate for horseradish peroxidase (HRP) and COX-2 at the peroxidase active site, resulting in formation of the bicyclopentadione products (Griesser et al. 2011). Similar oxidation to generate quinone methides in other polyphenols is catalyzed by both peroxidases and cytochrome P450 enzymes (Mahajan et al. 2011). Implicating the involvement of P450 enzymes in the catalysis of curcumin would suggest enzymatic transformation in the liver could contribute to the formation of the oxidized metabolites *in vivo.*

Human S9 liver fractions were used as a model to determine the contribution of liver metabolism in the oxidative transformation of curcumin *in vivo*. Experiments were performed using [$^{14}C_2$]curcumin as a tracer in order to account for potential novel, enzyme specific metabolites. Reactions were conducted in the presence (Figure 2.15B) or absence (Figure 2.15A) of NADPH.

NADPH dependent transformation of curcumin to the reduced hexahydrocurcumin product (identified by comparison to an authentic standard) was the only reaction detected. None of the oxidized products were detected.

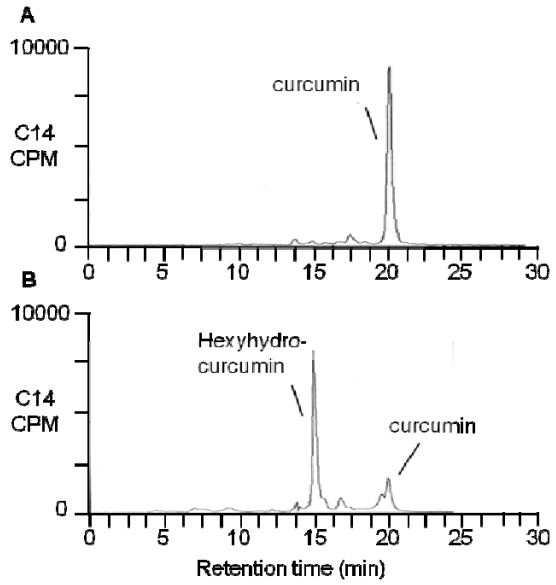

FIGURE 2.15. Radio-chromatogram showing reaction of [$^{14}C_2$]curcumin with S9 liver fractions. 25 μM [$^{14}C_2$]curcumin is incubated with 500 μL 0.1 M KPO_4 buffer pH 7.4, 2.5 mg S9 protein, 3 mM $MgCl_2$**,** with or without 2 mM NADPH for 30 min. The reaction was terminated by the addition of 1 mL MeCN, and the supernatant dried and reconstituted for HPLC-radio analysis.

This study indicates that the P450 enzymes in the liver may not be involved in the oxidation transformation of curcumin *in vivo*. Nonetheless, it is possible that peroxidase enzymes in other tissues may contribute to the

enzymatic formation of the oxidative metabolites. Many target tissues express peroxidase enzymes that are involved in oxidation activation of drugs to reactive metabolites in vivo, e.g., myloperoxidase (in leukocytes), P450 peroxidase, and the COX enzymes (expressed in multiple tissues) (O'Brien 1988; Stiborová et al. 2007). The relative contribution of enzymatic versus autoxidative transformation in the *in vivo* oxidation of curcumin has not been assessed.

2.4 Discussion

Mechanism of curcumin oxidation:

The isolation and structural identification of novel products and reaction intermediates, in conjunction with mechanistic studies using isotopic and structural analogs of curcumin (^{2}H-) or its metabolites (^{2}H- and ^{18}O-), allowed us to determine a mechanism of autoxidation (Figure 2.16). The reaction is initiated by hydrogen abstraction from either of the phenolic hydroxyls to form a phenoxyl radical. This radical is delocalized to a more stable carbon-centered position at C2 in the heptadieneone chain, also forming a quinone methide in the process. The secondary radical at C2 undergoes 5-exo cyclization reaction to form the cyclopentadione ring of C2 to C6. The resulting radical at C7 either reacts with O_2 to form a peroxyl radical (preferred reaction route) (Figure 2.16), or participates in a second cyclization reaction with the sp^2 carbon at C1 to form **5**, a minor reaction product (Figure 2.18). In the case of the reaction with O_2, the resulting peroxyl radical **III** also reacts with the sp^2 carbon at C1 to from an endoperoxide

with a tertiary radical at C1' **IV**. The endoperoxide radical undergoes two alternative reactions: The radical is quenched by H-donation to form a covalently complete endoperoxide **VI** that we propose is the precursor to **2, 3** and **4** (Figure 2.17). Alternatively, the radical performs S_Hi attack at the endoperoxide to form a spiroepoxide and alkoxyl radical **V** that is quenched to form the covalently complete **6**. Product **6** undergoes ring opening of the epoxide by C-C bond cleavage along with exchange of oxygen to form vinylether **7**. Addition of the hydroxyl of 7 across the C1-C2 double bond completes the formation of 8 as the major autoxidation product. Product **9** is presumably formed from the alkoxyl radical that can also undergo homolytic β-scission of the C1-C1' bond to release a methoxy phenol radical that dimerizes to give the final product (Figure 2.19). The formation of diguaiacol from curcumin autoxidation is unexpected, and our proposed mechanism is likely an oversimplification of a more complex mechanism. The dimerization of the methoxyphenol radical, which likely exists at very low concentrations, is puzzling.

^{18}O-labeling studies showed that **8** retains one of the oxygen initially incorporated from O_2, and has a second oxygen incorporated from H_2O. The oxygen from H_2O forms the ether bridge between C1 and C1' in the phenolic ring in **8** and, we presume, the similar ether bridge in **7**. This implicates that the exchange of oxygen occurs in conjunction with the epoxide opening in **6** during the formation of **7.** The opening of an epoxide in this manner to involve an oxygen exchange is unprecedented in the literature.

Our analysis further shows differential reaction rates for the transformation of the diastereomers of **6** and **7** during the formation of **8**. No scrambling of the stereoisomers occurred during this reaction, with **6a** going to form **8b**, **c** via **7a**, and **6b** going to **8a** through **7b,** suggesting that no racemization occurred during this transformation.

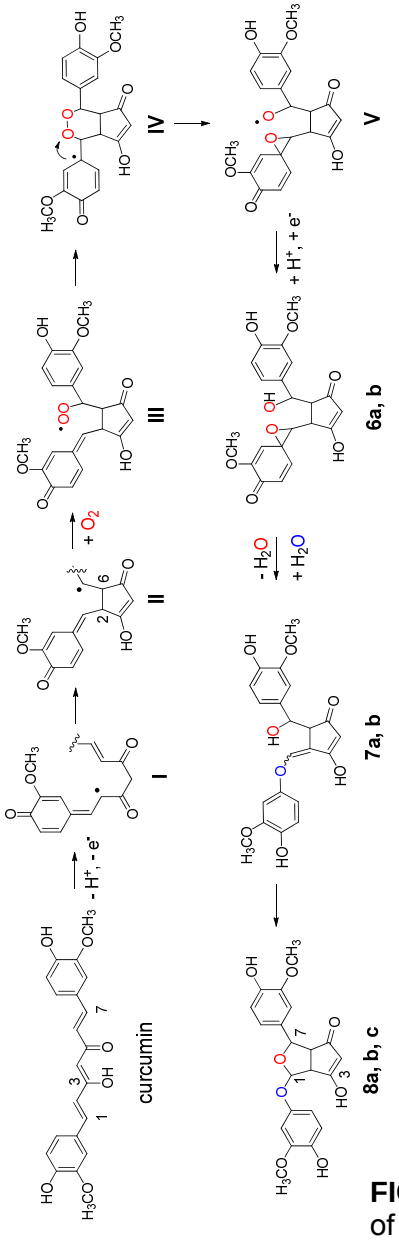

FIGURE 2.16 Proposed mechanism of autoxidation of curcumin.

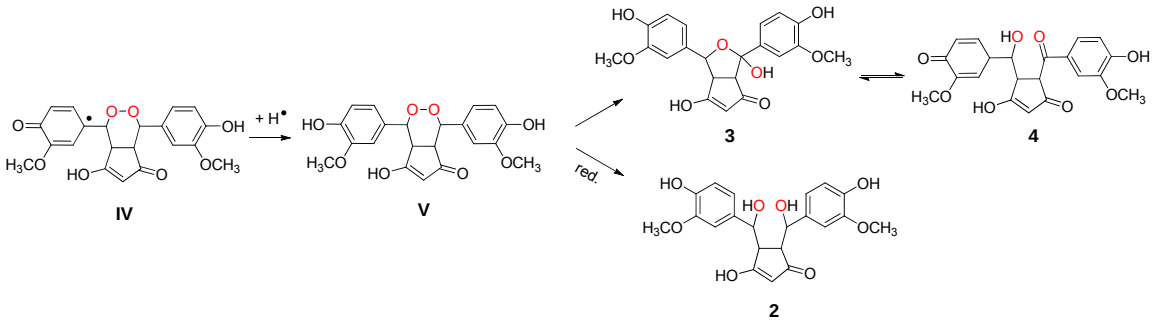

FIGURE 2.17 Proposed mechanism of formation of **2**, **3** and **4**.

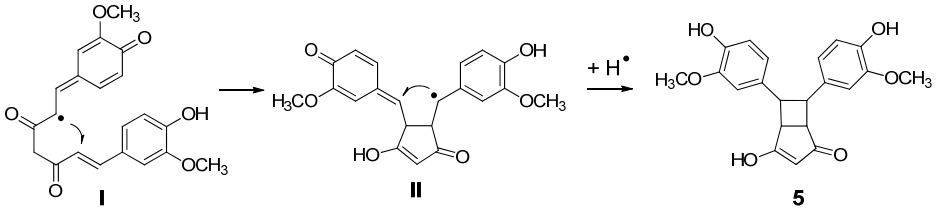

FIGURE 2.18 Proposed mechanism of formation of **5**.

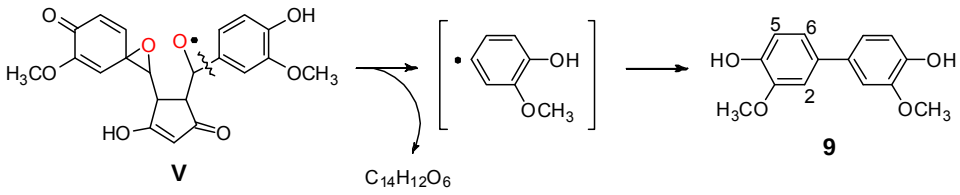

FIGURE 2.19 Proposed mechanism of formation of **9**.

Comparisons with the old mechanism

In the previously proposed mechanism of curcumin autoxidation, the secondary radical formed after migration of the phenoxyl radical also reacts with O_2, but the resulting peroxyl radical is quenched to form a hydroperoxide intermediate. The quinone methide is quenched by reaction with water (at C1) to account for the incorporation of oxygen from H_2O into the bicyclopentadione. Furthermore, the proposed spiroepoxide was formed from the hydroperoxide and placed across the C7 and C1" bond.

Our ^{18}O-labeling studies proved that the reaction with water does not occur at the quinone-methide, but at a later step in the reaction during the formation of **7** from **6**. Furthermore, the identification of the hemiketal and dihydroxy products points to the existence of an endoperoxide intermediate, supporting a reaction of the peroxyl radical with the quinone-methide, and argues against a hydroperoxide intermediate. Even though the spiroepoxide intermediate was proposed during the earlier mechanism, the epoxide was placed across C7 and C1''. The oxidation of methylcurcumin suggest that the epoxide exists across the C1 and C1' bond that formed part of the quinone-methide (Figure 2.20). Furthermore, our ^{18}O-labeleled studies of **8** showed that the oxygen atom from water formed the ether bond between C1 and C1', rather than being part of the tetrahydrofuran ring as previously proposed.

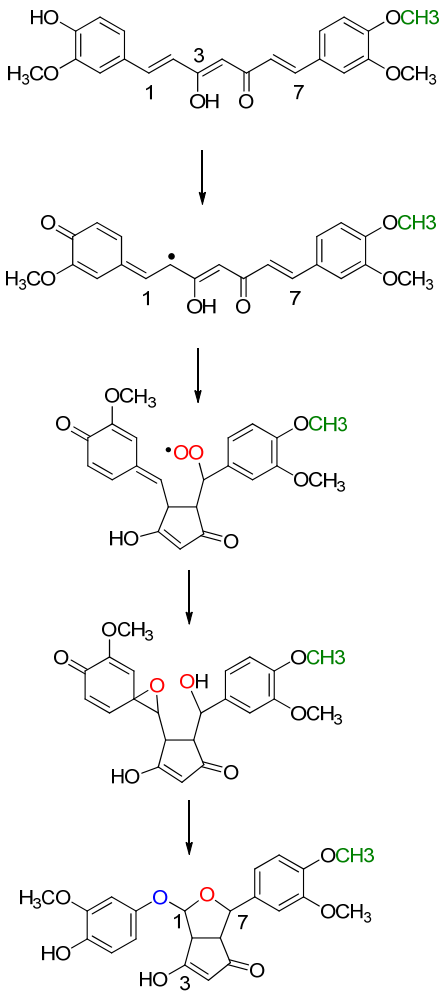

FIGURE 2.20 Proposed mechanism of oxidation of methylcurcumin.

Oxygen Exchange

The transformation mechanism elucidated for curcumin to incorporate oxygen from H_2O and O_2 is complex and is unprecedented in the oxidation of phenolic compounds. Individual steps during the transformation represent complex reactions and perhaps unprecedented chemistries as well. The most puzzling step of the reaction is the exchange of oxygen that occurs during the transformation of the **6** to **7.** Our data suggests that the exchange of oxygen

occurs in conjunction with the carbon-carbon bond cleavage during opening of the epoxide of **6**, rather than at QM as previously proposed. Suggesting a chemical mechanism to support this transformation proved non-trivial. In control experiments, no exchange of oxygen was detected after incubations of purified **6** and **7** in ^{18}O-labeled buffer, suggesting chemical reaction with water occurs during the transformation. The details of this transformation therefore remain to be explained.

The oxidative products are nucleophilic β-dicarbonyls

The extreme polarity of oxidative products **2**-**5,** as evident from their early elution time relative to **7** and **8**, is unusual given their very similar chemical features. Products **2**-**5** also share a common UV chromophore with prominent maximum absorbance at 263 - 265 nm, which is different than that of **7** and **8** (Figure 2.21A)**.** The differences in polarity and UV chromophore can both be attributed to differences in the nucleophilicity of the β-diketone moiety that acts as a carboxylic acid isostere. Products **2**-**5** exist as ionic species at pH 7.4 and are deprotonated at the central C4 position in the β-diketone moiety. ^{1}H NMR experiments suggest that the proton at C4 quickly exchanges for deuterium in 2-5. Protonation at C4 results in a reversible change in the chromophore of **2** to match that of **8** (Figure 2.21B). The nature of the substituent at C1 and C7 seems to affect the acidity at C4.

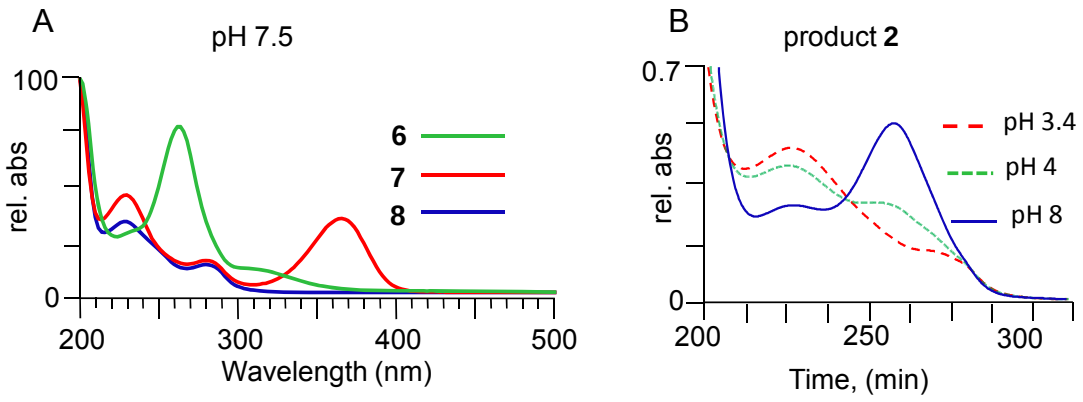

FIGURE 2.21 (A) UV/Vis spectra of **6, 7** and **8.** (B) UV/Vis spectra of **2a** at pH 3.4, 4 and 8.

Curcumin quinone methide poisons topoisomerase II

The analysis of the oxidative metabolites presented in this chapter is an initial step towards assessing their involvement in the bioactivities of curcumin. The first study to suggest a role for oxidative metabolism in the biological effects of curcumin was a collaborative effort between our laboratory and that of Dr. Osheroff. Our studies implicate the proposed quinone methide as the direct mediator of the topoisomerase poisoning effect of curcumin.

Curcumin can induce apoptosis in cancer cells and its effect on the topoisomerase enzymes is considered an important contributor (Pawar et al. 2012; López-Lázaro et al. 2007; Ketron et al. 2013). Topoisomerases regulate DNA integrity during replication by cutting and religating DNA strands to relieve tangles and supercoils. The two major classes of topoisomerases, type I and type II, act by forming a transient single or double-strand break, respectively. In the case of the type II topoisomerases, a covalent “cleavage complex”

intermediate is formed between an active site tyrosine residues and newly generated DNA termini (Wang 1996; Nitiss 1998). Several anti-cancer agents such as etoposide and doxorubicin act by stabilizing this cleavage complex, leading to eventual DNA strand breaks and apoptotic cell death. Drugs that act in this manner are referred to as topoisomerase poisons (Bender, Ham, and Osheroff 2007; Deweese and Osheroff 2009). Quinones form a class of topoisomerase poisons, and bind covalently to Cys-392 and Cys-405 in topoisomerase II to increases levels of cleavage complexes primarily by inhibiting DNA religation (Bender, Ham, and Osheroff 2007). Quinones exhibits both antitumor and carcinogenic activities (H. Wang et al. 2001).

Curcumin is a potent topoisomerase II poison in cells, showing greater activity than etoposide and other clinically used drugs that target that enzyme (López-Lázaro et al. 2007). In our study, we assessed the mechanism of action of curcumin against topoisomerase II *in vitro*. The assay used a purified recombinant enzyme and plasmid DNA. DNA cleavage was measured to indicate poisoning of the enzyme. Curcumin displayed no activity in this system when tested at 10 to 150 μM. In investigating the role of oxidative metabolism, we showed that curcumin is stable to autoxidation in the assay buffer due to the presence of $MgCl_2$ and antioxidants, and none of the oxidative products were formed (Figure 2.23A). Inducing oxidative transformation with stoichiometric concentrations of oxidizing agent potassium ferricyanide ($K_3Fe(CN)_6$) resulted in potent topoisomerase II poison activity, suggesting that oxidative transformation is required for this effect (Figure 2.23B). Stable curcumin analog

dimethylcurcumin did not induce DNA cleavage even after the addition of the $K_3Fe(CN)_6$ oxidant.

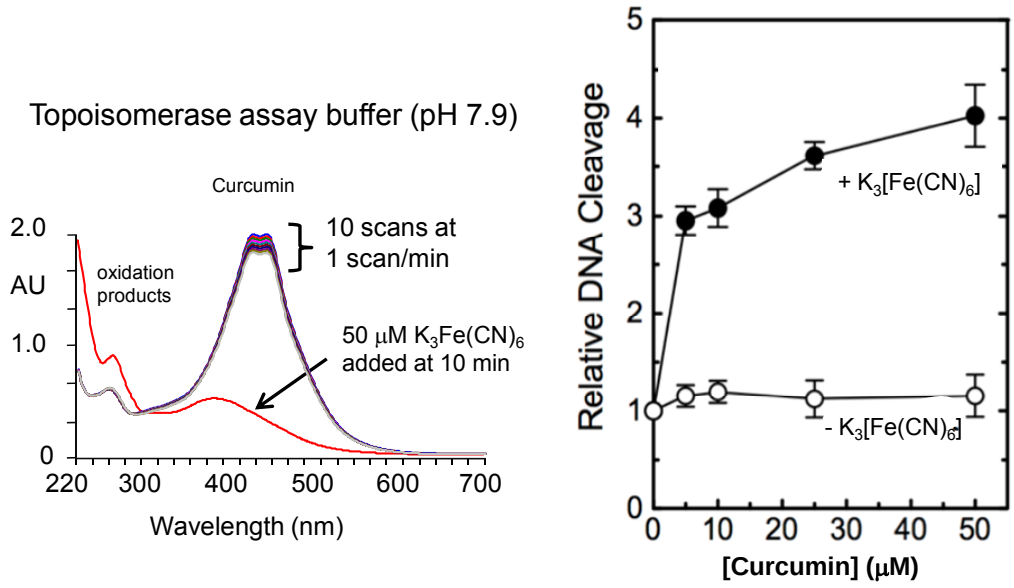

FIGURE 2.22 Topoisomerase-II poisoning effect of curcumin. (Left) Curcumin is stable in the assay buffer over 10 minutes after repetitive scanning in the spectrophotometer every 1 min. Addition of $K_3Fe(CN)_6$ induces oxidative degradation of curcumin. (Right) Curcumin shows no DNA cleavage when $K_3Fe(CN)_6$ is absent. Addition of $K_3Fe(CN)_6$ results in 4 fold increase in DNA cleavage (Ketron et al. 2012).

To support a redox-depended, covalent binding mechanism of action of curcumin, we showed that the addition of antioxidant DTT prior to the addition of the enzyme results in loss of the curcumin effect, presumably by preventing the covalent association of electrophile metabolite(s) of curcumin with the enzyme. The spiroepoxide **6**, which exhibits electrophilic properties in reactions with GSH

(Figure 4.4), was only 50% as potent in the topoisomerase poisoning assay compared to when curcumin is used. Neither the bicyclopentadione **8** nor a mixture of products **2** - **5** showed appreciable effect on topoisomerase. When curcumin is pre-incubated with topoisomerase and $K_3Fe(CN)_6$ prior to the addition of the DNA, the enzyme activity decreased to about zero with a half-life of 0.9 min, consistent with the prediction for redox-dependent poisons. These studies implicate the early quinone methide intermediate as the direct mediator of the topoisomerase effect of curcumin. This is the first instance where a curcumin target can be attributed to one of the oxidative metabolites (Ketron et al. 2013).

Establishing the involvement of the quinone methide in the topoisomerase effect of curcumin is an elegant explanation for the discrepancy between the *in vitro* and cellular data. Cells may possess the enzymatic machinery to oxidize curcumin, and this is lacking in the cell-free system. Our studies can serve as a model for assessing the involvement of the quinone methide against other curcumin targets.

Conclusions

The rapid degradation of curcumin at physiological pH has been recognized for many years, but the major products remained unidentified. A recent study by our group identified the degradation of curcumin as an autoxidation and the final product as a dioxygenated bicyclopentadione **8**. The discovery of **8** as the major product of curcumin degradation in buffer corrects

earlier literature reports stating that curcumin degradation in buffer is mainly a chain cleavage reaction generating vanillin and ferulic acid (Wang et al. 1997).

In the present study, I have isolated ten additional products of this transformation, including four reaction intermediates. We have refined and expanded on our previously proposed mechanism to include transformation through a proposed endoperoxide intermediate that proceeds through the isolated spiroepoxide **6** and vinylether **7** intermediates to form **8**. I have determined conditions for the isolation of the oxidative metabolites to allow for their evaluation in biological assays. We hypothesize that the oxidative metabolism of curcumin contributes to its therapeutic effects. This study represents the first example of the isolation and structural characterization of reactive intermediates formed during oxidative transformation of a natural polyphenolic agent of high medicinal interest.

CHAPTER 3

MECHANISTIC STUDIES INTO THE OXIDATIVE TRANSFORMATION OF CURCUMIN-GLUCURONIDE

3.1 Introduction

3.1.1 Curcumin glucuronidation

Glucuronidation is the most common route for the phase II metabolism of curcumin. Conjugation of curcumin with the glucuronic acid occurs in the liver and intestines. UDP-glucuronosyltransferases (UGTs) are a family of enzymes responsible for converting curcumin to the more polar conjugate through the nucleophilic addition of the glucuronic acid moiety (Ritter 2000). The *O*-glucuronide, in which the glucuronide is attached at one of the phenolic hydroxyls, is the abundant conjugation product of curcumin *in vivo* and has been found at much higher concentrations than the unconjugated curcumin (Pan, Huang, and Lin 1999). The comparatively high levels of curcumin-glucuronide in the plasma raise the question of its contribution to the pharmacological effects of curcumin. In rare cases, glucuronides of other drugs have been shown to have increased biological activity, or serve as a transporter form for the parent compound (Pasternak et al. 1987). The contribution of the curcumin-glucuronide to the biological activity of curcumin is unclear.

Autoxidative transformation is the major pathway for the *in vitro* degradation of curcumin, giving rise to dioxygenated derivatives. Oxidation of

curcumin involved hydrogen abstraction from either of its phenolic hydroxyls. The glucuronide conjugate of curcumin still has one free hydroxyl. We know from previous analysis of methylcurcumin that only one free hydroxyl is required for oxidative transformation to occur. However, blockage of the second hydroxyl group prevents autoxidation, and oxidative transformation then requires the action of peroxidase enzyme (e.g. HRP) or oxidant (e.g. $K_3Fe(CN)_6$). The chemical instability of the phenolic curcumin-glucuronide in aqueous buffer at pH 7.4 has been reported, but the products and reaction mechanism were not determined (Pfeiffer et al. 2006). The aims of the studies in this section were to investigate the oxidative transformation of curcumin glucuronide, and determine the reaction products.

3.2 Materials and Methods

3.2.1 Materials

Curcumin was synthesized from vanillin and acetylacetone as described. HRP (Type-II, 5 kU/ml; 25.9 mg/ml) was purchased from Sigma (P8250).

3.2.2 Synthesis of curcumin glucuronide

Curcumin glucuronide was synthesized following a protocol by Moon et al. (Moon et al. 2001). Curcumin (100 mg, 0.27 mmol) and acetobromo-α-D-glucuronic acid methyl ester (500 mg, 1.26 mmol) were dissolved in 5 ml dimethylformamide. K_2CO_3 (100 mg, 0.72 mmol) was added, and the solution

was stirred for 2 h at room temperature. Then 30 ml cooled H_2O were added and the solution was acidified using formic acid. Acidification resulted in the formation of a precipitate that was collected by centrifugation (4°C, 5000 rpm, 20 min). The precipitate was washed with 5 ml 0.2% formic acid and dissolved in 10 ml 50/50 MeOH/$CHCl_3$. The solvent was evaporated and the residue was dissolved in 5 ml dry MeOH. In order to remove the acetyl moieties 150 µl NaOH (28% in MeOH) were added, and the solution was stirred for 30 min at 4°C. The methyl ester was hydrolyzed by treatment with 5 ml H2O for 30 min at room temperature. Then 370 µl HCl (2.0 N) and a few drops of formic acid were added to acidy the solution. The solution was filtered, and the solvent evaporated. The product was purified by RP-HPLC (Econosil C18 column, 250 mm x 10 mm) eluted with a solvent of MeCN/H_2O (45/55) with 0.01% acetic acid at a flow rate of 4 ml/min. LC-MS: 543 ([M − H]−).^{1}H NMR (Acetone-d_6, 600 MHz): δ = 7.60 (d, 1H, J = 15.8), 7.59 (d, 1H, J = 15.7 Hz), 7.35 (d, 1H, J = 1.14 Hz), 7.33 (d, 1H, J = 1.7 Hz), 7.21 (m, 1H), 7.20 (m, 1H), 7.18 (dd, 1H, J = 8.2; 1.8 Hz) 6.87 (d, 1H, J = 8.2 Hz), 6.76 (d, 1H, J = 15.8 Hz), 7.71 (d, 1H, J = 15.8 Hz), 5.99 (s, 1H), 5.20 (d, 1H, J = 7.39 Hz), 4.10 (d, 1H, J = 9.8 Hz), 3.91 (s, 3H), 3.88 (s, 3H) ppm.

3.2.3 Analytical procedures for synthesized compounds

Products were analyzed and purified by RP-HPLC using an Agilent 1200 series diode array system equipped with a Waters Symmetry C18 5-µm column (4.6 × 250 mm). The column was eluted with a linear gradient of MeCN/H_2O/HOAc 20/80/0.01 to 80/20/0.01 (by vol.) over 20 min and a flow rate

of 1 ml/min (Method A). LC-MS was performed using a Thermo LTQ ion trap instrument equipped with an electrospray ionization interface. The instrument was operated in the negative ion mode, and mass spectra were acquired at a rate of 2 s/scan. The settings for the heated capillary (300 °C), spray voltage (4.0 kV), spray current (0.22 μA), auxiliary (37 mTorr), and sheath gas (16 mTorr). Samples were introduced using a Waters Symmetry Shield C18 3.5-μm column (2.1 × 100 mm) eluted with a gradient of MeCN/H_2O (5/95, by volume, containing .05% acetic acid) to MeCN/H_2O (95/5, by volume, containing .05% acetic acid) over 10 min. Curcumin glucuronide was identified based on comparison with an authentic commercial standard.

3.2.4 Oxidation of curcumin glucuronide

Curcumin glucuronide or curcumin (30 μM) were added to 500 μl 20 mM Na-phosphate buffer pH 7.5. The reaction was monitored in a UV/Vis spectrophotometer by repetitive scanning from 700 to 200 nm every 2 min or by following the disappearance of the chromophore at 430 nm in the time drive mode. To some reactions $K_3Fe(CN)_6$ (15 μM; from a 5 mM stock solution in water) or horseradish peroxidase (0.01 U/ml) and H_2O_2 (40 μM) were added.

A large scale incubation of curcumin glucuronide (1 mg) with 50 μM $K_3Fe(CN)_6$ was conducted in 40 ml of buffer for 20 minutes. Products were extracted after acidification on C18 cartridge eluted with methanol.

HPLC Analysis

The transformation reactions were analyzed using a Waters Symmetry C18 5-μm column (4.6 × 250 mm) eluted with a gradient of 20% MeCN to 80% MeCN in 0.05% aqueous acetic acid over 20 min. The samples run at flow rate of 1 ml/min. Elution of the products was monitored using an Agilent 1200 diode array detector.

LC-MS Analysis

For LC-MS analyses a Thermo Finnigan LTQ ion trap instrument. The settings for the heated capillary (300 °C), spray voltage (4.0 kV), spray current (0.22 μA), auxiliary (37 mTorr) and sheath gas (16 mTorr). Samples were introduced into the instrument using a Waters Symmetry Shield C18 3.5-μm column (2.1 × 100 mm) eluted with a gradient of 20% acetonitrile to 80% MeCN in 0.05% aqueous acetic acid over 5 min, followed by isocratic elution with 95% MeCN for 5 min.

NMR Analysis

Samples were dissolved in 150 μl of acetone $-d_6$ in a 3 mm tube, and the NMR spectra were recorded using a Bruker DRX 600 MHz spectrometer equipped with a cryoprobe. The pulse frequencies for the H,H-COSY, HSQC, and HMBC experiments were taken from the Bruker library. The spectra were acquired at 284 K. Chemical shifts are reported relative to residual acetone (δ = 2.05 ppm).

3.3 Results

3.3.1 Oxidation of curcumin-glucuronide

Following up on the transformation of curcumin in buffer, the reaction of curcumin-glucuronide was assessed under similar conditions. Spectrophotometric analysis shows that curcumin-glucuronide was stable to autoxidation in phosphate buffer pH 7.5 (not shown). The addition of HRP to the buffer resulted in little degradation over a 10 min time course with the further addition of the H_2O_2 catalyst resulting in the fast disappearance of the curcumin-glucuronide chromophore at λmax 430 nm (Figure 3.1).

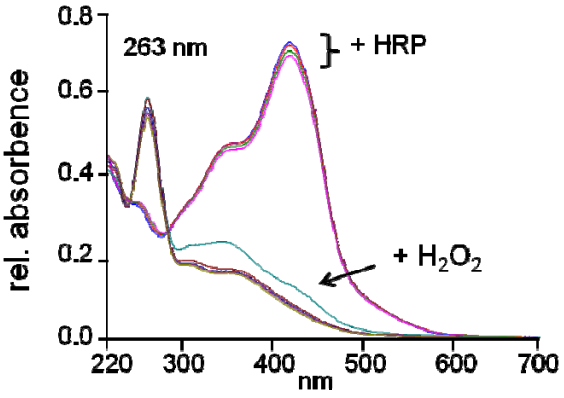

FIGURE 3.1 UV/VIS analysis of 30 μM curcumin-glucuronide oxidation in 500 μl 20 mM Na-phosphate buffer pH 7.5. The reaction is scanned repetitively from 700-200 for 5 min in the presence of HRP before H_2O_2 is added for 3 min. Scan rate: 1 min^{-1}.

The addition of a half-stoichiometric amount of the oxidizing agent potassium ferricyanide ($K_3Fe(CN)_6$) also catalyzed this transformation. The disappearance of the 420 nm chromophore was associated with the formation of a new chromophore at 263 nm, matching that seen during curcumin oxidation and suggesting the same type of transformation.

I conducted kinetic analysis in a spectrophotometer to compare the rate of autoxidative, $K_3Fe(CN)_6$ catalyzed, and HRP/H_2O_2-catalyzed transformations of curcumin and curcumin-glucuronide in pH 7.5 buffer. The assay measured the change in the absorbance of curcumin (430 nm) or curcumin glucuronide (420 nm) over the first 45 sec upon the addition of the enzyme or oxidant. The obtained values are the average of three repeats performed for each experiment.

Substrate	Initial rate +/- S.D. (μM/min)				Turnover number for HRP (min^{-1}; at 40 μM H_2O_2)
	Autoxidation	$K_3Fe(CN)_6$	HRP	HRP + H_2O_2	
Curcumin	1.8 +/- 0.4	54.2 +/- 9.2	4.1 +/- 0.1	40.6 +/- 1.8	3.4×10^4 +/- 1.5×10^3
Curcumin glucuronide	0.1 +/- 0.05	28.6 +/- 2.2	3.6 +/- 0.1	33.3 +/- 3.5	2.8×10^4 +/- 2.9×10^3

TABLE 3.1 Kinetic analyses of the oxidation of curcumin and curcumin-glucuronide.

As shown in Table 3.1, curcumin-glucuronide was practically stable under autoxidative conditions when compared to curcumin. Curcumin-glucuronide transformation was about 80% as fast with the enzyme (HRP/H_2O_2) and about 50% as fast with the oxidant ($K_3Fe(CN)_6$) compared to curcumin. Curcumin-glucuronide was therefore an efficient substrate for the oxidant and enzyme, howbeit not as efficient as curcumin.

3.3.2 HPLC and LC-MS analyses of curcumin-glucuronide oxidation.

Curcumin-glucuronide oxidation reactions were conducted using HRP/H_2O_2. The reactions were acidified and the products separated on RP-HPLC system with diode-array detection. The chromatogram, presented in Figure 3.2A, shows two polar products eluting at 7 and 7.5 min retention time with the same UV/Vis spectra as the curcumin bicyclopentadiones. A similar reaction conducted in parallel was treated with β-glucuronidase in order to remove the glucuronic acid moiety from the products and starting material. After hydrolysis, the two products were shifted to the same retention time as the bicyclopentadione isomers formed by autoxidation of curcumin (Figure. 3.2B and C). LC-ESI/MS analysis in negative ion mode of the major reaction product in Figure 3.2A shows *m/z* 575 representing an increase in 32 (2O) above the molecular weight of curcumin-glucuronide (*m/z* 543). These data suggest that the major product of curcumin-glucuronide oxidation is the bicyclopentadione-glucuronide. Products from $K_3Fe(CN)_6$ and peroxidase-catalyzed reactions were identical based on RP-HPLC-UV and LC-MS/MS analysis.

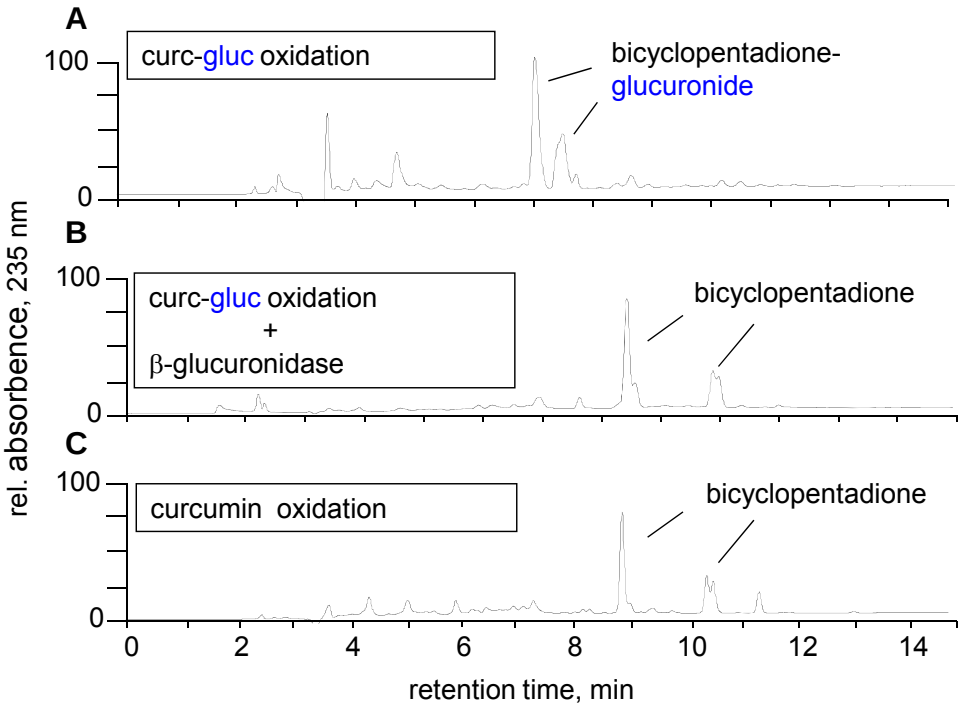

FIGURE 3.2 RP-HPLC analysis of enzymatic transformation products of curcumin glucuronide. (A) 30 μM Curcumin glucuronide was reacted with HRP and H_2O_2 (40 μM). (B) A reaction conducted in parallel in analyzed after hydrolysis with β-glucuronidase (pH4, 1 h at 37°C). (C) Transformation products of curcumin by HRP/H_2O_2)

3.3.3 Characterization of the bicyclopentadione-glucuronide by NMR.

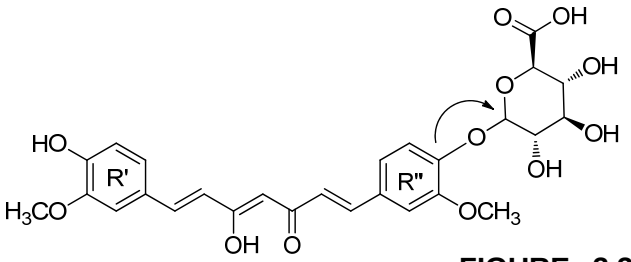

FIGURE 3.3 Biclyclopentadione-glucuronide. The arrow shows the 3-bond ^{1}H to ^{13}C HMBC cross peak.

	δ^1H (ppm)	
No.	BCP	BCP-glucu
1′	–	
2′	6.85	6.84
3′	–	–
4′	–	–
5′	6.84	6.82
6′	6.66	6.65
3′-OMe	3.87	3.85
1″	–	
2″	6.74	6.88
3″	–	–
4″	–	–
5″	6.69	7.13
6″	6.71	6.86
3″-OMe	3.76	3.79

TABLE 3.2 Proton chemical shifts of the aromatic signals of the bicyclopentadione (BCP) and bicyclopentadione glucuronide (BCP-Glucu)

To confirm the identification of the bicyclopentadione-glucuronide, and to determine which of the phenolic rings has the glucuronide moiety, NMR analysis was conducted on the major reaction product in Figure 3.3A after a large scale reaction.

^{1}H NMR spectra closely matched that of the curcumin derived bicyclopentadione. Signals for the aromatic hydrogens H5' and H6' were shifted by 0.44 and 0.15 ppm, respectively, relative to those of the free bicyclopentadione indicating that the glucuronic acid moiety is attached to that ring. We detected HMBC cross peak between a glucuronic acid carbon and C4" as shown in Figure 3.3.

3.4 Discussion

Oxidative transformation of curcumin-glucuronide in our study required the addition of HRP/H_2O_2 or the oxidizing agent $K_3Fe(CN)_6$. The rate of catalysis was

about 80% that of curcumin for the enzyme, and 50% for the oxidant. Using LC-MS and NMR studies, the major products of the HRP and $K_3Fe(CN)_6$ mediated transformations were identified as the glucuronidated analog of the bicyclopentadione isomers. These studies imply that curcumin glucuronide can undergo the same oxidative transformation described for curcumin (Figure 3.4), and that curcumin-glucuronide could be subjected to further metabolism by peroxidase enzymes *in vivo*. The products of curcumin-glucuronide oxidation could contribute to the biological activities of curcumin.

The study by Pfeiffer et al found rapid degradtion of curcumin-glucuronide in pH 7.5 phosphate buffer at 37 ºC at rates higher than that of curcumin (Pfeiffer et al. 2006). In contrast, we found that the curcumin-glucuronide showed virtually no reactivity in ammonium acetate buffer at the same pH 7.5 at room temperature, compared to the rapid degradation of curcumin in the same system. It is not clear what accounts for the differences seen in these studies, even though the higher temperature (37 ºC) employed the first study is expected to increase the reaction rates overall.

The inhibitory effect of the glucuronic acid substituent on the autoxidation of curcumin is similar to what was observed for methylcurcumin; blocking one of the phenolic hydroxyls resulted in marked decrease in the autoxidation rate but still allowed for chemical and peroxidase-catalyzed oxidation. The steps following the initial hydrogen abstraction, including radical cyclization, oxygenation, and exchange of water to form bicyclopentadiones, are presumed to occur without

further interference from the glucuronide. The glucuronic acid moiety was attached to the hydroxyl of the R" ring in the bicyclopentadione.

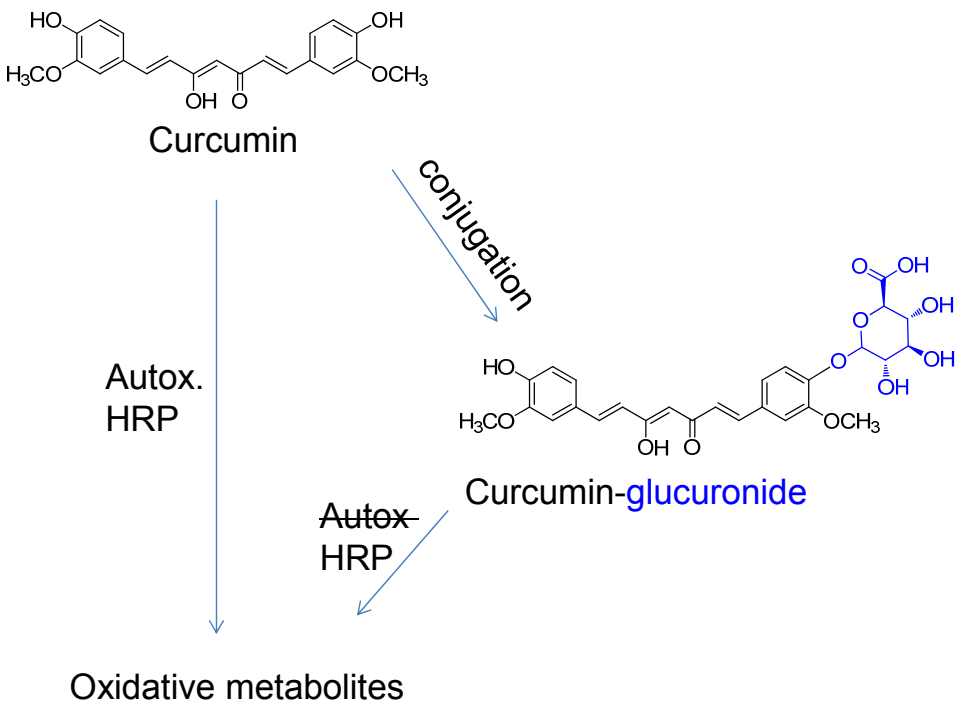

FIGURE 3.4 Oxidative transformation of curcumin and curcumin-glucuronide.

Curcumin-glucuronide as a metabolism dependent pro-drug

Our data suggests that curcumin-glucuronide is not an inert phase II metabolite of curcumin but can be further oxygenated by peroxidase enzymes to generate potentially bioactive products. There are other exceptions to the notion that glucuronidation is solely a detoxifying mechanism. This long-accepted view changed with the discovery that morphine 6-glucuronide was up to 20 fold more potent than morphine (Pasternak et al. 1987) Subsequently, glucuronides were found to represent pharmacologically active forms of other drugs such as the

serotonin 5-HT2A-receptor antagonist sarpogrelate, or the CYP2C8 inhibitor gemfibrozil (Kim et al. 2013; Ogilvie et al. 2006). Gemfibrozil is a presumed metabolism-dependent inhibitor of its target, requiring further transformation to reactive aldehydes that adduct to the protein.

We hypothesize that curcumin glucuronide can exhibit metabolism-dependent activity, requiring oxidative activation to reactive products. Even though glucuronides are typically too hydrophilic to penetrate the cells, the unusual lipophilicity of curcumin-glucuronide has been reported, which could allow for its distribution into different organs (Pfeiffer et al. 2006). In fact, morphine 6-glucuronide shows high penetration into the brain despite its high polarity and low blood brain barrier permeability, possibly due to the involvement of active transport systems (Sattari, Routledge, and Mashayekhi 2011).

Glucuronidation may also contribute to the biological activities of curcumin by serving as a storage mechanism. The glucuronide conjugate of curcumin is more stable to autoxidation, and could be less susceptible to further metabolism, allow for 'intact' transportation to the sites as action where hydrolysis occurs. The notion that glucuronide conjugates may represents a 'transporter form' of a drug is well established, and has been exploited to deliver drugs directly to the site of cancers, e.g. doxorubicin (Weyel et al. 2000).

CHAPTER 4

SUMMARY AND FUTURE DIRECTIONS

The oxidative transformation of curcumin to a dioxygenated bicyclopentadione is a recent discovery in our laboratory. We hypothesize that the products of this transformation are direct mediators of some of the many bioactivities of curcumin. My approach in testing this hypothesis has been (1) to isolate and identify the oxidative products from *in vitro* model reactions, and (2), to elucidate the mechanism of formation of the isolated products.

I have successfully isolated ten novel products of this transformation, including four reaction intermediates, and have completed their structural identification using HPLC-UV, LC-MS, and a combination of 1D and 2D NMR methods. Mechanistic studies on the incorporation of ^{2}H and ^{18}O into the oxidative metabolites during reactions with $^{2}H_2O$, $H_2{}^{18}O$, and $^{18}O_2$, enabled us to determine the mechanism of oxidative transformation of curcumin. The reaction is initiated by H-abstraction from either of the phenolic hydroxyls. The resulting phenoxyl radical migrates into the heptadienedione chain to form a quinone methide and carbon centered radical at C2. The radical participates in 5-exo cyclization to form a cyclopentadione ring of C-2 to C6. Oxygen addition to the resulting radical (at C-7) forms a peroxyl radical and subsequently an endoperoxide, followed by S_Hi carbon radical attack on the endoperoxide to form a spiroepoxide. The spiroepoxide **6** undergoes water exchange during

transformation to a vinylether **7** that is an immediate precursor to the final bicyclopentadione **8** (Figure 2.16). The phenolic glucuronide of curcumin undergoes enzymatic oxidative transformation to generate the bicyclopentadione-glucuronide, suggesting the same reaction mechanism as curcumin. The curcumin quinone methide is implicated as the direct mediator of the topoisomerase-poisoning effect of curcumin, supporting our hypothesis of the oxidative metabolites as contributors to the bioactivities of curcumin.

Establishing the *in vivo* formation of the oxidative metabolites of curcumin (and of that of its glucuronide conjugate) is an important part in supporting a role for oxidative metabolism in the biological activities of curcumin. We have developed stable isotope dilution mass spectrometry (MS) methods to detect and quantify curcumin, curcumin glucuronide, and their respective bicyclopentadione products in plasma. We have synthesized d_6-labeled standards to be used in the quantification. Preliminary data by our group shows that the final bicyclopentadione product of curcumin oxidation is found in human and mouse plasma after oral dosage of curcumin.

Future pharmacokinetic studies in the laboratory will help determine the rate and extent of the formation of the oxidative metabolites in human subjects and in mice. Mouse studies will allow for tissue distribution to be evaluated by harvesting organs after administration of [$^{14}C_2$]curcumin tracer. The formation of reactive intermediates during the oxidation transformation of curcumin should be an important consideration in these studies, as adduction to biomolecules is expected to limit the amount of free compound that can be detected in the

tissues. The amounts of the free metabolites detected therefore are likely to be a partial reflection of the extent of oxidative transformation *in vivo*. Further, it may be that failure to find abundant levels of these metabolites, or at all, does not preclude their formation, especially at the sites of action. Exploring contribution of peroxidase enzymes versus autoxidative transformation to the formation of the oxidative metabolites is also an interesting avenue of study.

Are the oxidative metabolites biologically active?

Curcumin modulates more than 100 cellular targets, and many of these are presumed to be through direct interaction. The antioxidant and electrophilic properties of curcumin primarily are implicated in its ability to modulate signaling in cells. As an antioxidant, curcumin can modulate the oxidative tone in cells due to its ability to inhibit lipid peroxidation and reduce ROS (Jat et al. 2013). Its electrophilic properties allow for covalent interaction with protein thiols and other nucleophilic protein residues (Awasthi et al. 2000). However, it is unlikely that curcumin's antioxidant and weak electrophilic properties can account for its effects on more than 100 proteins. The exact nature of the chemical interaction between curcumin and its targets therefore remains to be determined.

Furthermore, curcumin has shown systemic effects in a wide range of preclinical disease models despite what one would consider to be sub-therapeutic plasma levels. The IC_{50} values reported for curcumin *in vitro* against anti-inflammatory targets COX-2 and NF-κB are typically in the 10 μM to 20 μM range, which is orders of magnitude higher than the maximum reported plasma

levels (Gafner et al. 2004). Additionally, plasma levels of curcumin are sustained for short periods, with rapid clearance through the kidneys and bile reported (Yang et al. 2007; Lao et al. 2006). Given curcumin's virtual absence in tissues where efficacy has been demonstrated, it has been posited that its effects could be ultimately mediated by its more abundant and/or more potent metabolites (Heger et al. 2014b; Shen and Ji 2012). The pleiotropic effects of curcumin could be reconciled by implicating the involvement of multiple, chemically diverse metabolites, such as those formed during oxidative transformation.

The known curcumin metabolites (e.g., reduction, conjugation and cleavage products) have been shown to retain bioactivity against some targets, but are generally less potent than curcumin (Heger et al. 2014; Pfeiffer et al. 2006). None of these metabolites are implicated as ultimate mediators of curcumin’s effects (Shen and Ji 2012; Heger et al. 2014). The oxidative metabolites represent novel players in the discussion of potentially bioactive curcumin metabolites. The oxidative metabolites represent a range of different-strength nucleophiles (**2**-**8**) and electrophiles (quinone methide and **6**) and are likely to affect different targets. The proposed reaction of the quinone methide with cysteine thiols is illustrated in figure 4.1. The isolation and identification of these metabolites now allow us to assess their biological effects. The overarching hypothesis is that the oxidative metabolites are the ultimate mediators of some of the biological effects of curcumin.

Curcumin quinone methide and spiroepoxide can adduct to protein thiols

There are several examples of phenolic compounds for which bioactivation to a quinone methide is implicated in its biological effects (e.g., eugenol and quercetin) (Thompson, Barhoumi, and Burghardt 1998; Mahmoud et al. 2000). Quinone methides exhibit a wide range of reactivity and biological effects. They mediate the therapeutic effects of anti-cancer agents and through covalent interactions with proteins (tamoxifen) and DNA (mitomycin C), or exert cytoprotective effects due to the induction of NRF2 signaling (nitric oxide-donating aspirin prodrugs) (Fan and Bolton 2001; Peterson and Fisher 1986; Dunlap et al. 2012).

We have already shown data that suggest the curcumin quinone methide acts as an electrophile to mediate its effect on topoisomerase. Many other targets of curcumin are similarly regulated by electrophilic adduction to reactive quinone methides. These include the transcription factor NF-κB. NF-κB is an important target due to its prominent roles in cancer and inflammation. Reactive electrophiles, such as quinone methides and epoxides, inhibit NF-κB activation through covalent modification of Cys-179 in the activation loop of IKKβ (Pandey et al. 2007). Curcumin is a weak electrophile, and preliminary data in our lab suggest that is does not readily adduct to the $IKK\beta_{173\text{-}187}$ peptide. LC-MS analysis of the $IKK\beta_{173\text{-}187}$ peptide before (Figure 4.2A) and after (Figure 4.2B) reaction with autoxidizing curcumin shows that, in the presence of curcumin, the detected *m*/*z* for the peptide increase by 400 amu, equivalent to the addition of **6**, or

curcumin quinone methide + O_2. No adduct was detected with the untransformed curcumin or with the stable curcumin analog, methylcurcumin. We hypothesize that the inhibition of NF-κB by curcumin depends on its oxidative activation to the more reactive quinone methide or spiroepoxide that ultimately adduct to IKK.

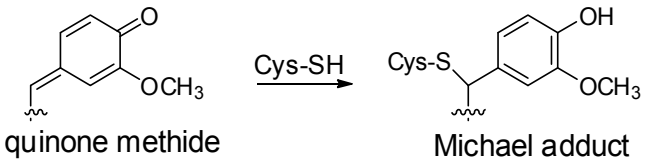

FIGURE 4.1 Proposed reaction of curcumin quinone methide with cysteine thiols.

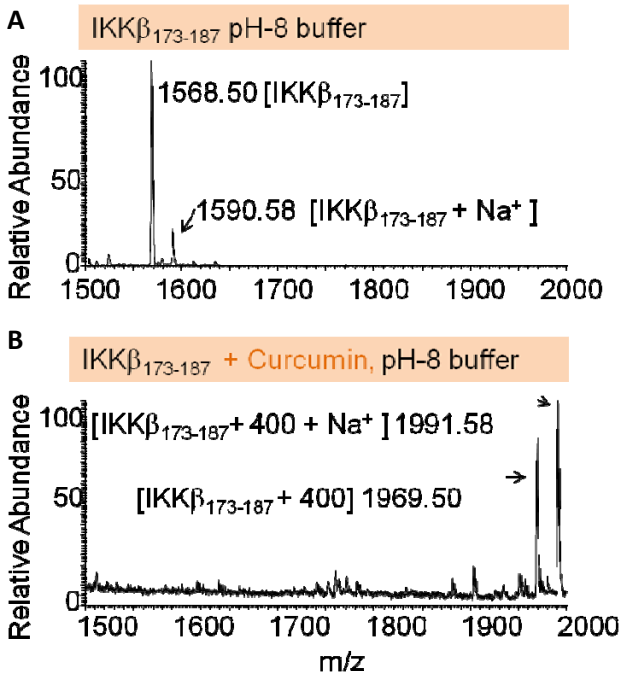

FIGURE 4.2 Reaction of curcumin oxidative metabolite with IKKβ$_{173-187}$.

Preliminary studies also suggest that the spiroepoxide **6** can act as an electrophile and exhibits reactivity towards model cysteine thiol GSH. HPLC analysis shows the consumption of **6a** and **6b** upon the addition of 2 mM GSH

(Figure 4.3A). The putative spiroepoxide-GSH conjugate co-eluted with the left over GSH at 1.9 min in (Figure 4.3B). LC-MS analysis of a reaction of isolated **6** with GSH shows a peak at *m*/*z* 577, representing the expected mass of the adduct (*m*/*z* 706) with the characteristic neutral loss of glutamate (*m*/*z* 129) (Figure 4.3C & D).

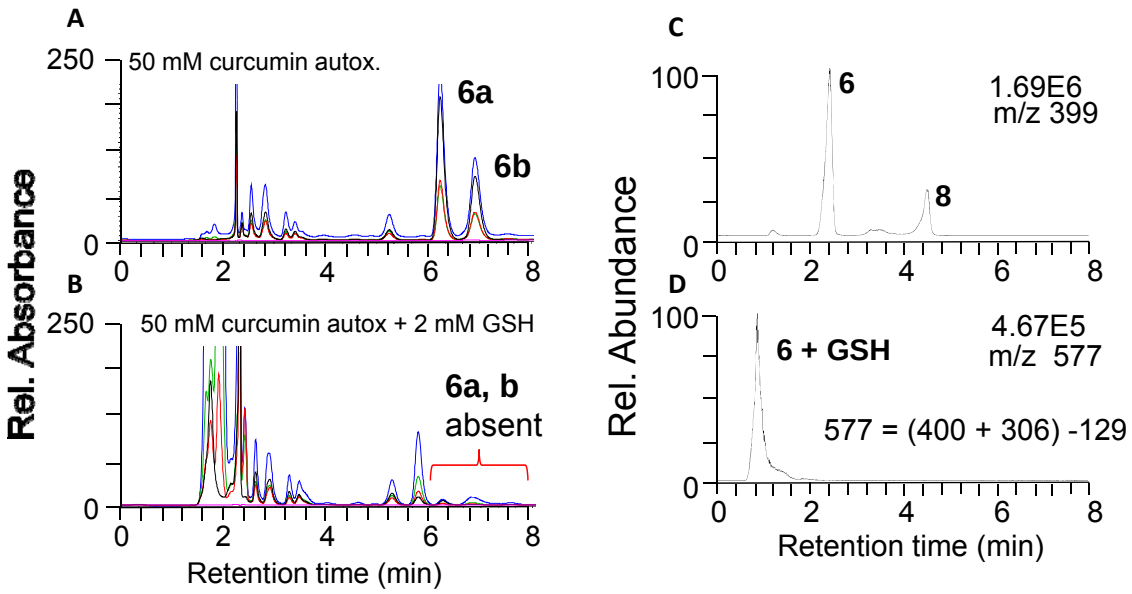

FIGURE 4.3: Reaction of the spiroepoxide **6** with GSH. A and B show HPLC analysis of curcumin autoxidation reactions before and after the addition of 2mM GSH, respectively. C and D show LC-MS analysis of isolated **6a** and **6b** before and after the addition of 2mM GSH, respectively.

The complex nature of the effects of reactive electrophiles is illustrated in the fact that GSH depletion by quinone methide is associated with both cytoprotective as well as cytotoxic effects (Guyton, Thompson, and Kensler 2014). The mutagenic effects of quinone methides is associated with its anticancer bioactivity, but also hepatic toxicity and leukemia (Sharma et al. 2012). Whether the formation of quinone methide and spiroepoxide *in vivo* will

result in protective or toxic effects effects seems to be based on narrow margins. Therefore, the formation of reactive quinone methide and epoxide intermediates usually elicits some concern of possible toxic effects. This concern is greatly lessened in the case of curcumin since no significant adverse effects have so far been reported despite centuries of use.

Curcumin β-diketones may adduct to protein sulfenic acids.

Sullfenic acid modification in proteins has been detected due to specific reactivity with a model compound dimedone. Dimedone is a β-diketone, a feature shared by the bicyclopentadione and the other products of curcumin autoxidation. In fact, the oxidative metabolites represents a range of nucleophilic β-diketones as can be inferred from the extreme polarity of the compounds in HPLC and rapid rate of exchange in the proton attached at C4 from ^{1}H NMR experiments. We hypothesize that the β-diketone moiety of the oxidative metabolites will permit selective reactivity with protein sulfenic acid to inhibit NF-κB, and other proteins regulated by sulfenic acids (Figure 4.4).

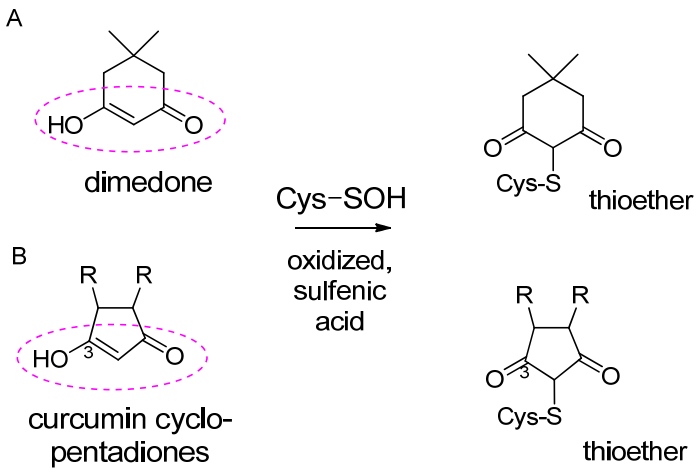

FIGURE 4.4 Proposed reaction of sulfenic acids (Cys-SOH) with dimenone (A) and curcumin cyclopentadione (B)

In conclusion, our studies for the first time present a complete profile of the products of curcumin oxidative transformation and detail their mechanism of formation. The isolation and identification of the oxidative products, along with the elucidation of the reaction mechanism, will allow for future studies in further assessing their involvement in the biological activities of curcumin. Moreover, the oxidative reaction mechanism we describe, and the biological effects we propose for these metabolites, can serve as a model for the metabolism of mechanism of action for other phenolic compounds.

APPENDIX

TABLE A1: ESI/HR/MS and LC-MS/MS analysis of curcumin oxidation products.

Product	Major Product Ions	HR-MS (ESI) $[M-H]^-$		
		Found	Calculated	Error (ppm)
2a	249; 151	401.1249	401.1236	3.2
2b	249; 151	401.1261	401.1236	6.2
3	247; 151; 355; 313	399.1099	399.1080	4.8
4	247; 151; 355; 313	399.1084	399.1080	1.0
5	173; 217; 271	367.1195	367.1182	3.5
6a	259; 315; 355	399.1088	399.1080	2.0
6b	259; 313; 355	399.1086	399.1080	1.5
7a	247; 151	399.1092	399.1080	2.3

Table B1-8: ^{1}H and ^{13}C NMR chemical shifts and couplings of curcumin oxidation products. The spectra were recorded on a Bruker AV-II 600 MHz spectrometer equipped with a cryoprobe. ^{13}C chemical shifts were determined from HMBC and HSQC experiments.

TABLE B1: ^{1}H and ^{13}C NMR chemical shifts and couplings of product **2a** (600.13 MHz, MeOD).

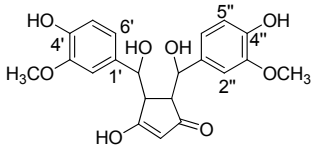

Position	^{1}H (ppm)	Multi-plicity	J (Hz)	^{13}C (ppm)	COSY	HMBC
1	3.76	d	3.18	46	2	2';6'
2	3.34	d	3.18	47	1	1'
3	-	-	-	206	-	-
4	4.7	s	-	104	-	-
5	-	-	-	206	-	-
6	3.34	d	3.18	47	7	1''
7	3.76	d	3.18	46	6	6'';2"
1'	-	-	-	132	-	-
2'	6.41	d	1.8	120	6'	1;6'2'
3'	-	-	-	147	-	-
4'	-	-	-	144	-	-
5'	6.55	d	8.1	112	6'	3';1'
6'	6.59	dd	8.1, 1.86	114	2	1;5';
-OCH_3'	3.62	s	-	54.8	-	3'
1"	-	-	-	132	-	-
2"	6.41	d	1.8	120	6"	1;6"2"
3"	-	-	-	147	-	-
4"	-	-	-	144	-	-
5"	6.55	d	8.1	112	6"	3";1"
6"	6.59	dd	8.1, 1.86	114	2	1;5"
-OCH_3"	3.62	s	-	54.8	-	3"

TABLE B2: ^{1}H and ^{13}C NMR chemical shifts and couplings of product **2b** (600.13 MHz, MeOD).

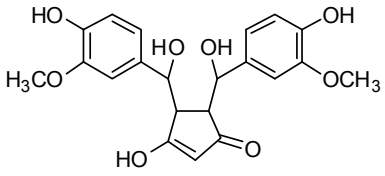

Position	^{1}H (ppm)	Multi-plicity	J (Hz)	^{13}C (ppm)	COSY	HMBC
1	4.51	d	9.0	77	2	2';6';1';3
2	2.30	dd	8.9;2.9	51	1;6	7;1;1';3
3	-	-	-	207	-	-
4	3.84	s	-	x	-	-
5	-	-	-	x	-	-
6	2.52	dd	2.8;3.9	52	2;7	7;1"
7	4.34	d	3.4	73	6	-
1'	-	-	-	x	-	-
2'	6.69	d	1.8	109	$-OCH_3'$	1;6';4'
3'	-	-	-	x	-	-
4'	-	-	-	x	-	-
5'	6.65	d	8.1	114	-	1';3'
6'	6.64	dd	8.2;1.7	119	-	1;2'
$-OCH_3'$	-	s	-	55	2'	3'
1"	-	-	-	x	-	-
2"	6.59	d	1.8	109	$-OCH_3''$	7;6";4"
3"	-	-	-	x	-	-
4"	-	-	-	x	-	-
5"	6.61	d	8.1	114	-	1";3"
6"	6.52	dd	7.9;2.1	118	-	7;2";4"
$-OCH_3''$	-	s	-	55	2"	3"

X = Expected signal not seen.

TABLE B3: ^{1}H and ^{13}C NMR chemical shifts and couplings of product **3** (600.13 MHz, MeOD).

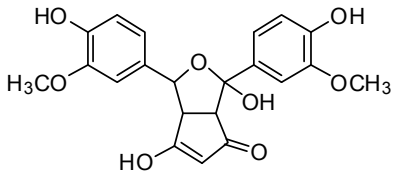

Position	^{1}H (ppm)	Multi-plicity	J (Hz)	^{13}C (ppm)	COSY	HMBC
1	5.23	d	2.4	70	-	2
2	2.57	s	-	64	3	1;6
3	-	-	-	x	-	-
4	5.07	s	-	104	-	-
5	-	-	-	x	-	-
6	3.51	d	2.2	50	5;1';	2
7	-	-	-	x	-	-
1'	-	-	-	135.4	-	-
2'	6.95	d	1.62	108	1; 6';4'	6'
3'	-	-	-	147	-	-
4'	-	-	-	145/144	-	-
5'	6.72	d	8.1	112	1';3'	6'
6'	6.85	dd	8.1;x	118	1,2';4'	2';5'
$-OCH_3$'	3.75/3.58	-	s	55.4	-	3"
1"	-	-		134.8	-	-
2"	6.01	d	1.6	111	4";6"	6"
3"	-	-	-	146.5	-	-
4"	-	-	-	143.6/143	-	-
5"	6.52	d	8.1	112	1";3"	6"
6"	6.29	dd	8.2;1.9	119	2";4"	2";5"
$-OCH_3$"	3.75/3.58	-	s	55.4	-	3"

X = Expected signal not seen.

TABLE B4: ^{1}H and ^{13}C NMR chemical shifts and couplings of product **4** (600.13 MHz, MeOD).

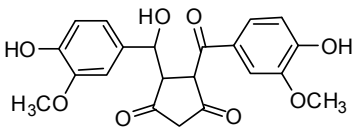

Position	^{1}H (ppm)	Multi-plicity	J (Hz)	^{13}C (ppm)	COSY	HMBC
1	5.26	s	-	69.6	-	2
2	3.23	s	-	58	-	1,6
3	-	-	-	x	-	-
4	x	-	-	x	-	-
5	-	-	-	x	-	-
6	4.66	s	-	53	-	2
7	x	-	-	x	-	-
1’	-	-	-	135.7	-	-
2’	6.80	d	1.2	108	6';4'	6’2’
3’	-	-	-	146.5	-	-
4’	-	-	-	144	-	-
5’	6.54	d	8.1	114	1';3'	3’;1’
6’	6.70	dd	1.44;1.08;7.8;8.16	117.5	2';4'	1;5’;
-OCH_3'	3.86/3.57	s	-	54	3'	3'
1”	-	-	-	134.5		-
2”	7.31	-	1.44	111	6";4"	6"2"
3”	-	-	-	147	-	-
4”	-	-	-	151	-	-
5”	6.75	-	8.28	114	1";3"	3";1"
6”	7.39	dd	1.5;1.74;8.28,8.52	124	2";4"	1;5"
-OCH_3"	3.86/3.57	s	-	54	3"	3"

X = Expected signal not seen.

TABLE B5: ^{1}H and ^{13}C NMR chemical shifts and couplings of product **5** (600.13 MHz, MeOD).

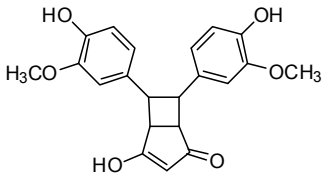

Position	^{1}H (ppm)	Multi-plicity	J (Hz)	^{13}C (ppm)	COSY	HMBC
1	4.55	s	-	72	2	2;2';6';3
2	2.64	d	2.45	51	1	1;5
3	-	-	-	206	-	-
4	x	-	-	x	-	-
5	-	-	-	206	-	-
6	2.64	d	2.45	51	7	7;2
7	4.55	s	-	72	6	6;2";6";5
1'	-	-	-	134	-	-
2';2"	6.71	d	1.68	109	1;6	1;6'; 4'
3';3"	-	-	-	146.7	-	-
4',4"	-	-	-	145	-	-
5';5"	6.66	d	8.1	114	6;	1',3'
6',5"	6.54	dd	8.04, 1.68	118	5;1	1;2';4'
$-OCH_3'$	3.79	s	-	54.7	-	3'
1"	-	-	-	134	-	-
2"	6.71	d	1.68	109	1;6	1;6"; 4"
3"	-	-	-	146.7	-	-
4"	-	-	-	145	-	-
5"	6.66	d	8.1	114	6;	1",3"
6"	6.54	dd	8.04, 1.68	118	5;1	1;2";4"
$-OCH_3"$	3.79	s	-	54.7	-	3"

X = Expected signal not seen.

TABLE B6: ^{1}H and ^{13}C NMR chemical shifts and couplings of product **6a** (MeOD).

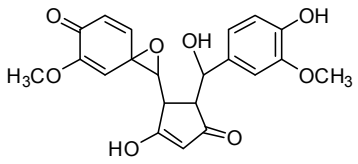

Position	^{1}H (ppm)	Multi-plicity	J (Hz)	^{13}C (ppm)	COSY	HMBC	NOESY
1	3.28	d	9	68.2	2	6';3	-
2	2.63	dd	1.8, 8.9	44.5	1;6	3,1',1	2";6";6
3	-	-	-	203	-	-	-
4	4.90	s	-	103.5	-	-	-
5	-	-	-	204	-	-	-
6	2.91	dd	2.7, 2.2	57.0	1;7	5;1;2	2;2";6"
7	5.20	d	2.7;	71.5	6	2;6";1"5	6;2";6"
1'	-	-	-	59.2	-	-	-
2'	5.25	d	2.34	111.5	6'	4';6';1'	2
3'	-	-	-	153.5	-	-	-
4'	-	-	-	184	-	-	-
5'	6.32	d	9.90	130.2	6'	3';1'	-
6'	6.52	dd	2.46, 9.96	150.3	5';2'	4',2'	1
$-OCH_3'$	3.6	s	-	54	-	3'	-
1"	-	-	-	135.5	-	-	-
2"	7.06	d	1.9	109.5	6"	7,6",4"	6;2;7
3"	-	-	-	147.3	-	-	-
4"	-	-	-	144.7	-	-	-
5"	6.74	d	8.16	114.0	6"	1";3"	-
6"	6.89	dd	2.0, 8.1	118	5";2"	2";7;4"	6;2;7
$-OCH_3"$	3.8	s	-	55	-	4'	-

-

TABLE B7: ^{1}H and ^{13}C NMR chemical shifts and couplings of product **6b** (600.13 MHz, MeOD).

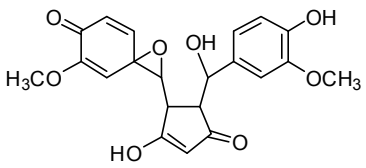

Position	^{1}H (ppm)	Multi-plicity	J (Hz)	^{13}C (ppm)	COSY	HMBC
1	3.40	d	8.26	67.6	2	2;6’
2	2.37	dd	8.34,2.04	42	6,1	3;7;1;6
3	-	-	-	202	-	-
4	4.76	s	-	101.7	-	-
5	-	-	-	205	-	-
6	2.97	dd	7.71, 2.10	55	7;2	1;7;1”5
7	4.82	d	7.60	76	6	2;2”6”;5
1’	-	-	-	59.5	-	
2’	5.28	d	2.44	111	6’	4’;3’,6’
3’	-	-	-	153.5	-	-
4’	-	-	-	181	-	-
5’	6.36	d	9.90	130	6’	3’;1'
6’	6.59	dd	2.48,9.90	149.8	5’;2’	4’;2’
$-OCH_3$'	3.6	s	-	54	-	3’
1”	-	-	-	132	-	-
2”	7.01	d	1.74	110.5	6”;	7;6”;4”
3”	-	-	-	147	-	-
4”	-	-	-	146	-	-
5”	6.72	d	8.10	114	6”	1”;3”
6”	6.84	dd	8.10,1.92	119.8	5”;2”	2”;7;4”
$-OCH_3$"	3.8	s	-	54	-	4’

TABLE B8: ^{1}H and ^{13}C NMR chemical shifts and couplings of product **7a** (600.13 MHz, $CDCl_3$)

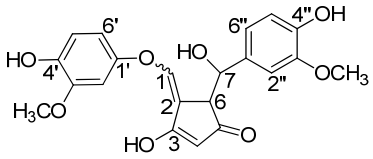

Position	^{1}H (ppm)	Multi-plicity	J (Hz)	^{13}C (ppm)	COSY	HMBC
1	7.15	d	1.20	142.3	6	6; 2; 3
2	-	-	-	108.7	-	-
3	-	-	-	187.6	-	-
4	4.60	s	-	103.6	-	6; 2
5	-	-	-	210.7	-	-
6	6.68	dd	4.04, 1.43	55.2	7; 1	5
7	5.30	d	4.08	73.1	6	2
1’	-	-	-	147	-	-
2’	6.43	d	2.72	104.1	6’	6’; 4’
3’	-	-	-	147.3	-	-
4’	-	-	-	143.5	-	-
5’	6.70	d	8.65	113.5	6’	3’
6’	6.37	dd	8.62; 2.72	111.4	5’; 2’	2’; 4’; 3’
$-OCH_3$’	3.76	-	-	55.3	-	-
1”	-	-	-	131.8	-	-
2”	6.80	d	2.00	109.8	6”	1; 6”; 4”
3”	-	-	-	147.3	-	-
4”	-	-	-	142.7	-	-
5”	6.74	d	8.11	114.2	6”	3”
6”	6.65	dd	8.12; 1.84	118.9	5”; 2”	1; 2”4”
$-OCH_3$”	3.73	-	-	55.3	-	-

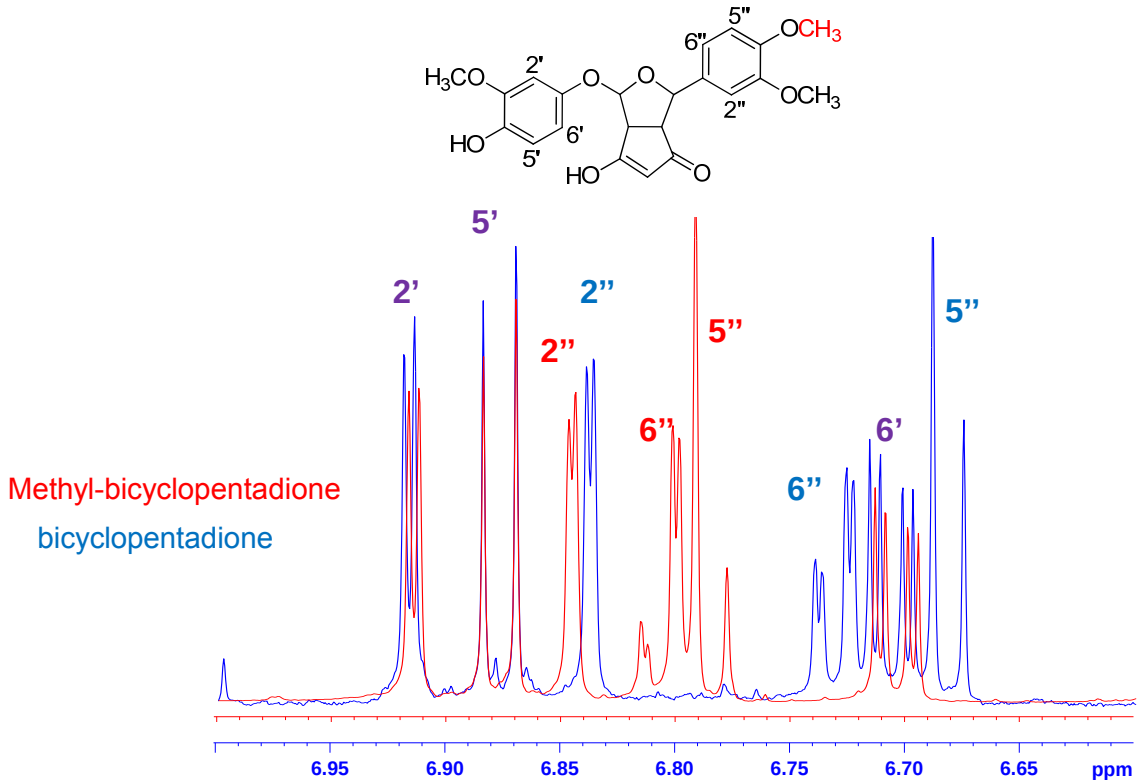

FIGURE B1: Partial ^{1}H NMR Spectra of the bicyclopentadione **8** and Methyl-bicyclopentadione. Protons in the R" ring of methyl-bicyclopentadione are shifted relative to those of **8**. The spectra were acquired in acetone-d_3.

FIGURE B2: NMR Spectra of **2a**

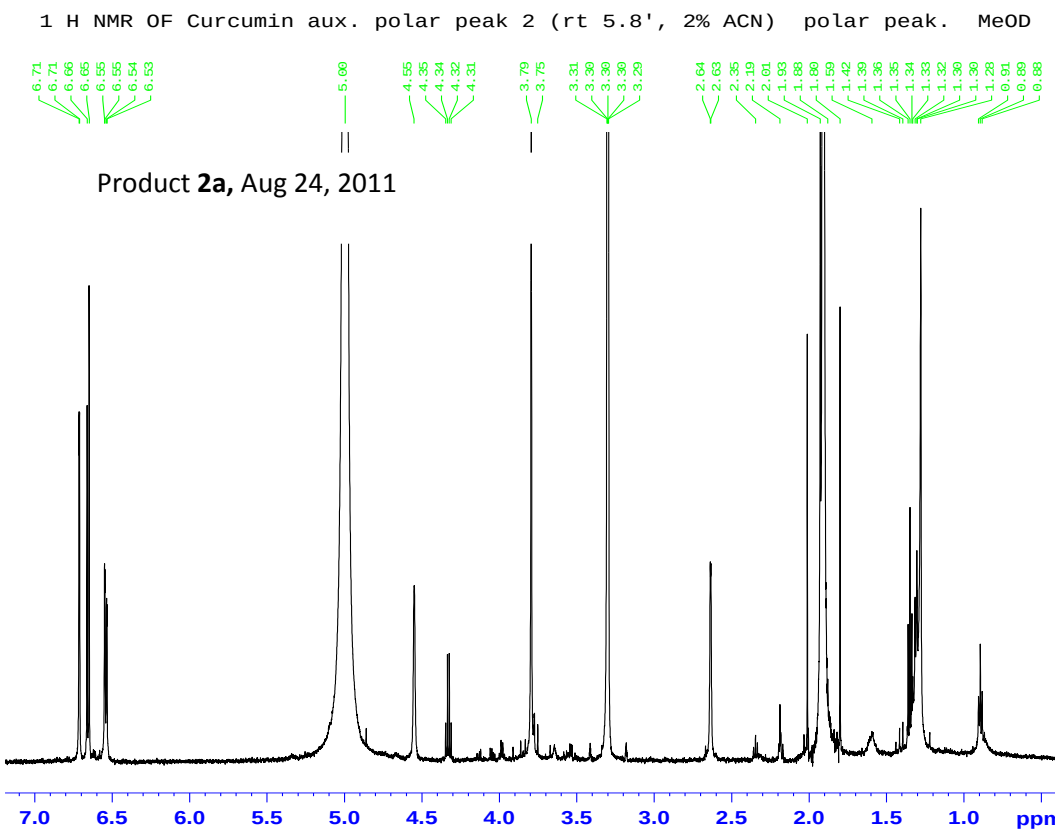

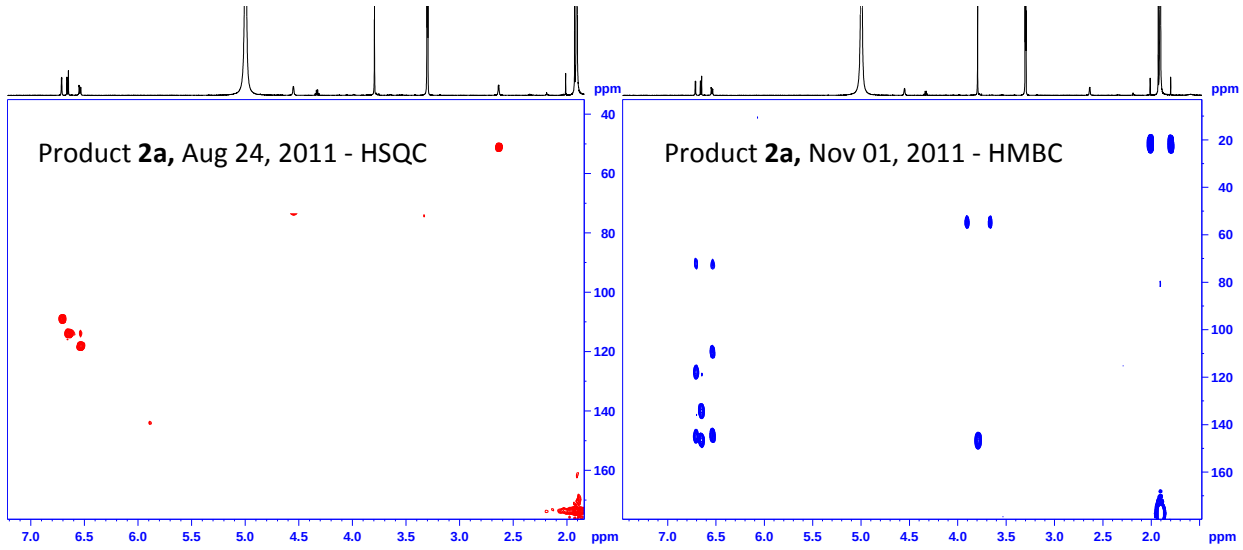

FIGURE B3: NMR Spectra of **2b**

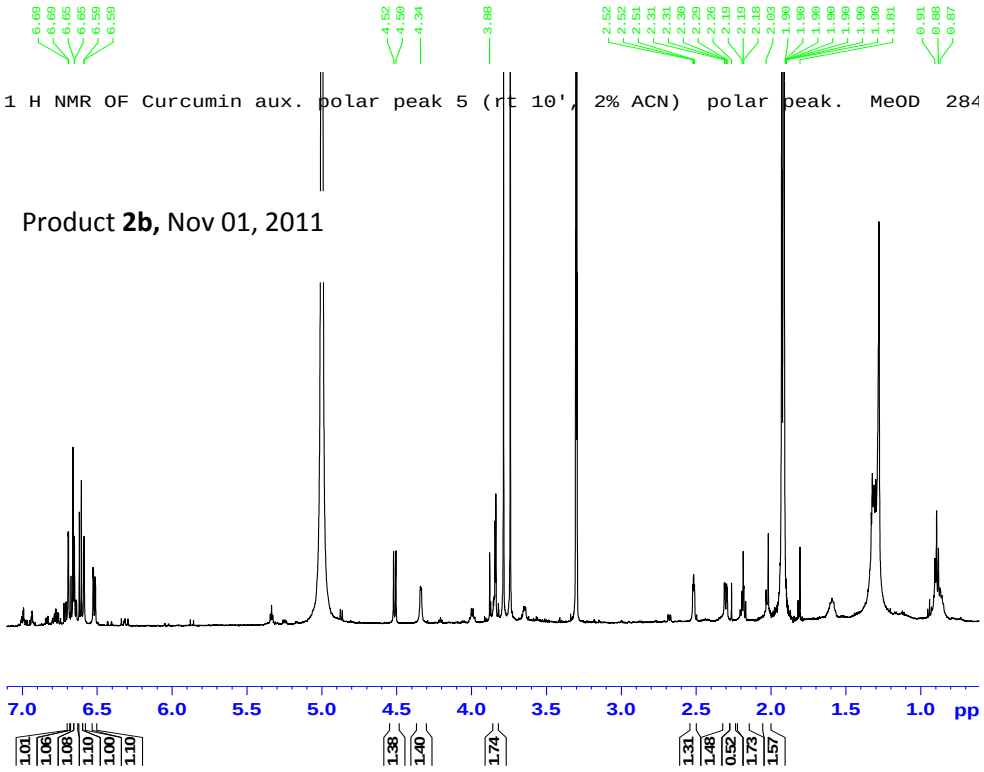

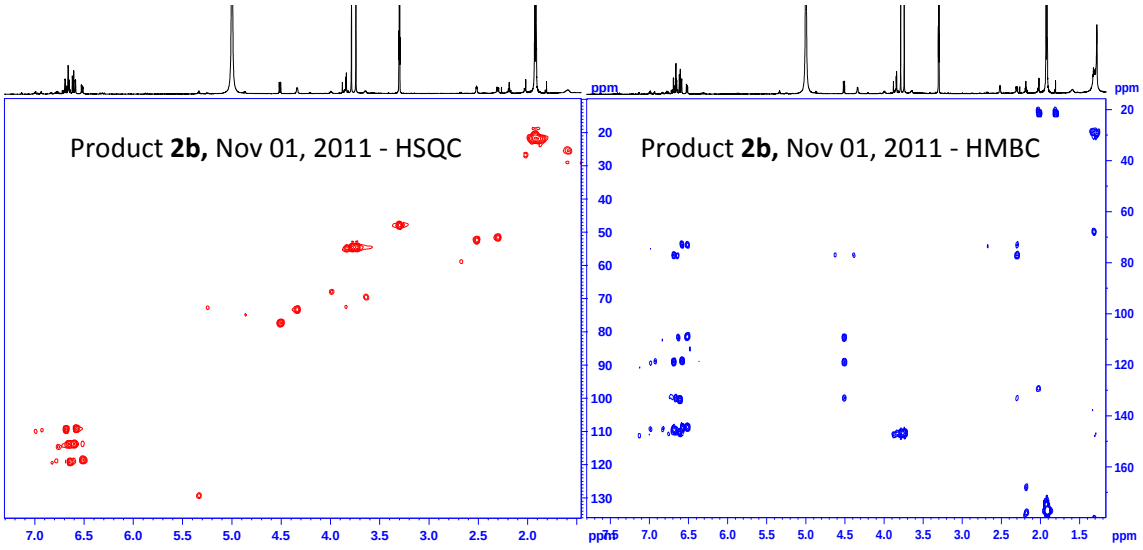

FIGURE B4: NMR Spectra of **3**

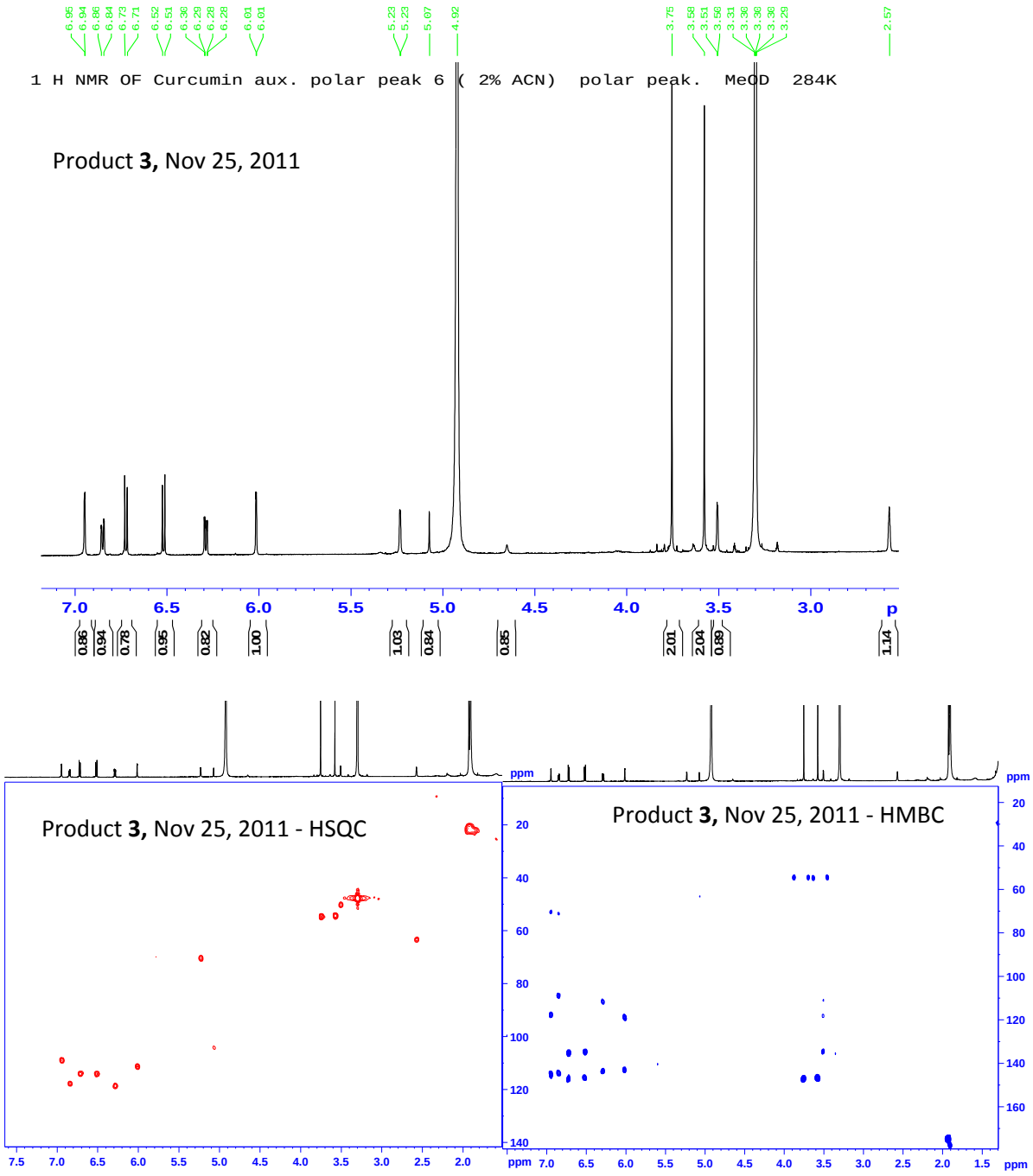

FIGURE B5: NMR Spectra of **4**

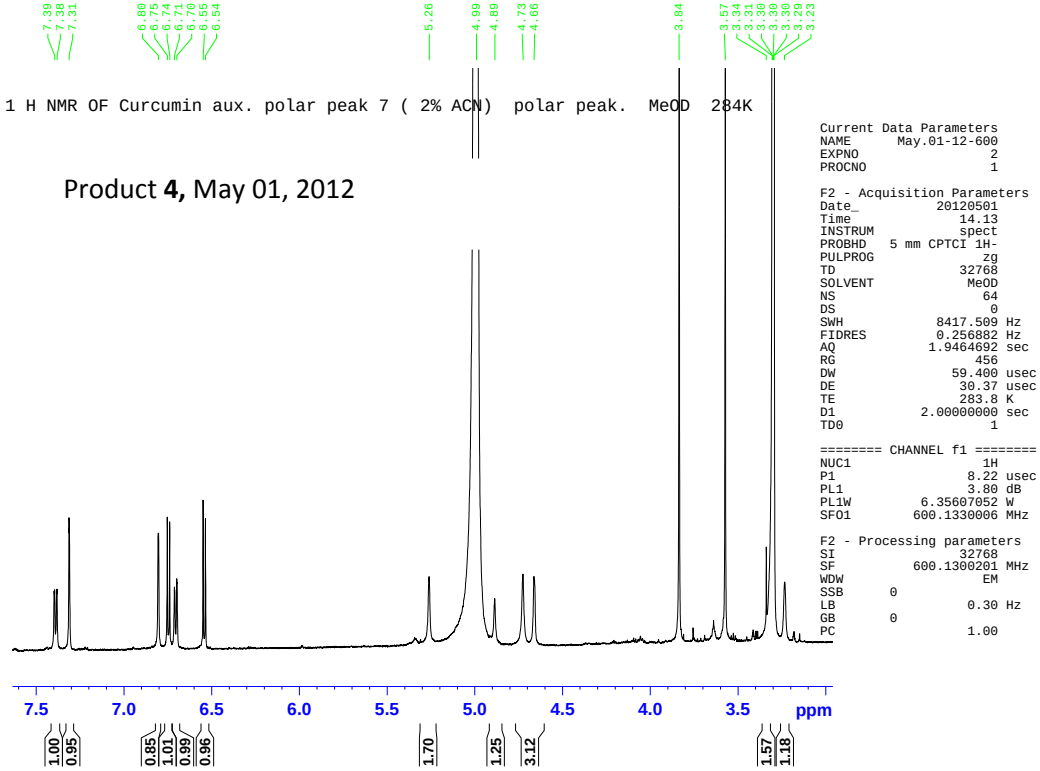

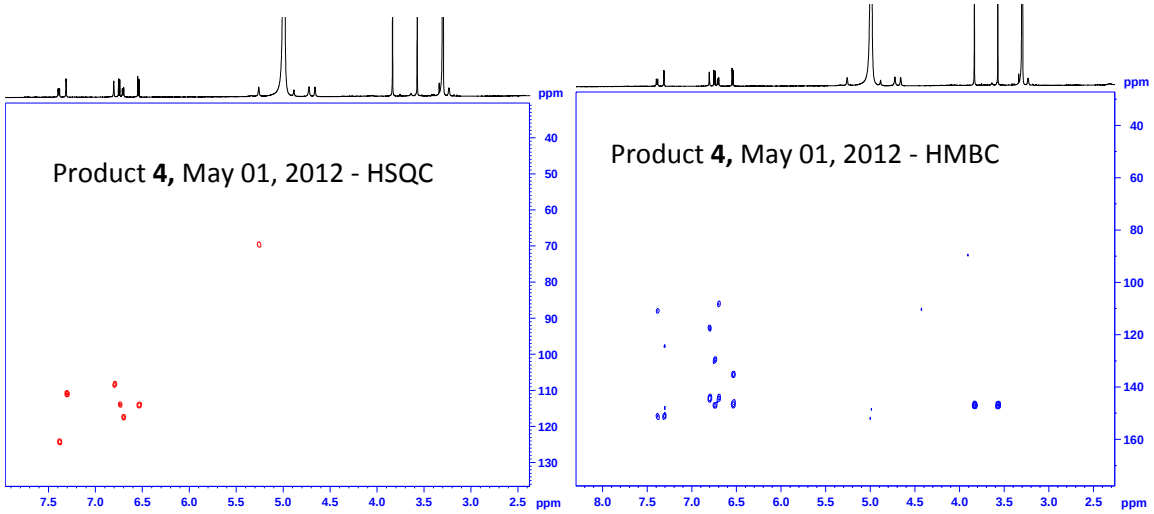

FIGURE B6: NMR Spectra of **5**

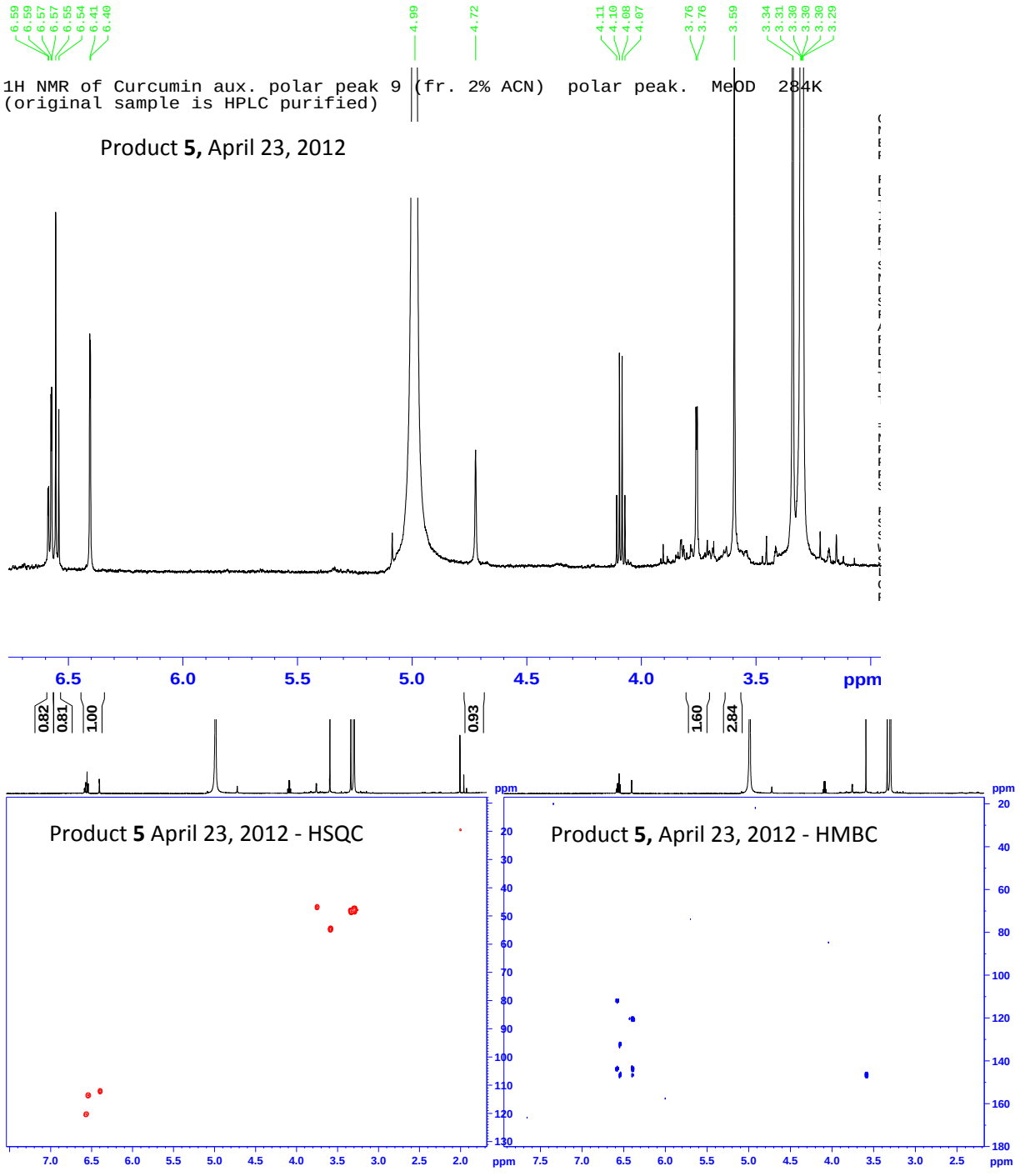

FIGURE B7: NMR Spectra of **6a**

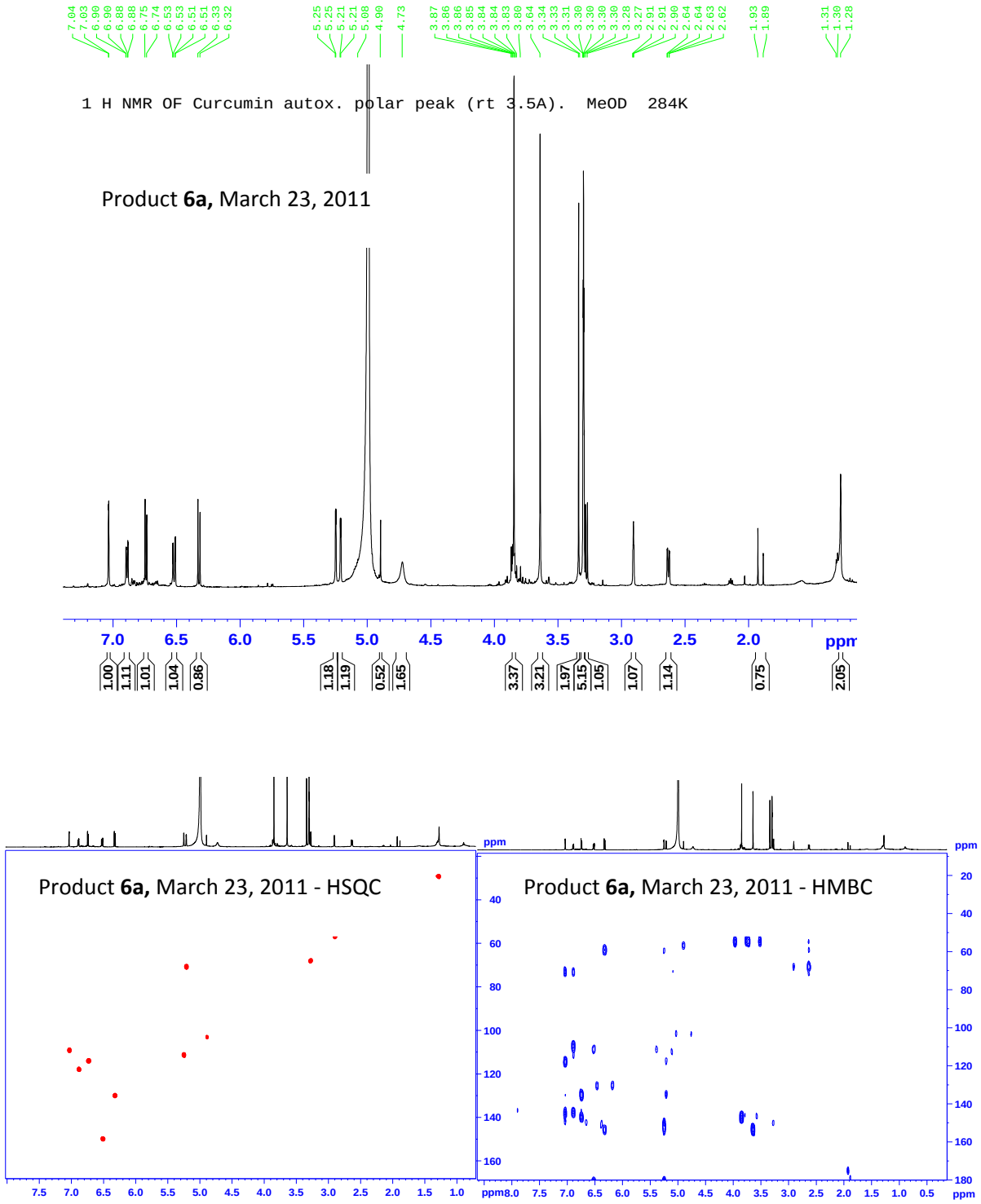

FIGURE B8: NMR Spectra of **6b**

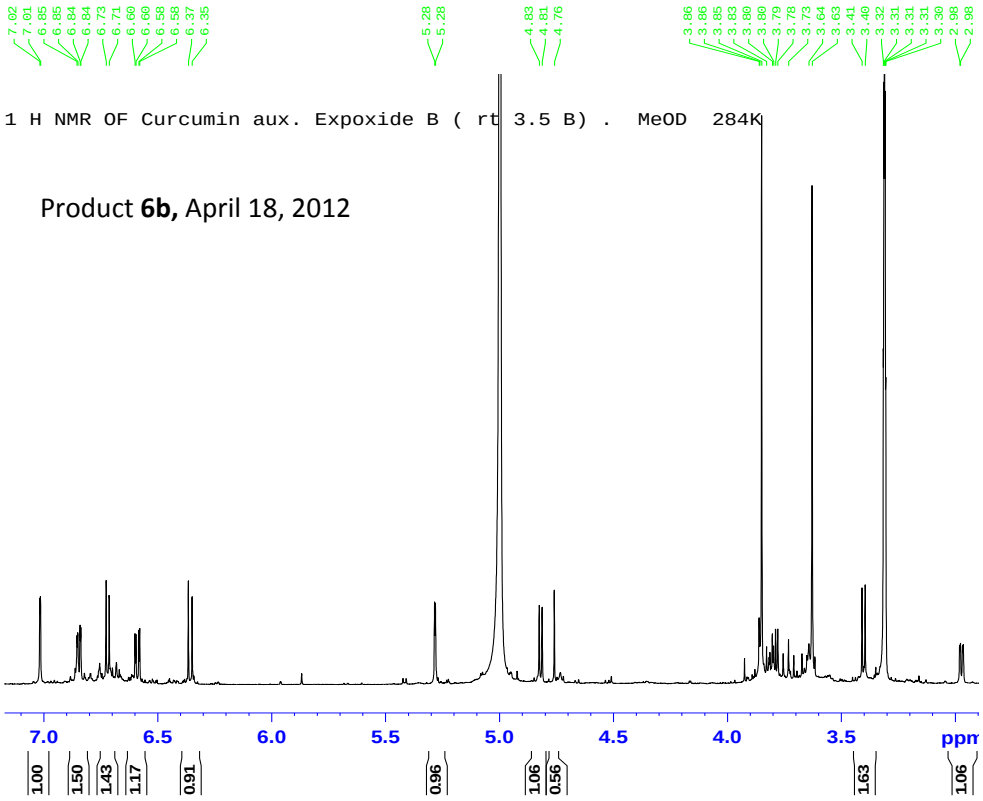

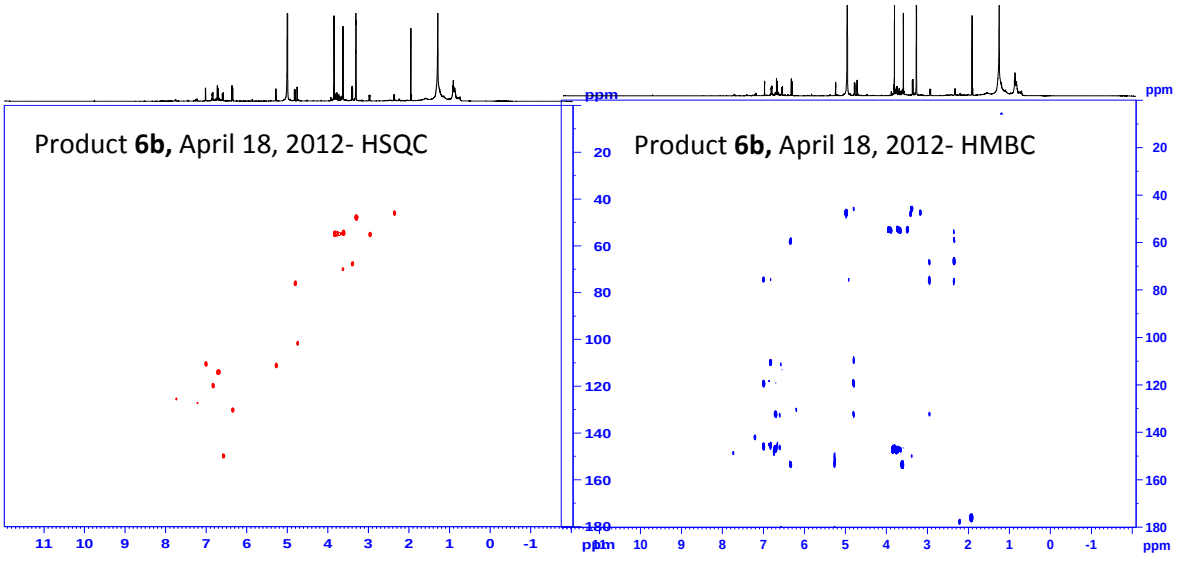

FIGURE B9: NMR Spectra of **7a**

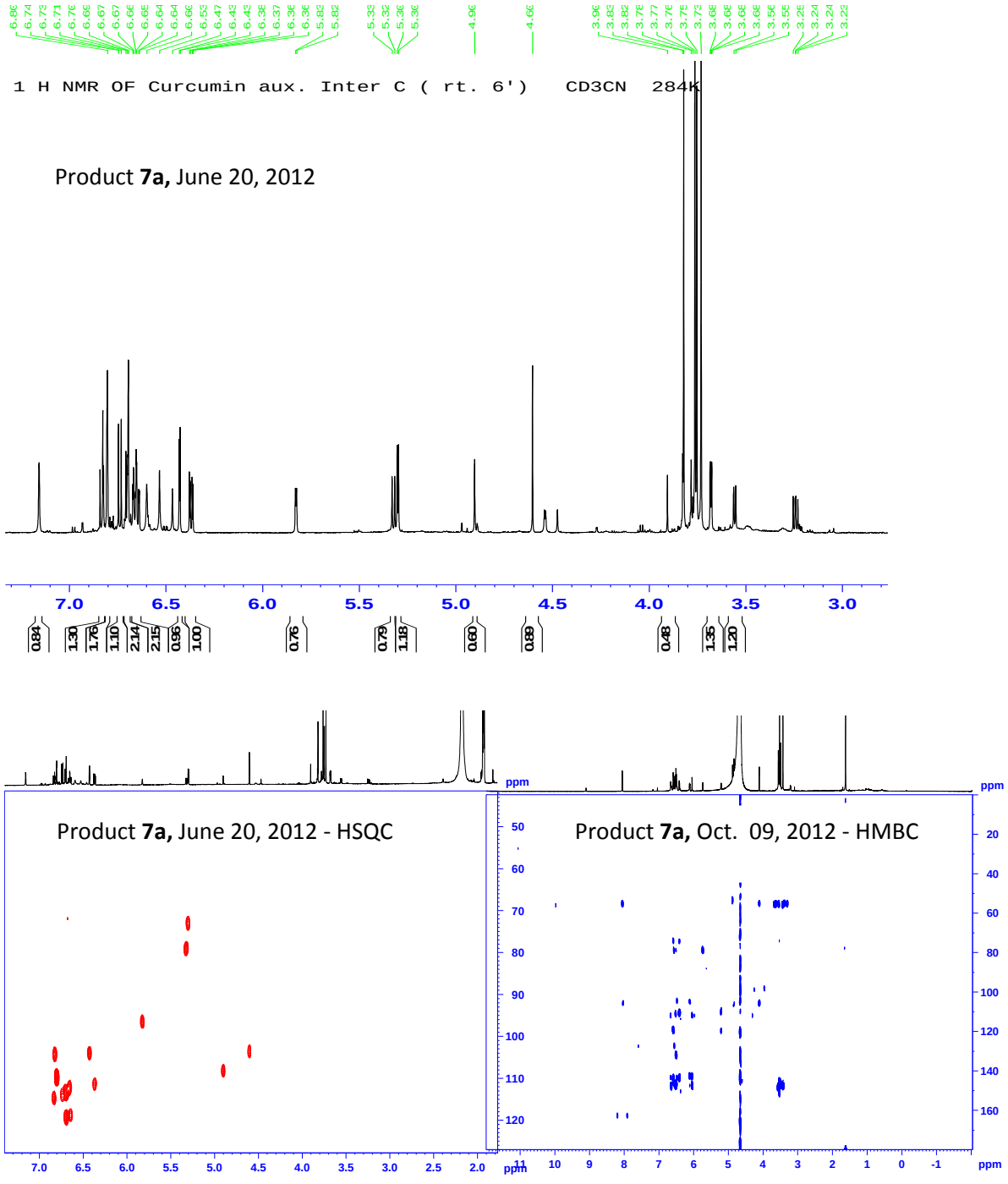

REFERENCES

Aggarwal, B. B., & Harikumar, K. B. (2009). Potential therapeutic effects of curcumin, the anti-inflammatory agent, against neurodegenerative, cardiovascular, pulmonary, metabolic, autoimmune and neoplastic diseases. *The International Journal of Biochemistry & Cell Biology*, *41*(1), 40–59.

Al-Amiery, A. A., Kadhum, A. A. H., et al. (2013). Synthesis and antioxidant activities of novel 5-chlorocurcumin, complemented by semiempirical calculations. *Bioinorganic Chemistry and Applications*, *2013*, 354982.

Anand, P., Thomas, S. G., et al. (2008). Biological activities of curcumin and its analogues (Congeners) made by man and Mother Nature. *Biochemical Pharmacology*, *76*(11), 1590–1611.

Aoki, H., Takada, Y., et al. (2007). Evidence that curcumin suppresses the growth of malignant gliomas in vitro and in vivo through induction of autophagy: role of Akt and extracellular signal-regulated kinase signaling pathways. *Molecular Pharmacology*, *72*(1), 29–39.

Awasthi, S., Pandya, U., et al. (2000). Curcumin–glutathione interactions and the role of human glutathione S-transferase P1-1. *Chemico-Biological Interactions*, *128*(1), 19–38.

Balasubramanian, K. (2006). Molecular Orbital Basis for Yellow Curry Spice Curcumin’s Prevention of Alzheimer's Disease. *Journal of Agricultural and Food Chemistry*, *54*(10), 3512–3520.

Barclay, L. R., Vinqvist, M. R., et al. (2000). On the antioxidant mechanism of curcumin: classical methods are needed to determine antioxidant mechanism and activity. *Organic Letters*, *2*(18), 2841–3.

Barzegar, A., & Moosavi-Movahedi, A. A. (2011). Intracellular ROS protection efficiency and free radical-scavenging activity of curcumin. *PloS One*, *6*(10), e26012.

Belcaro, G., Cesarone, M. R., et al. (2010). Efficacy and safety of Meriva®, a curcumin-phosphatidylcholine complex, during extended administration in osteoarthritis patients. *Alternative Medicine Review*, *15*(4), 337–44.

Bender, R. P., Ham, L., & Osheroff, N. (2007). Quinone-induced enhancement of DNA cleavage by human topoisomerase IIalpha: adduction of cysteine residues 392 and 405. *Biochemistry*, *46*(10), 2856–64.

Bera, R., Sahoo, B. K., Ghosh, K. S., & Dasgupta, S. (2008). Studies on the interaction of isoxazolcurcumin with calf thymus DNA. *International Journal of Biological Macromolecules*, *42*(1), 14–21.

Chandran, B., & Goel, A. (2012). A randomized, pilot study to assess the efficacy and safety of curcumin in patients with active rheumatoid arthritis. *Phytotherapy Research : PTR*, *26*(11), 1719–25.

Chanpoo, M., Petchpiboonthai, H., et al. (2010). Effect of curcumin in the amelioration of pancreatic islets in streptozotocin-induced diabetic mice. *Journal of the Medical Association of Thailand*, S152–9.

Chen, F., & Shi, X. (2002). Signaling from toxic metals to NF-kappaB and beyond: not just a matter of reactive oxygen species. *Environmental Health Perspectives*, *110 Suppl* , 807–11.

Chen, Y., Shu, W., et al. (2007). Curcumin, both histone deacetylase and p300/CBP-specific inhibitor, represses the activity of nuclear factor kappa B and Notch 1 in Raji cells. Basic & Clinical Pharmacology & Toxicology, 101(6), 427–33.

Chignell, C. F., Bilskj, P., et al. (1994). Spectral and photochemical properties of curcumin. *Photochemistry and Photobiology*, *59*(3), 295–302.

Chuengsamarn, S., Rattanamongkolgul, S., et al. (2014). Reduction of atherogenic risk in patients with type 2 diabetes by curcuminoid extract: a randomized controlled trial. *The Journal of Nutritional Biochemistry*, *25*(2), 144–50.

Cooper, C. E., Patel, R. P., et al. (2002). Nanotransducers in cellular redox signaling: modification of thiols by reactive oxygen and nitrogen species. *Trends in Biochemical Sciences*, *27*(10), 489–492.

Denk, A., Goebeler, M., et al. (2001). Activation of NF-kappa B via the Ikappa B kinase complex is both essential and sufficient for proinflammatory gene expression in primary endothelial cells. *The Journal of Biological Chemistry*, *276*(30), 28451–8.

Dennehy, M. K., Richards, K. A. M., et al. (2006). Cytosolic and nuclear protein targets of thiol-reactive electrophiles. *Chemical Research in Toxicology*, *19*(1), 20–9.

Deweese, J. E., & Osheroff, N. (2009). The DNA cleavage reaction of topoisomerase II: wolf in sheep's clothing. *Nucleic Acids Research*, *37*(3), 738–48.

Dunlap, T., Piyankarage, S. C., et al. (2012). Quinone-induced activation of Keap1/Nrf2 signaling by aspirin prodrugs masquerading as nitric oxide. *Chemical Research in Toxicology*, *25*(12), 2725–36.

Fan, P. W., & Bolton, J. L. (2001). Bioactivation of tamoxifen to metabolite E quinone methide: reaction with glutathione and DNA. *Drug Metabolism and Disposition*, *29*(6), 891–6.

Gafner, S., Lee, S., et al. (2004). Biologic evaluation of curcumin and structural derivatives in cancer chemoprevention model systems. *Phytochemistry*, *65*(21), 2849–59.

Goel, A., Kunnumakkara, A. B., & Aggarwal, B. B. (2008). Curcumin as "Curecumin": From kitchen to clinic. *Biochemical Pharmacology*, *75*(4), 787–809.

Gordon, O. N., & Schneider, C. (2012). Vanillin and ferulic acid: not the major degradation products of curcumin. *Trends in Molecular Medicine*, *18*(7), 361–363.

Griesser, M., Pistis, V., et al. (2011). Autoxidative and Cyclooxygenase-2 Catalyzed Transformation of the Dietary Chemopreventive Agent Curcumin. *Journal of Biological Chemistry*, *286*(2), 1114–1124.

Grynkiewicz, G., & Ślifirski, P. (2012). Curcumin and curcuminoids in quest for medicinal status. *Acta Biochimica Polonica*, *59*(2), 201–12.

Guyton, K. Z., Thompson, J. A., & Kensler, T. W. (1993). Role of quinone methide in the in vitro toxicity of the skin tumor promoter butylated hydroxytoluene hydroperoxide. *Chemical Research in Toxicology*, *6*(5), 731–8.

Hanai, H., Iida, T., et al. (2006). Curcumin maintenance therapy for ulcerative colitis: randomized, multicenter, double-blind, placebo-controlled trial. *Clinical Gastroenterology and Hepatology, 4*(12), 1502–6.

He, Z., Shi, C., et al. (2011). Upregulation of p53 expression in patients with colorectal cancer by administration of curcumin. *Cancer Investigation*, *29*(3), 208–13.

Heger, M., van Golen, R. F., et al. (2014). The molecular basis for the pharmacokinetics and pharmacodynamics of curcumin and its metabolites in relation to cancer. *Pharmacological Reviews*, *66*(1), 222–307.

Hishikawa, N., Takahashi, Y., et al. (2012). Effects of turmeric on Alzheimer's disease with behavioral and psychological symptoms of dementia. *Ayu*, *33*(4), 499–504.

Hoehle, S. I., Pfeiffer, E., Sólyom, A. M., & Metzler, M. (2006). Metabolism of curcuminoids in tissue slices and subcellular fractions from rat liver. *Journal of Agricultural and Food Chemistry*, *54*(3), 756–64.

Holder, G. M., Plummer, J. L., & Ryan, A. J. (1978). The Metabolism and Excretion of Curcumin (1,7-Bis-(4-hydroxy-3-methoxyphenyl)-1,6-heptadiene-3,5-dione) in the Rat. *Xenobiotica*, *8*(12), 761–768.

Hong, D., Zeng, X., et al. (2010). Altered profiles of gene expression in curcumin-treated rats with experimentally induced myocardial infarction. *Pharmacological Research*, *61*(2), 142–8.

Huang, M. T., Lou, Y. R., et al. (1998). Effect of dietary curcumin and dibenzoylmethane on formation of 7,12-dimethylbenz[a]anthracene-induced mammary tumors and lymphomas/leukemias in Sencar mice. *Carcinogenesis*, *19*(9), 1697–700.

Huang, M. T., Newmark, H. L., & Frenkel, K. (1997). Inhibitory effects of curcumin on tumorigenesis in mice. *Journal of Cellular Biochemistry. Supplement*, *27*, 26–34.

Ireson, C., Orr, S., et al. (2001). Characterization of Metabolites of the Chemopreventive Agent Curcumin in Human and Rat Hepatocytes and in the Rat in Vivo, and Evaluation of Their Ability to Inhibit Phorbol Ester-induced Prostaglandin E2 Production. *Cancer Res.*, *61*(3), 1058–1064.

Jacob, A., Wu, R., Zhou, M., & Wang, P. (2007). Mechanism of the Anti-inflammatory Effect of Curcumin: PPAR-gamma Activation. *PPAR Research*, *2007*, 89369.

Jat, D., Parihar, P., et al.. (2013). Curcumin reduces oxidative damage by increasing reduced glutathione and preventing membrane permeability transition in isolated brain mitochondria. *Cellular and Molecular Biology, 59 Suppl*, OL1899–905.

Jeong, J., Jung, Y., et al. (2011). Novel oxidative modifications in redox-active cysteine residues. *Molecular & Cellular Proteomics*, *10*(3), M110.000513.

Johnson, J. J., & Mukhtar, H. (2007). Curcumin for chemoprevention of colon cancer. *Cancer Letters*, *255*(2), 170–181.

Jovanovic, S. V., Boone, C. W., et al. (2001). How Curcumin Works Preferentially with Water Soluble Antioxidants. *Journal of the American Chemical Society*, *123*(13), 3064–3068.

Jurrmann, N., Brigelius-Flohe, R., & Bol, G. (2005). Curcumin Blocks Interleukin-1 (IL-1) Signaling by Inhibiting the Recruitment of the IL-1 Receptor-Associated Kinase IRAK in Murine Thymoma EL-4 Cells. *J. Nutr.*, *135*(8), 1859–1864.

Ketron, A. C., Gordon, O. N., et al. (2013). Oxidative metabolites of curcumin poison human type II topoisomerases. *Biochemistry*, *52*(1), 221–7.

Ketterer, B. (1988). Protective role of glutathione and glutathione transferases in mutagenesis and carcinogenesis. *Mutation Research*, *202*(2), 343–361.

Khurana, A., & Ho, C. (1988). High Performance Liquid Chromatographic Analysis of Curcuminoids and Their Photo-oxidative Decomposition Compounds in Curcuma Longa L. *Journal of Liquid Chromatography*, *11*(11), 2295–2304.

Kim, H., Jeong, E. S., et al. (2013). Glucuronidation of a sarpogrelate active metabolite is mediated by UDP-glucuronosyltransferases 1A4, 1A9, and 2B4. *Drug Metabolism and Disposition*, *41*(8), 1529–37.

Koonammackal, M. V., Nellipparambil, U. V. N., & Sudarsanakumar, C. (2011). Molecular dynamics simulations and binding free energy analysis of DNA minor groove complexes of curcumin. *Journal of Molecular Modeling*, *17*(11), 2805–16.

Lao, C. D., Ruffin, M. T., et al. (2006). Dose escalation of a curcuminoid formulation. *BMC Complementary and Alternative Medicine*, *6*, 10.

Lee, B. H., Choi, H. A., et al. (2013). Changes in chemical stability and bioactivities of curcumin by ultraviolet radiation. *Food Science and Biotechnology*, *22*(1), 279–282.

Leong-Skornicková, J., Sída, O., et al. (2007). Chromosome numbers and genome size variation in Indian species of Curcuma (Zingiberaceae). *Annals of Botany*, *100*(3), 505–26.

Leung, M. H. M., & Kee, T. W. (2009). Effective stabilization of curcumin by association to plasma proteins: human serum albumin and fibrinogen. *Langmuir*, *25*(10), 5773–7.

Li, Z., Ouyang, K., et al. (2009). Curcumin induces apoptosis and inhibits growth of human Burkitt's lymphoma in xenograft mouse model. *Molecules and Cells*, *27*(3), 283–9.

Litwinienko, G., & Ingold, K. U. (2004). Abnormal solvent effects on hydrogen atom abstraction. 2. Resolution of the curcumin antioxidant controversy. The role of sequential proton loss electron transfer. *The Journal of Organic Chemistry*, *69*(18), 5888–96.

Liu, Y., Yang, Z., et al. (2008). Interaction of curcumin with intravenous immunoglobulin: a fluorescence quenching and Fourier transformation infrared spectroscopy study. *Immunobiology*, *213*(8), 651–61.

Lopachin, R. M., & Decaprio, A. P. (2005). Protein adduct formation as a molecular mechanism in neurotoxicity. *Toxicological Sciences, 86*(2), 214–25.

López-Lázaro, M., Willmore, E., et al. (2007). Curcumin Induces High Levels of Topoisomerase I− and II−DNA Complexes in K562 Leukemia Cells. *Journal of Natural Products*, *70*(12), 1884–1888.

Mahajan, M. K., Uttamsingh, V., et al. (2011). In vitro metabolism of oxymetazoline: evidence for bioactivation to a reactive metabolite. *Drug Metabolism and Disposition*, *39*(4), 693–702.

Mahmoud, N. N., Carothers, A. M., et al. (2000). Plant phenolics decrease intestinal tumors in an animal model of familial adenomatous polyposis. *Carcinogenesis*, *21*(5), 921–7.

Marczylo, T. H., Verschoyle, R. D., et al. (2007). Comparison of systemic availability of curcumin with that of curcumin formulated with phosphatidylcholine. *Cancer Chemotherapy and Pharmacology*, *60*(2), 171–7.

Mashayekhi, S. O., Sattari, M. R., & Routledge, P. A. (2010). Evidence of active transport involvement in morphine transport via MDCKII and MDCK-PGP cell lines. *Research in Pharmaceutical Sciences*, 5(2), 99–106.

Masuda, T., Hidaka, K., et al. (1999). Chemical Studies on Antioxidant Mechanism of Curcuminoid: Analysis of Radical Reaction Products from Curcumin. *Journal of Agricultural and Food Chemistry*, *47*(1), 71–77.

Metzler, M., Pfeiffer, E., Schulz, S. I., & Dempe, J. S. (2013). Curcumin uptake and metabolism. *BioFactors*, *39*(1), 14–20.

Nafisi, S., Adelzadeh, M., Norouzi, Z., & Sarbolouki, M. N. (2009). Curcumin binding to DNA and RNA. *DNA and Cell Biology*, *28*(4), 201–8.

Nitiss, J. L. (1998). Investigating the biological functions of DNA topoisomerases in eukaryotic cells. *Biochimica et Biophysica Acta*, *1400*(1-3), 63–81.

O'Brien, P. J. (1988). Radical formation during the peroxidase catalyzed metabolism of carcinogens and xenobiotics: the reactivity of these radicals with GSH, DNA, and unsaturated lipid. *Free Radical Biology & Medicine*, *4*(3), 169–83.

Ogilvie, B. W., Zhang, D., et al. (2006). Glucuronidation converts gemfibrozil to a potent, metabolism-dependent inhibitor of CYP2C8: implications for drug-drug interactions. *Drug Metabolism and Disposition*, *34*(1), 191–7.

Olszanecki, R., Jawień, J., et al. (2005). Effect of curcumin on atherosclerosis in apoE/LDLR-double knockout mice. *Journal of Physiology and Pharmacology, 56*(4), 627–35.

Ono, K., Hasegawa, K., et al. (2004). Curcumin has potent anti-amyloidogenic effects for Alzheimer's beta-amyloid fibrils in vitro. *Journal of Neuroscience Research*, *75*(6), 742–50.

Pabon, H. J. J. (1964). A synthesis of curcumin and related compounds. *Recueil Des Travaux Chimiques Des Pays-Bas*, *83*(4), 379–386.

Pan, M., Huang, T., & Lin, J. (1999). Biotransformation of Curcumin Through Reduction and Glucuronidation in Mice. *Drug Metab. Dispos.*, *27*(4), 486–494.

Pandey, M. K., Sandur, S. K., et al. (2007). Butein, a tetrahydroxychalcone, inhibits nuclear factor (NF)-κB and NF-κB-regulated gene expression through direct inhibition of IKKβ on cysteine 179 residue. *The Journal of Biological Chemistry*, *282*(24),

Pandya, A., Goswami, H., et al. (2012). A novel nanoaggregation detection technique of TNT using selective and ultrasensitive nanocurcumin as a probe. *The Analyst*, *137*(8), 1771–4.

Pasternak, G. W., Bodnar, R. J., et al. (1987). Morphine-6-glucuronide, a potent mu agonist. *Life Sciences*, *41*(26), 2845–9.

Pawar, Y. B., Munjal, B., et al. (2012). Bioavailability of a lipidic formulation of curcumin in healthy human volunteers. *Pharmaceutics*, *4*(4), 517–30.

Perry, M., Demeule, M., et al. (2010). Curcumin inhibits tumor growth and angiogenesis in glioblastoma xenografts. *Molecular Nutrition & Food Research*, *54*(8), 1192–201.

Peterson, D. M., & Fisher, J. (1986). Autocatalytic quinone methide formation from mitomycin c. *Biochemistry*, *25*(14), 4077–84.

Pfeiffer, E., Hoehle, S. I., et al. (2006). Curcuminoids Form Reactive Glucuronides In Vitro. *Journal of Agricultural and Food Chemistry*, *55*(2), 538–544.

Poole, L. B., Zeng, B., et al. Synthesis of chemical probes to map sulfenic acid modifications on proteins. *Bioconjugate Chemistry*, *16*(6), 1624–8. doi:

Priyadarsini, K. I., Maity, D. K., et al. (2003). Role of phenolic O-H and methylene hydrogen on the free radical reactions and antioxidant activity of curcumin. *Free Radical Biology & Medicine*, *35*(5), 475–84.

Quitschke, W. W., Steinhauff, N., & Rooney, J. (2013). The effect of cyclodextrin-solubilized curcuminoids on amyloid plaques in Alzheimer transgenic mice: brain uptake and metabolism after intravenous and subcutaneous injection. *Alzheimer's Research & Therapy*, *5*(2), 16.

Ranjan, A. P., Mukerjee, A., et al. (2013). Efficacy of Liposomal Curcumin in a Human Pancreatic Tumor Xenograft Model: Inhibition of Tumor Growth and Angiogenesis. *Anticancer Res*, *33*(9), 3603–3609.

Ravindran, J., Prasad, S., & Aggarwal, B. B. (2009). Curcumin and cancer cells: how many ways can curry kill tumor cells selectively? *AAPS J*, *11*(3), 495–510.

Ravindranath, V., & Chandrasekhara, N. (1980). Absorption and tissue distribution of curcumin in rats. *Toxicology*, *16*(3), 259–265.

Ravindranath, V., & Chandrasekhara, N. (1981). Metabolism of curcumn-studies with [^{3}H]curcumin. *Toxicology*, *22*(4), 337–344.

Reddie, K. G., & Carroll, K. S. (2008). Expanding the functional diversity of proteins through cysteine oxidation. *Current Opinion in Chemical Biology*, *12*(6), 746–54.

Ritter, J. K. (2000). Roles of glucuronidation and UDP-glucuronosyltransferases in xenobiotic bioactivation reactions. *Chemico-Biological Interactions*, *129*(1-2), 171–193.

Sanphui, P., Goud, N. R., et al. (2011). New polymorphs of curcumin. *Chemical Communications, 47*(17),

Sasikumar, B. (2005). Genetic resources of Curcuma: diversity, characterization and utilization. *Plant Genetic Resources*, *3*(2), 230–251.

Selvam, C., Jachak, S. M., Thilagavathi, R., & Chakraborti, A. K. (2005). Design, synthesis, biological evaluation and molecular docking of curcumin analogues as antioxidant, cyclooxygenase inhibitory and anti-inflammatory agents. *Bioorganic & Medicinal Chemistry Letters*, *15*(7), 1793–7.

Sharma, A. M., Li, Y., et al. (2012). Bioactivation of nevirapine to a reactive quinone methide: implications for liver injury. *Chemical Research in Toxicology*, *25*(8), 1708–19.

Shen, L., & Ji, H.-F. (2009). Contribution of degradation products to the anticancer activity of curcumin. *Clinical Cancer Research*, *15*(22), 7108;

Shen, L., & Ji, H. (2012). The pharmacology of curcumin: is it the degradation products? *Trends in Molecular Medicine*, *18*(3), 138–44.

Singh, M., Ramos, I., Asafu-Adjei, D., et al. (2013). Curcumin improves the therapeutic efficacy of Listeria(at)-Mage-b vaccine in correlation with improved T-cell responses in blood of a triple-negative breast cancer model 4T1. *Cancer Medicine*, *2*(4), 571–82.

Singh, S., & Khar, A. (2006). Biological effects of curcumin and its role in cancer chemoprevention and therapy. *Anticancer Agents in Medicinal Chemistry*, *6*(3), 259–270.

Sinha, R., Anderson, D. E., McDonald, S. S., & Greenwald, P. (2003). Cancer risk and diet in India. *Journal of Postgraduate Medicine*, *49*(3), 222–8.

Sperker, B., Backman, J. T., & Kroemer, H. K. (1997). The role of beta-glucuronidase in drug disposition and drug targeting in humans. *Clinical Pharmacokinetics*, *33*(1), 18–31.

Sperker, B., Werner, U., et al. (2000). Expression and function of β-glucuronidase in pancreatic cancer: potential role in drug targeting. *Naunyn-Schmiedeberg's Archives of Pharmacology*, *362*(2), 110–115.

Stiborová, M., Poljaková, J., et al. (2007). Mammalian peroxidases activate anticancer drug ellipticine to intermediates forming deoxyguanosine adducts in DNA identical to those found in vivo and generated from 12-hydroxyellipticine and 13-hydroxyellipticine. *International Journal of Cancer*, *120*(2), 243–51.

Strimpakos, A. S., & Sharma, R. A. (2008). Curcumin: preventive and therapeutic properties in laboratory studies and clinical trials. *Antioxidants & Redox Signaling*, *4*(14), 2909–2911.

Su, C., Yang, J., Lu, C., et al. (2010). Curcumin inhibits human lung large cell carcinoma cancer tumour growth in a murine xenograft model. *Phytotherapy Research*, *24*(2), 189–92.

Sun, Y., Wang, R., Yuan, S., Lin, X., & Liu, C. (2010). Theoretical study on the antioxidant activity of curcumin. *Chinese Journal of Chemistry*, *22*(8), 827–

Sun, Y., Zhang, H., Chen, D., & Liu, C. (2002). Theoretical Elucidation on the Antioxidant Mechanism of Curcumin: A DFT Study. *Organic Letters*, *4*(17), 2909–2911.

Suzuki, M., Betsuyaku, T., et al. (2009). Curcumin attenuates elastase- and cigarette smoke-induced pulmonary emphysema in mice. *American Journal of Physiology. Lung Cellular and Molecular Physiology*, *296*(4), L614–23.

Szewczuk, L. M., Lee, S. H., et al. (2005). Viniferin formation by COX-1: evidence for radical intermediates during co-oxidation of resveratrol. *Journal of Natural Products*, *68*(1), 36–42.

Thompson, D. C., Barhoumi, R., & Burghardt, R. C. (1998). Comparative toxicity of eugenol and its quinone methide metabolite in cultured liver cells using kinetic fluorescence bioassays. *Toxicology and Applied Pharmacology*, *149*(1), 55–63.

Tonnesen, H. H., & Karlsen, J. (1985). Studies on curcumin and curcuminoids. *Zeitschrift Fur Lebensmittel-Untersuchung Und -Forschung*, *180*(2), 132–134.

Vaidya, V., Ingold, K. U., & Pratt, D. A. (2009). Garlic: Source of the Ultimate Antioxidants-Sulfenic Acids. *Angewandte Chemie*, *121*(1), 163–166.

Valacchi, G., Pagnin, E. et al (2004). Inhibition of NFkappaB activation and IL-8 expression in human bronchial epithelial cells by acrolein. *Antioxidants & Redox Signaling*, *7*(1-2), 25–31.

Vareed, S. K., Kakarala, M., et al. (2008). Pharmacokinetics of curcumin conjugate metabolites in healthy human subjects. *Cancer Epidemiology, Biomarkers & Prevention, 17*(6), 1411–7.

Wahlström, B., & Blennow, G. (1978). A study on the fate of curcumin in the rat. *Acta Pharmacologica et Toxicologica*, *43*(2), 86–92.

Wang, H., Mao, Y. et al. (2001). Stimulation of Topoisomerase II-Mediated DNA Damage via a Mechanism Involving Protein Thiolation. *Biochemistry*, *40*(11), 3316–3323.

Wang, J. C. (1996). DNA topoisomerases. *Annual Review of Biochemistry*, *65*, 635–92.

Wang, L., Li, C., Guo, H. et al. (2011). Curcumin inhibits neuronal and vascular degeneration in retina after ischemia and reperfusion injury. *PloS One*, *6*(8), e23194.

Wang, Y., Pan, M., Cheng, A. et al. (1997). Stability of curcumin in buffer solutions and characterization of its degradation products. *Journal of Pharmaceutical and Biomedical Analysis*, *15*(12), 1867–1876.

Weber, W. M., Hunsaker, L. A. et al. (2006). Activation of NFkB is inhibited by curcumin and related enones. *Bioorganic Medicinal Chemistry*, *14*(7), 2450–2461.

Weisberg, S. P., Leibel, R., & Tortoriello, D. V. (2008). Dietary curcumin significantly improves obesity-associated inflammation and diabetes in mouse models of diabesity. *Endocrinology*, *149*(7), 3549–58.

Wetzelberger, K., Baba, S. P., et al. (2010). Postischemic deactivation of cardiac aldose reductase: role of glutathione S-transferase P and glutaredoxin in regeneration of reduced thiols from sulfenic acids. *The Journal of Biological Chemistry*, *285*(34), 26135–48.

Weyel, D., Sedlacek, H. H., et al. (2000). Secreted human beta-glucuronidase: a novel tool for gene-directed enzyme prodrug therapy. *Gene Therapy*, *7*(3), 224–31.

Wilken, R., Veena, M. S., Wang, M. B., & Srivatsan, E. S. (2011). Curcumin: A review of anti-cancer properties and therapeutic activity in head and neck squamous cell carcinoma. *Molecular Cancer*, *10*, 12.

Yang, K., Lin, L., Tseng, T., Wang, S., & Tsai, T. (2007). Oral bioavailability of curcumin in rat and the herbal analysis from Curcuma longa by LC-MS/MS. *Journal of Chromatography. B, Analytical Technologies in the Biomedical and Life Sciences*, *853*(1-2), 183–9.

Zebib, B., Mouloungui, Z., & Noirot, V. (2010). Stabilization of curcumin by complexation with divalent cations in glycerol/water system. *Bioinorganic Chemistry and Applications*, 292760.

Zhao, X., C. Wang, et al. (2013). "Chronic curcumin treatment normalizes depression-like behaviors in mice with mononeuropathy: involvement of supraspinal serotonergic system and GABAA receptor." Psychopharmacology: 1-17.